Technical Report Documentation Page

1. Report No. FHWA/TX-14/0-6723-1	2. Government Accession No.	3. Recipient's Catalog No.
4. Title and Subtitle Development of Rapid, Cement-based Repair Materials for Transportation Structures: Final Report		5. Report Date January 2015; Published July 2015 6. Performing Organization Code
7. Author(s) Mitchell Dornak, Jose Zuniga, Anthony Garcia, Thano Drimalas, and Kevin J. Folliard		8. Performing Organization Report No. 0-6723-1
9. Performing Organization Name and Address Center for Transportation Research The University of Texas at Austin 1616 Guadalupe St., Suite 4.202 Austin, TX 78701		10. Work Unit No. (TRAIS) 11. Contract or Grant No. 0-6723
12. Sponsoring Agency Name and Address Texas Department of Transportation Research and Technology Implementation Office P.O. Box 5080 Austin, TX 78763-5080		13. Type of Report and Period Covered Technical Report September 2011–August 2014 14. Sponsoring Agency Code
15. Supplementary Notes Project performed in cooperation with the Texas Department of Transportation and the Federal Highway Administration.		
16. Abstract The state of Texas has been plagued by various durability-related issues in recent years, including deterioration from alkali-silica reaction (ASR), delayed ettringite formation (DEF), corrosion of reinforcing steel, and volume changes (plastic shrinkage, drying shrinkage, thermal effects, etc.), just to name a few. These durability-related issues, coupled with other factors that contribute to reductions in service life (e.g., service loads, defects, vehicle impact, etc.), have resulted in the need to repair concrete structures and to do so in a timely, efficient fashion, with minimal disruption to the traveling public. Thus, the need for rapid, cement-based repair materials has emerged, especially in highly congested urban areas. This project included a comprehensive laboratory-based program, as well as a significant field component, aimed at addressing this critical infrastructure need. The goals of the research project were to evaluate a range of rapid repair materials and to provide recommendations on the most efficient, economical, and durable repair materials and methodologies.		
17. Key Words rapid repair materials, calcium aluminate cement, calcium sulfoaluminate cement, durability, volume changes	18. Distribution Statement No restrictions. This document is available to the public through the National Technical Information Service, Springfield, Virginia 22161; www.ntis.gov.	

19. Security Classif. (of report)	20. Security Classif. (of this page)	21. No. of pages	22. Price
Unclassified	Unclassified	288	

Form DOT F 1700.7 (8-72) Reproduction of completed page authorized

THE UNIVERSITY OF TEXAS AT AUSTIN
CENTER FOR TRANSPORTATION RESEARCH

Development of Rapid, Cement-based Repair Materials for Transportation Structures: Final Report

Mitchell Dornak
Jose Zuniga
Anthony Garcia
Thano Drimalas
Kevin J. Folliard

CTR Technical Report:	0-6723-1
Report Date:	October 2014; Revised January 2015
Project:	0-6723
Project Title:	Development of Rapid, Cement-based Repair Materials for Transportation Structures
Sponsoring Agency:	Texas Department of Transportation
Performing Agency:	Center for Transportation Research at The University of Texas at Austin

Project performed in cooperation with the Texas Department of Transportation and the Federal Highway Administration.

Center for Transportation Research
The University of Texas at Austin
1616 Guadalupe St, Suite 4.202
Austin, TX 78701

http://ctr.utexas.edu

Disclaimers

Author's Disclaimer: The contents of this report reflect the views of the authors, who are responsible for the facts and the accuracy of the data presented herein. The contents do not necessarily reflect the official view or policies of the Federal Highway Administration or the Texas Department of Transportation (TxDOT). This report does not constitute a standard, specification, or regulation.

Patent Disclaimer: There was no invention or discovery conceived or first actually reduced to practice in the course of or under this contract, including any art, method, process, machine manufacture, design or composition of matter, or any new useful improvement thereof, or any variety of plant, which is or may be patentable under the patent laws of the United States of America or any foreign country.

Engineering Disclaimer

NOT INTENDED FOR CONSTRUCTION, BIDDING, OR PERMIT PURPOSES.

Project Engineer: Dr. David W. Fowler
Professional Engineer License State and Number: Texas No. 27859
P. E. Designation: Researcher

Acknowledgments

The authors express appreciation to the TxDOT Project Director, members of the Project Monitoring Committee, and the staff at the Concrete Durability Center.

Table of Contents

List of Figures

List of Tables

Glossary

ACI	American Concrete Institute
ASR	alkali-silica reaction
CA	monocalcium aluminate
CAC	calcium aluminate cement
CH	calcium hydroxide
CSA	calcium sulfoaluminate cement
C-S-H	calcium silicate hydrates
CTE	coefficient of thermal expansion
FSF	free shrinkage frame
MOE	modulus of elasticity
OPC	ordinary portland cement
RCF	rigid cracking frame
RCPT	rapid chloride permeability test
SBR	styrene butadiene rubber
SCM	supplementary cementitious material
w/c	water-to-cement ratio
w/cm	water-to-cementitious-materials ratio
XRD	x-ray diffraction
XRF	x-ray fluorescence

Chapter 1. Introduction and Scope

There are a variety of reasons why concrete structures, in general, and transportation structures, in particular, may require repair during their intended service lives. Many of the underlying mechanisms responsible for concrete deterioration may be occurring simultaneously, requiring a holistic viewpoint to capture this overall issue, as depicted in Figure 1.1 (Mehta and Monteiro, 1993).

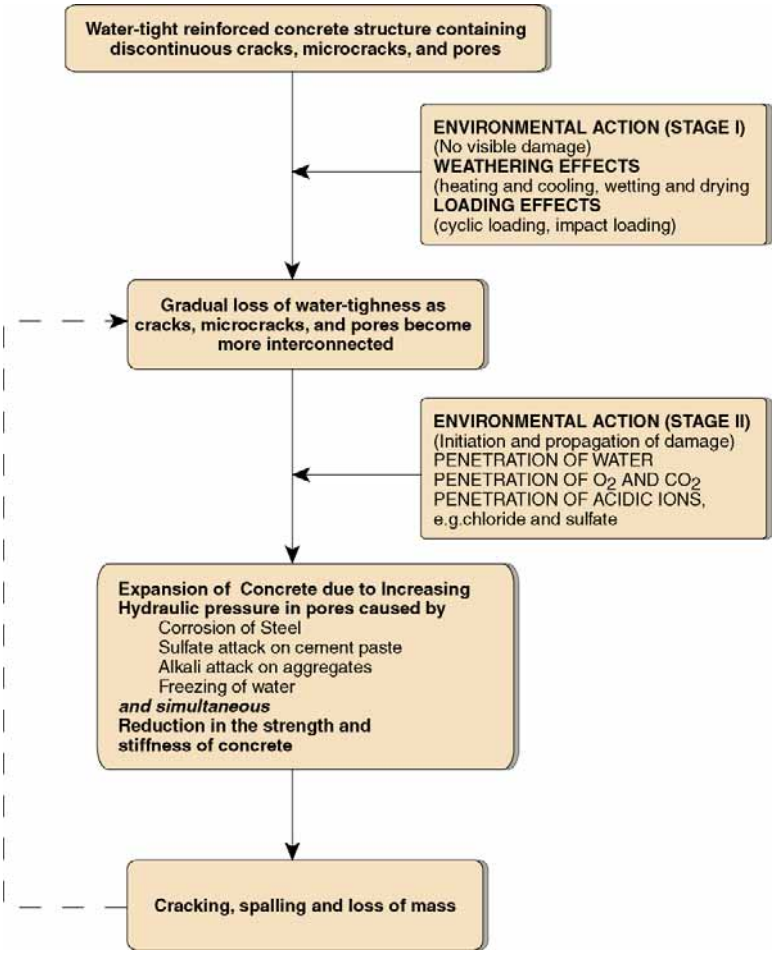

Figure 1.1: A holistic approach to understanding the mechanisms of concrete deterioration (Mehta and Monteiro, 1993)

In addition to the various causes of concrete degradation shown in Figure 1.1, repairs may be necessitated simply by the need to build or rebuild to meet increased capacity, specifically increased population and vehicular traffic. This has been the case in areas such as Dallas/Fort Worth and Houston over the years, and Austin is heading in the same direction, in terms of increasing population and traffic and inadequacies in the current infrastructure (relative to demand). Regardless of the need for repair, when it is necessary in congested, urban areas,

speed of construction and the ability to open to traffic as soon as possible become paramount, and repair materials/methods are needed to meet this need.

Over the past 20 years or so, many in the transportation arena have used the adage "Get in, get out, stay out" to capture the essence that repairs need to be quick and long-lasting. However, oftentimes, the actual performance of repairs to pavements and bridge decks is not consistent with this adage, and reality often becomes "Get in, get out, get in again." The failure of rapid repair materials is unfortunately quite common, mainly due to the highly technical demands for a rapid yet durable repair material for pavements and bridge decks. Issues such as incompatibility (thermal, elastic, or viscoelastic) with the base concrete, heavy traffic loading, durability problems, and environmental exposure conditions can all adversely impact the service life of a given repair application.

The focus of this project, funded by the Texas Department of Transportation (TxDOT), was to evaluate a range of repair materials across a range of properties (fresh, hardened, and durability) that affect the performance of horizontal repairs, such as pavements and bridge decks. This project included a significant laboratory and field evaluation program, evaluated several classes of rapid concrete, including calcium aluminate cement (CAC) concrete, high early-strength portland cement concrete, calcium sulfoaluminate cement (CSA) concrete, and concrete containing fly ash as the sole binder.

1.1 Report Organization and Outline

This report summarizes the main findings from TxDOT Project 6723, *Development of Rapid, Cement-based Repair Materials for Transportation Structures,* a three-year laboratory-based project that focused primarily on evaluating rapid repair materials. For convenience and organizational purposes the research focusing on rapid-repair materials is presented in the following chapters:

- **Chapter 2** presents a concise literature review on various rapid repair materials used in transportation applications.
- **Chapter 3** describes the materials used in the laboratory and field testing programs.
- **Chapter 4** describes the Phase I laboratory screening program, where a wide range of materials and mixture proportions were evaluated to determine which materials/proportions would be selected for more detailed evaluations.
- **Chapter 5** presents the results of tests performed to determine key engineering properties for various repair materials, including elastic modulus, coefficient of thermal expansion, and bond strength.
- **Chapter 6** describes research performed evaluating the early-age volume changes (restrained and unrestrained) for various repair materials and mixtures.
- **Chapter 7** presents the results of calorimetry studies on various repair materials.
- **Chapter 8** summarizes the findings from field evaluations involving rapid repair materials, including large-scale bridge deck repairs at The University of Texas at Austin and field surveys of repaired pavements in Cotulla, Texas.
- **Chapter 9** describes the results of laboratory testing related to the resistance of rapid repair concrete mixtures to freezing and thawing and salt scaling.

- **Chapter 10** describes the results of laboratory tests related to the resistance of rapid repair concrete mixtures to alkali-silica reaction.
- **Chapter 11** provides the results of laboratory tests related to the resistance of rapid repair materials to sulfate attack.
- **Chapter 12** provides the results of permeability and corrosion results of rapid repair materials.
- **Chapter 13** provides the conclusions of the laboratory and field performance results for the durability of rapid-repair materials.

Chapter 2. Literature Review of Rapid-Repair Materials

2.1 Introduction

The focus of this literature review is to bring to light some of the needs and requirements for repair materials, along with the benefits that today's popular binders bring to a high early-strength rapid repair job. This chapter also includes any special provisions or specifications for these binders that serve as a starting guide for the durability research needs for this project.

2.2 Needs and Requirements

The increase in deterioration to today's infrastructure's pavements has led to an increase in the number of binders and types of mixture designs available for rapid repair and rehabilitation. Typical ordinary portland cement (OPC) mixtures are acceptable for new pavement construction because contractors do not rely on high early strengths soon after placement. On the other hand, roads and bridge decks that have been open to traffic especially in densely populated areas, cannot be simply shut down to allow for repairs because this causes large traffic delays and involves high costs to keep the lanes closed to ensure the safety of construction workers for the duration of the repair. For this reason the implementation of rapid early-strength materials for fast-track concrete repair has become quite popular with transportation officials. These rapid-setting materials can be very expensive in comparison to OPC concrete, but the high early strengths, durability, and speed of construction compensate for the higher upfront material cost.

Typical short-term requirements for these fast-track jobs are 3000 psi compressive strength at 3 hours or 400 psi flexural strength at 4 hours, a reasonable working time, and a reasonable flow of the concrete mixture. Certain binders have become popular for these high early-strength jobs such as CAC, CSA, accelerated Type III portland cement, alkali-activated fly ash binders, and also prepackaged proprietary blends. These binders typically have no problems meeting the short-term goals of strength but their durability properties have not been extensively tested. Potential detriments to durability include the alkali-silica reaction (ASR), delayed ettringite formation, sulfate attack, freezing and thawing, and corrosion. The selected mixes from Phase I of this project will be subjected to a comprehensive laboratory program that will test the durability of the materials in the face of these forms of attack to determine whether these binders will meet the long-term durability requirements for fast-track concrete placement.

2.3 Types of Materials

Various binders that exhibit high rates of reaction and early-age strength have been developed within the past century and have been harnessed for rapid repair construction to minimize traffic delays and improve performance. The most popular binders to date were selected to conduct an extensive laboratory testing regime to test the fresh, hardened, and durability properties. A detailed literature review for each of these binders is described below.

2.3.1 Calcium Aluminate Cement Concrete

2.3.1.1 Introduction

CAC started to appear in the late 19th and early 20th centuries in Europe. Different in composition from OPC, this blend was engineered to be resistant to high sulfate environments and seawater. Work done by L. J. Vicat in the 1840s to change the chemical makeup of cements—especially the ratio of silica+alumina to that of calcium+magnesium—was one of the precursors to the development of CAC (Gosselin, 2009). A few years later, this work was continued by Jules Bied, who experimented with these ratios and came up with a cement low in silica and high in alumina, and finally patented the blend as Ciment Fondu Lafarge in 1908. Nowadays the use of bauxite, a relatively pure and expensive raw material, is the primary source of alumina for the manufacture of CAC (Gosselin, 2009). CAC is typically around four to five times more expensive when compared to OPC. For this reason, CAC is not a major competitor for OPC; its use is limited to special areas such as refractory, dry mix mortars, self-leveling compounds, and rapid repair. A brief description of the chemical composition and hydration process of CACs is explained in the following sections.

2.3.1.2 Chemical Composition

Several grades of CAC exist, with varying alumina and iron contents; their compositions are shown in Table 2.1. Two different types of bauxite are used to manufacture CAC. Red bauxite typically contains around 20% of iron oxides and typically forms a brown to dark grey cement, while white bauxite contains little to no iron oxides and forms a light grey to white cement. For the purposes of this research Ciment Fondu was chosen as our source for CAC as it is most readily available and the most common blend used for these rapid repair applications. For this specific blend of CAC typical ranges for alumina content are around 40 to 60%.

Table 2.1: Composition ranges for calcium aluminate cements from Scrivener (2003)

Grade	Colour	Al_2O_3	CaO	SiO_2	Fe_2O_3 + FeO	TiO_2	MgO	Na_2O	K_2O	Countries of manufacture
'Standard' low alumina	Grey or buff to black	36–42	36–42	3–8	12–20	<2	~1	~0.1	~0.15	France, Spain, Croatia, USA, India, Eastern Europe
Low alumina, low iron	Light buff or grey to white	48–60	36–42	3–8	1–3	<2	~0.1	~0.1	~0.05	France, USA, India, Korea, Brazil
Medium alumina	White	65–75	25–35	<0.5	<0.5	<0.05	~0.1	<0.3	~0.05	France, UK, USA, Japan, China, India, Korea, Brazil
High alumina	White	⩾80	<20	<0.2	<0.2	<0.05	<0.1	<0.2	~0.05	USA, France, Japan, Brazil, Korea

The main compound in any CAC is monocalcium aluminate (CA) and typically comprises 40 to 60% of the cement. The second most available compound in CAC is $C_{12}A_7$, also called *mayenite*; this phase is important and contributes greatly to the setting of the cement. Too much of this phase can cause flash setting in the concrete, however, so its percentage is typically regulated in the manufacturing process. Other phases in CAC include C_2S (belite), C_2AS (gehlenite), ferrite solid solution, and other phases containing iron and silicon. The percentages of these secondary phases can reach up to 50% total of the cement but their reactivity is far less

and much slower than CA and $C_{12}A_7$, so their early age contributions are not as readily analyzed (Scrivener, 2003).

2.3.1.3 Hydration and Conversion

As mentioned above, the main hydration reactant is CA, and it follows some of the same hydration rules as OPC. The first step is the dissolution of the CA into Ca^{2+} and $Al(OH)^{4-}$ ions, and then precipitation into its hydrates. The main products in CAC are formed according to the reactions shown as Equations 2.1 to 2.3.

$$CA + 10H \rightarrow CAH_{10} \tag{2.1}$$

$$2CA + 11H \rightarrow C_2AH_8 + AH_3 \tag{2.2}$$

$$3CA + 12H \rightarrow C_3AH_6 + 2AH_3 \tag{2.3}$$

The main difference between these calcium aluminate hydrates and the calcium silicates formed though OPC hydration is the fact that some of these hydrates are metastable and thermodynamically wish to exist as the stable phases of AH_3 or C_3AH_6. The metastable phases, CAH_{10} and C_2AH_8, form temporarily and are sensitive to the water availability in the solution and temperature. For example, the more readily available water is in the solution (typically a water-to-cement ratio [w/c] greater than 0.7 for concrete mixtures), the more the chemistry favors the formation of the metastable phases. With lower w/c, there is not enough water to fully hydrate the metastable phases, so some formation of the stable phases can be seen.

Temperature also dictates which hydrates will be favored in the hydration process. The formation of CAH_{10} is favored up to a temperature of 75 to 100 °F; at temperatures above 150 °F the nucleation of C_3AH_6 occurs; and at temperatures in between, the formation of C_2AH_8 and AH_3 most commonly arises. The process by which these metastable phases transform to the thermodynamically stable phases is called *conversion* and the transformation of these phases follows Equations 2.4 and 2.5.

$$2CAH_{10} \rightarrow C_2AH_8 + AH_3 + 9H \tag{2.4}$$

$$3C_2AH_8 \rightarrow 2C_3AH_6 + AH_3 + 9H \tag{2.5}$$

This process can be slow and take decades to complete if high w/c and the ambient temperature is below 95 °F. On the other hand if low w/c are used and the mixture sees temperatures above 150 °F in the first hours of hydration conversion can take place within the first few days. If the metastable and stable phases were similar in morphology there would be no problem with conversion, but the different amounts of combined water and densities of these phases cause problems in the concrete matrix. The amount of combined water is much less in stable phases (AH_3 or C_3AH_6) than in metastable phases (CAH_{10} or C_2AH_8) so their densities increase as conversion takes place (Campas & Scrivener, 1998). Typical densities and combined water values are shown in Table 2.2.

Table 2.2: Density and combined water for calcium aluminate hydrates from Campas & Scrivener (1998)

Phase	Density (kg/m^3)	Combined water (%)
CAH_{10}	1720	53
C_2AH_8	1750	40
C_3AH_6	2520	28
AH_3	2400	35

This densification of the stable phases brings about a reduction in the solid volume in the matrix as well as an increase in the porosity which in turn causes a decrease in strength. Up to a 50% reduction in strength has been seen in certain cases (Barborak, 2010). This reduction in strength caused several CAC structures to collapse in the UK after World War II when CAC was used as a construction material in Europe (Campas & Scrivener, 1998). Conversion was not given 100% of the blame as forensic analysis of the structures showed structural design problems. Since then, the conversion process has been studied further but CAC still remains banned in certain structural applications. Although conversion is inevitable, researchers have found ways to determine the converted reduced strength of CAC mixtures by casting cylinders in an insulated box and allowing the temperature to reach 140 °F (Barborak, 2010). This degree of heat drives the formation of the stable hydrates and effectively creates the final composition that the mixture will see in its lifetime, including the highest levels of porosity and thermodynamically stable phases. It is important to note that once the concrete has attained these stable phases, the compressive strength of the material remains stable and might see a slight increase in time with hydration of unhydrated cement grains. Special provision such as TxDOT's SS-4491 allows this process to be used to attain the converted compressive strength and use that value as the final design strength of the mixture (Barborak, 2010). CAC concrete may be different in chemistry and behavior but once the mechanisms are understood the use and implementation of CAC concrete can be very simple and straightforward.

2.3.1.4 Benefits of Using CAC Concrete

Some of the benefits that CAC concrete has over OPC concrete include the following:

- high resistance to temperature and chemical attack
- high sulfate resistance
- high resistance to ASR
- lower CO_2 emissions during production
- higher early strengths upon setting

The original purpose for creating CACs was to provide sulfate resistant cement. External sulfate attack usually consists of sulfates from the environment, either from soils or groundwater, reacting with the AFM phases in traditional OPC concrete. The external sulfates convert the AFM phases, particularly monosulfate, to the more stable ettringite causing expansion and consequently the deterioration of the concrete. In CAC concrete the main products, both stable

and metastable, are calcium aluminate hydrates such as CAH_{10}, C_2AH_8, AH_3 and C_3AH_6. With minimal to no amount of monosulfate phases in CAC concrete to react with the external sulfates and form ettringite there is little to no sulfate attack. Another difference from OPC concrete is the lower pH of CAC concrete, typically around 11.97 to 12.4, as compared to 13.4 for OPC concrete. This low pH is still able to passivate the steel just like OPC concrete but corrosion may still occur by either the lowering of the pH by carbonation or by the ingress of chlorides (Macias, 1996). Minimal research has been conducted to determine any chloride ingress relationships for CAC concrete but field behavior and durability can be seen in existing CAC members. CAC concrete members in marine environments have shown a dense surface layer up to 50mm thick containing chlorides, monosulfate, and Friedel's salt. Even though chlorides have been found to that depth in those concrete elements, no signs of corrosion in the reinforcing steel were observed (Scrivener, 2003).

2.3.2 Calcium Sulfoaluminate Cements

2.3.2.1 Introduction

CSAs were developed in China in the 1970s and classified as China's "Third Cement Series" (Pera & Ambroise, 2004). The raw materials used to form CSA are limestone, gypsum, and bauxite, which combine to create a sulfate-based clinker as opposed to the silicates of OPC. CSA clinker's main chemical composition includes the following phases: belite (C_2S), tetracalcium trialuminate sulfate ($C_4A_3\$$) (also known as ye'elemite), and gypsum. The rapid growth of ettrigite is the mechanism by which CSA cements attain strength. There are two different mechanisms by which ettringite forms in CSA depending on the availability of CH (Liao & Wei, 2011). These mechanisms will be discussed in the next section. Some of the properties achieved by the use of CSAs include these:

- high early strength
- expansive and self-stressing mixtures
- shrinkage compensating mixtures

The limited availability of raw materials, especially bauxite (source of alumina), increases the cost of the cement and inhibits the widespread use of CSA as an alternative to portland cement.

2.3.2.2 Chemical Composition

CSA cement is produced when burning limestone, bauxite, and gypsum in a rotary kiln at 1250 °C, 200 degrees lower than portland cement. CSA contains some of the same chemical compounds contained in OPC, such as C_2S, $C\$$, C_4AF, and also $C_4A_3\$$ (known ye'elemite or Klein's compound) (Winnefeld, 2010). A comparison of the different percentages of each compound for OPC and CSA are shown in Table 2.3. Minor phases in CSA include C_4AF, $C_{12}A_7$, C_3A, and C_6AF_2.

Table 2.3: Comparison of portland cement and CSA from Bescher & Ramseyer (2008)

Portland Cement Composition					
ASTM TYPE	C_3S	C_2S	C_3A	C_4AF	C$
I	59	15	12	8	2.9
II	46	29	6-8	12	2.8
III	60	12	12-15	8	3.9
IV	30	46	5-7	13	2.9
V	43	36	4-5	12	2.7
CSA Cement Composition					
	C_3S	C_2S	C_3A	C_4AF	C$
	30	45	0	2	15

The lack of iron phases in the chemistry of the cement gives it a light grey color. Figure 2.1 shows a sample of the CSA cement used for this research. The hydration products formed from these compounds along with mechanistic behavior of the reactions are described in the following section.

Figure 2.1: Sample CSA showing light grey color

2.3.2.3 Hydration

The most important reaction in CSA is the formation of ettringite ($C_6A\$_3H_{32}$). Ettringite forms from the reaction of ye'elemite with gypsum according to Equations 2.6 and 2.7, depending on the amount of calcium hydroxide in solution.

$$C_4A_3\$ + 2C\$H_2 + 36H \rightarrow C_6A\$_3H_{32} + 2AH_3 \quad (2.6)$$

$$C_4A_3\$ + 8C\$H_2 + 6CH + 74H \rightarrow 3C_6A\$_3H_{32} \quad (2.7)$$

When calcium hydroxide is not present as in reaction (2.6), the ettringite growth is non-expansive but does result in high early strengths, typically around 4000 psi compressive strengths by 3 or 4 hours for a well-designed mixture. In the presence of calcium hydroxide, reaction (2.7), the formation of ettringite is expansive and is used for self-stressing concrete elements and shrinkage resistant cement. The ettringite crystal microstructure influences the setting time, strength development, and shrinkage of the concrete (Pera & Ambroise, 2004). The difference in behavior depending on the overall composition of the cement has been exploited by

cement producers to target their specific needs: either shrinkage-compensating concrete, expansive and self-stressing concrete, or high early-strength concrete.

2.3.2.4 Benefits of Using CSA Concrete

Several benefits of using CSA cement are observed even before mixing with water. The production of CSA cement occurs at 2280 °F, 360 degrees lower than portland cement, effectively reducing the amount of energy during production. The amount of limestone calcined in order to produce CSA cement is also considerably lower than that needed to produce the calcium silicates of portland cement (Juenger, 2011). Sulfate-based clinkers are also more porous than OPC clinker and thus require less energy to grind (Winnefeld & Pelletier-Chaignat, 2011). So overall the energy needed for the total production of CSA for calcining, and grinding is considerably less than that needed for portland cements and CO_2 emissions can be reduced by 80% (Juenger, 2011). Although the savings in energy are recognized the production of CSA is still more expensive due to the cost of bauxite as a raw material.

These CSA cements also exhibit high sulfate resistance. The unique chemistry of this binder leads to the formation of stable ettringite as the main hydration product along with minor amounts of AFm phases, C-S-H (calcium silicate hydrates) gel, and gibbsite. For this reason any additional sulfates in the environment do not cause a deleterious effect on the concrete. These sulfate cements also show high impermeability and chemical resistance, low drying shrinkage due to their expansive nature, and low alkalinity. Typical pH values for CSA concrete are around 10.5 to 11, much lower than portland cement concrete, which is above 13. This lower alkalinity prevents the dissolution of silicate particles and thus reduces the chance of ASR occurring in the concrete (Scrivener, 2003). The other benefits have already been discussed in the previous sections, and those included the rapid strength gain, the expansive behavior, and shrinkage compensating properties of the concrete.

2.3.3 Latex-Modified Concrete

2.3.3.1 Introduction

Bridge decks contain large amounts of reinforcing steel that should be protected from corrosion. In cold weather, bridge decks tend to suffer from freezing due to cold winds through the top and bottom of the structure so DOTs use deicing salts to prevent snow or ice buildup. Microcracking of bridge decks allows the migration of these chlorides into the reinforcement layers and cause corrosion of the steel. For this reason, low permeability concrete and proper curing has been used for years to prevent early age cracking and slow down or prevent chlorides from penetrating into the structural steel (BASF, 2011).

Latex-modified concrete has been used for decades to create a durable and low permeability bridge deck concrete overlay. Dow Chemical began researching modified concrete in 1952 by and five years later conducted their first field trials on US 23 in Cheboygan, MI (DOW, 1995). The latex modifier used for these mixtures was a styrene butadiene rubber (SBR) latex polymer consisting of approximately 48% solids and 52% water, and these proportions are still being used today. Latex-modified concrete has typically been created with CSA cement, portland cement, or a mixture of the two. For this research project, latex will be added to CSA and CAC concrete mixtures only.

2.3.3.2 Specifications and Criteria

Research conducted in the late 1950s and 1960s by Dow Chemical aimed to achieve a combination of styrene-butadiene polymer with concrete mixtures to decrease the permeability to chlorides and increase flexural properties of the concrete. Addition of latex polymer ranged from 5 to 20% by weight of cement. All the research done by Dow Chemical as well as private laboratories led to the formation of guidelines for the construction of latex-modified concrete. The American Concrete Institute (ACI) developed a set of rules and guidelines for proper placement and design for latex-modified concrete in ACI 548.4 *Specification for Latex-Modified Concrete Overlays*, which sets a minimum of 15% latex addition by solids (ACI 548.4, 2011). Contractors and mixture designers need to take into account that the styrene-butadiene polymer comes in an approximate 50/50 suspension, so the amount of water added to the mixture should be adjusted accordingly. Some specifications and requirements for the proper implementation of a very-early-strength latex-modified concrete overlay include (ACI 548.4, 2011) the following:

- One-third calcium sulfoaluminate and two-thirds dicalcium silicate or any other hydraulic cement meeting strength requirements
- Overlay thickness of 1.25 to 4 in.
- 15% latex addition minimum
- Maximum w/c of 0.40
- Fine aggregate range by weight of total aggregate should be within 55–70%
- Moist curing by damp burlap and plastic sheeting should be applied as soon as possible until the opening of traffic.

The development of more sophisticated technological equipment, screeds, and volumetric mixers has led to more specified construction and efficiently placed overlays for latex-modified concrete. The added benefits of using latex-modified concrete are described in the following section.

2.3.3.3 Benefits of Latex-Modified Concrete

The original properties sought through latex-modified concrete research were reduced permeability, increased flexural and increased tensile strength of the concrete. Compressive strengths were reduced at early ages but by 28 days the strengths were equivalent to non-latex concrete mixtures. During concrete hydration micro-cracks start to form within the concrete matrix and compromise durability even before it is opened to traffic (Won, 2011). When using latex-modified concrete, the latex fills in these micro-cracks and reduces the permeability of the concrete by creating links that overlap over these cracks as shown in Figure 2.2. Research data for latex-modified concrete has proven these added benefits and typical results are shown in Figure 2.3. The addition of latex requires lower w/c which generally produce lower porosity and higher strengths, and have also shown a decrease in the modulus of elasticity of the concrete which makes for better performance when subjected to traffic loading.

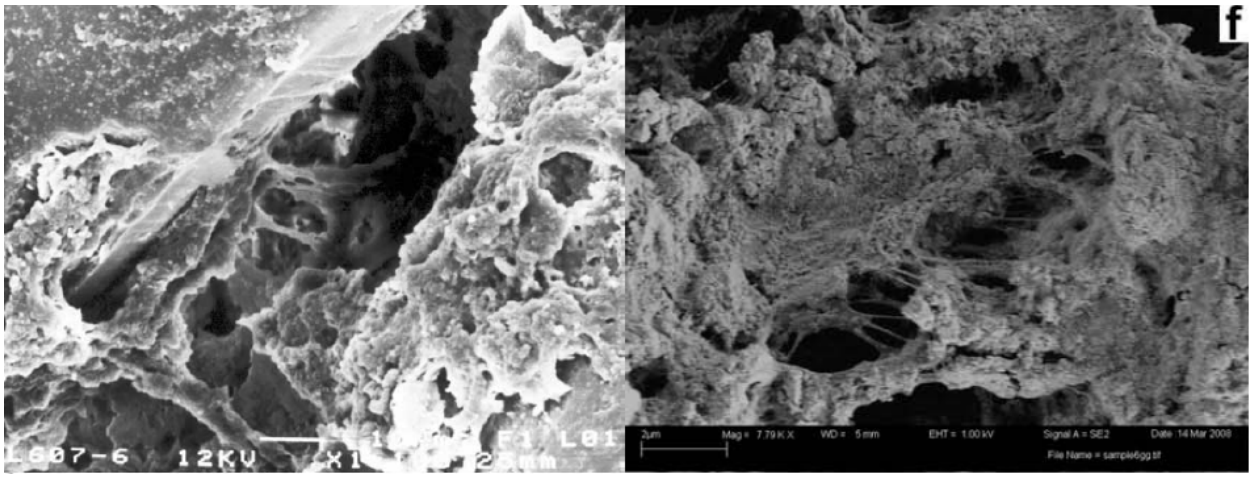

Figure 2.2: SEM images of SBR-modified mortars from Vincke & Wanseele (2002) left and from Yang & Shi (2009) right

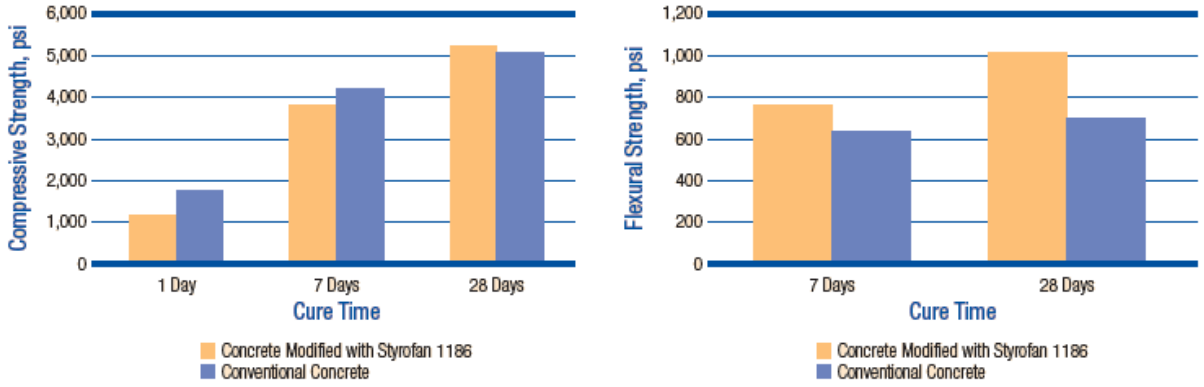

Figure 2.3: Average compressive and flexural strengths for latex-modified concrete from BASF (2011)

Latex also improves bonding to substrate when used as an overlay by providing a stronger adhesion by the polymer links described above. Latex serves as a mild air-entraining admixture as well and typically results in 4±1% entrained air that, along with the stronger polymer bonds, provides durability against salt scaling, and freezing and thawing cycles. For this reason, mixtures containing latex will be subjected to freezing and thawing cycles without any additional air-entraining agents.

2.3.4 Alkali-Activated Fly Ash

2.3.4.1 Introduction

With sustainability as one of the hottest words these days, the need for an innovative and waste incorporating concrete mixture has been the topic of much interest in the research community. The use of fly ash, slag, and silica fume has been used for decades to reduce the amounts of cement used and to benefit from the pozzolanic or hydraulic reactions from these supplementary cementitious materials (SCMs) (PCA, 2010). Research done in the 1930s and

1940s looked at the cementitious properties of clinkerless cements. These cement blends consisted of either slag or fly ash activated by alkaline solutions. The most common activators used are potassium hydroxide, sodium hydroxide, or "waterglass," a sodium silicate solution. These cements aim to be a competitor and alternative to portland cements that positively impacts the environment.

2.3.4.2 Chemical Composition

The chemical composition of most of the alkali-activated cements varies widely with the type of SCM and the origin of each material. The most common materials used for these cements include slag, class F fly ash (low calcium ash), and class C fly ash (high calcium ash). Class F ash is pozzolanic in nature, slag is hydraulic, and class C ash is generally somewhere in between the two. Typical chemical analysis for these materials is shown in Table 2.4. The American Society for Testing and Materials (ASTM) standard C618 specifies the criteria for fly ash and natural pozzolans and requires the sum of SiO_2, Al_2O_3, and Fe_2O_3 to be a minimum of 70% for class F ash and 50% for class C ash (ASTM C 618, 2011).

Table 2.4: Chemical analysis and typical fineness for selected SCMs from PCA (2010)

Composition, %	Class F fly ash	Class C fly ash	Ground slag
SiO_2	52	35	35
Al_2O_3	23	18	12
Fe_2O_3	11	6	1
CaO	5	21	40
SO_3	0.8	4.1	9.0
Na_2O	1.0	5.8	0.3
K_2O	2.0	0.7	0.4
Total Na eq. alk	2.2	6.3	0.6
LOI	2.8	0.5	1.0
Blaine fineness, m^2/kg	420	420	400

The alkali activators used for these materials include sodium silicate solutions (Na_2SiO_3), sodium hydroxide (NaOH), or potassium hydroxide (KOH). These solutions are usually 8–12M and very caustic in nature and thus require delicate use to prevent any harm to the users or the environment (Komljenovic, 2010). The chemical composition of the materials used should be determined to better select the type of solution and molarity that leads to the best quality product.

2.3.4.3 Hydration

As Table 2.4 indicates, the main components of the waste materials used for alkali-activated concrete are Al_2O_3, SiO_2, and CaO. The amount of reactive CaO (not all the calcium from the waste materials will react) in the mixture affects the type of hydration products that will precipitate in solution. The high quantities of calcium in class C ash and slag tend to create C-(A)-S-H gel much like the C-S-H in OPC concrete and can be analyzed using similar techniques (Juenger, 2011). The hydration between low calcium ash and the alkali-activator forms an amorphous alumino-silcate gel, N-A-S-H, and full analysis of the hydration is yet to be performed.

High molar solutions of either NaOH or KOH are typically used to dissolve the aluminosilicates into solution (Fernandez-Jimenez, 2005). As mentioned above, the nature of the materials used will determine the primary gel formed during precipitation, including the Ca/Si ratio and alumina content within that gel, but a mixture of both types of gels is not uncommon, especially with high calcium ash. After precipitation of the gel, the moisture content and any heat will drive the products to form a more thermodynamically stable, dense, and crystalline form. A simplified hydration schematic is shown in Figure 2.4.

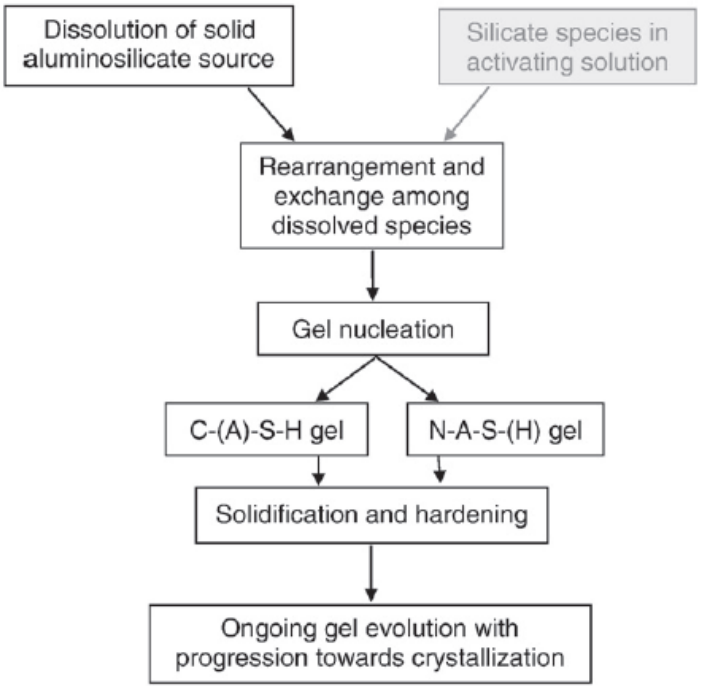

Figure 2.4: Alkali activation process schematic from Juenger (2011)

Although heat curing will increase the strength and maturity of the concrete, it is not necessary and high early strengths can be achieved through the proper dose and chemistry of the activator. Careful analysis of the raw material composition should be done in order to dial in the activator quantities to achieve high strengths at room temperature. With proper chemical analyses of the cementitious materials of these waste products, both strength and durability comparable to that of good quality portland cement concrete can be achieved (Shi & Fernandez-Jimenez, 2011).

2.3.4.4 Benefits of Using Alkali-Activated Fly Ash

The main benefit of using alkali-activated cement is primarily the positive environmental impact through the use of waste materials, which reduce the need for portland cement and CO_2 emissions. Similar strengths to portland cement can be achieved through the use of high molar alkaline solutions and heat curing. Depending on the chemical makeup of the fly ash and the alkali-activator, the following properties for alkali-activated concrete can be obtained:

- reduced setting time

- accelerated strength gain
- higher flexural strength than OPC concrete in some cases
- high heat resistance due to the lack of free $Ca(OH)_2$
- high acid and sulfate resistance
- lower water and chloride permeability in moist conditions

All of these benefits make alkali-activated concrete a promising and probable replacement for OPC at some point in the future, but some durability issues have been noted.

- It has been shown that carbonation in alkali-activated concrete can occur much faster than in portland cement concrete, which allows for corrosion of the steel.
- The use of reactive aggregate also makes alkali-activated fly ash concrete more susceptible to ASR.
- Admixtures such as superplasticizers, water reducers, and air entrainers are usually ineffective as they tend to disintegrate in the highly alkaline environment (Shi & Roy, 2005)

These durability issues, along with unclear hydration kinetics, curing regime, caustic activating solutions, and the variation in composition of the waste material of alkali-activated concrete, make alkali-activated concrete difficult to use as a replacement for OPC concrete. Nevertheless, the positive impacts that alkali-activated systems can have on the environment should encourage further research to establish a set of guidelines for its use as an alternative to portland cement.

2.3.5 Accelerated Portland Cement Mixtures

2.3.5.1 Introduction

Accelerated portland cement concrete has been used for years to obtain high-strength concrete within a few hours after placement to repair deteriorated pavements. These high early-strength concrete mixtures are not rapid-setting but are nonetheless more expensive than new pavement concrete because of the addition of chemical admixtures, higher cement content per cubic yard, and the equipment used for placement (Macadam & Folwer, 1984). With the incorporation of curing blankets and the use of heated material, these concrete mixtures result in 3000 psi compressive strength and 350 psi flexural strength in as little as 6 hours. These concrete mixtures are sometimes referred to as "fast-track" or "Class K concrete" and typically require a minimum of seven sacks of cement per cubic yard, air entrainment, large doses of non-chloride accelerator, and low w/c with the aid of polycarboxylate superplasticizers (Temple & Ballou, 1984).

2.3.5.2 Chemical Composition

For accelerated portland cement concrete, ASTM Type III cement is used to achieve the high early strengths needed for a "fast-track mix." Type III is a portland cement containing the

same composition as any portland cement, including C_3S, C_2S, C_3A, C_4AF, and gypsum. Typical composition percentages for Type III cements are shown in Table 2.5.

Table 2.5: Typical Type III cement composition

Portland Cement Composition					
	C_3S	C_2S	C_3A	C_4AF	C$
ASTM TYPE III	60	12	12-15	8	3.9

Type III portland cement contains about 12 to 15% C_3A, which has one of the highest reaction rates of any phase in portland cement. This hydration is slowed down by the addition of gypsum during the grinding process; otherwise C_3A can cause flash setting of the concrete. The cement is also ground much finer than any of the other ASTM Type cements (generally around 5480 cm^2/g Blaine fineness) to promote a higher reactivity and heat generation that will then produce higher early strengths in concrete (ASTM C 150, 2012). The higher heats of hydration and early strength gain make it a preferred material for prestressed concrete (Chen, 2009).

Alite, or C_3S, comprises roughly 60% of the total hydration reactants of Type III cement and is the main early-strength component in OPC. This phase hydrates quickly and provides the initial and final sets of the concrete (Chen, 2009). During hydration this phase creates more calcium hydroxide than C_2S, which does not add to the strength of the concrete but this fact is usually overlooked in a construction project focused on speed.

C_2S is present in the portland cement at around 12% and has a slower reaction rate than C_3S. This phase contributes mainly in the long-term strength gain. It requires less energy to create in the production process but the need for early strength favors the production of alite.

C_4AF is a minor phase in OPC that comes from the flux agent added during the production process to reduce the temperature needed to melt the raw materials (Chen, 2009).

2.3.5.3 Hydration

The hydration of portland cement has been known for decades and will not be described in full depth in this literature review. C_2S and C_3S hydrate according to Equations 2.8 and 2.9 to form calcium silicate hydrates referred to here as *C-S-H*.

$$2C_3S + 11H \rightarrow C_3S_2H_8 + 3CH \quad (2.8)$$

$$2C_2S + 9H \rightarrow C_3S_2H_8 + CH \quad (2.9)$$

C-S-H is the main load bearing component in concrete and is what gives portland cement concrete its strength. Calcium hydroxide (CH) is also a main product in OPC concrete but does not add to the strength of the concrete and is readily attacked by acids and sulfates. SCMs have been used for years to reduce the amount of CH in the matrix by having it react with the available silica in these SCMs, thereby reducing the permeability of the concrete through additional C-S-H. C_3A reacts with water to form calcium aluminate hydrates such as C_2AH_8 and hydrogarnet (C_3AH_6), as shown in Equations 2.10 and 2.11.

$$2C_3A + 27H \rightarrow C_4AH_{19} + C_2AH_8 \quad (2.10)$$

$$C_4AH_{19} + C_2AH_8 \rightarrow 2C_3AH_6 \quad (2.11)$$

In the presence of gypsum (CH_2$) (as in OPC), C_3A forms AFm and AFt phases as shown in the reactions presented in Equations 2.12 through 2.14. First it reacts with gypsum to form ettringite ($C_6A\$_3H_{32}$); when gypsum is then consumed, additional C_3A reacts with ettringite to form monosulfate ($C_4A\$H_{12}$). This phase is readily attacked by sulfates in the environment, causing such problems as delayed ettringite formation, external sulfate attack, and even thaumasite. For this reason Type III is not used in high sulfate environments and the ACI code limits the C_3A content for cements used in those types of environments (ACI 318, 2011).

$$C_3A + 3C\$H_2 + 26H \rightarrow C_6A\$_3H_{32} \quad (2.12)$$
C_3A in the presence of gypsum

$$C_3A\$_3H_{32} + 2C_3A + 4H \rightarrow 3C_4A\$H_{12} \quad (2.13)$$
C_3A reaction when gypsum is consumed

$$C_4A\$H_{12} + xC_3A + xCH + 12H \rightarrow C_4A\$_xH_{12+x} \quad (2.14)$$
C_3A when ettringite is consumed

C_4AF phases in OPC follow similar reactions to C_3A, first forming AFt phases with gypsum, then AFm phases when gypsum is consumed. This is a minor phase in concrete and hydrates quickly but not as fast as C_3A hydration.

2.3.5.4 Benefits of Using Accelerated Portland Cement Concrete

The main benefit of using an accelerated portland cement concrete mixture is the familiarity the contractors and DOT departments have with this particular cement. This is not a rapid-setting formulation so flash setting is not a problem. These mixtures usually require high doses of accelerators and superplasticizers, the use of heated material, and insulated curing blankets.

The first accelerators used with portland cement were chloride based but issues with corrosion led to the banning of such products in structural elements. For this reason, non-chloride accelerators such as calcium nitrate or calcium nitrite have been developed. For these high early-strength concrete mixtures, the highest dosage of accelerators is usually used to obtain the strengths needed. Most of these accelerators are in liquid suspensions and thus caution should be used when calculating the total water in the mixture by subtracting the amount of accelerator from the mixing water. If powder-based accelerators are used, their proper dosage weight is added to the total mixing water and stirred.

The maturity of portland cement concrete is well established; we know that curing at higher temperatures generally leads to faster strength gain. In the field, higher temperatures are reached by the use of heated materials and by trapping the heat of hydration within the concrete matrix through the use of insulated blankets (Kurtz, Balaguru, Consolazio, & Maher, 1997). Records have shown that by using Type III portland cement strengths of 3000 psi have been attained within six to nine hours of placement. The higher cement contents and low w/c

(typically at or above 700 lbs per cubic yard and 0.35 respectively) result in a less permeable material but make it more susceptible to drying shrinkage, ASR, and sulfate attack because of the higher C_3A content, and alkalis in the bulk concrete. Testing for these forms of attack will be done for these mixes as well to determine how the durability of the concrete may be affected by these specific proportions. These mixtures are by no means inexpensive either—the use of accelerators and insulated blankets add an additional $1.00 per 1.67 m^2 of pavement and costs easily and quickly add up (Ghafoori & Tays, 2007).

2.3.6 Proprietary Blends

2.3.6.1 Introduction

Throughout the years companies have developed their own proprietary rapid-hardening mixtures for highway repair. The main use for these proprietary blends is for rapid repair of small sections of pavement; they are usually sold as individual bagged units typically around $0.5ft^3$. Specifications, site preparations, and mixing procedures are located on these products. For this research project, each individual proprietary blend was mixed according to the company's recommendations.

2.3.6.2 Chemical Composition

Several chemical compositions for rapid setting cements exist for the general public, including magnesium phosphate, gypsum-modified portland cements, alkali-activated blends, accelerated portland and silica fume cements, and even polymer-based "cements." Most of these proprietary blends obtain the necessary strength requirements with no complications but some are notorious for not providing the durability properties that pavements require and needing constant maintenance.

2.3.6.3 Hydration

Most of these proprietary cements are sold as "ready-to-use" and only require mixing with a prescribed amount of water. Polymer-based rapid repair blends are usually sold all together and only require mixing resins and hardeners along with aggregates. Most of the hydration of these cements occurs within the first hours and not much occurs after hardening of the concrete.

2.3.6.4 Benefits of Proprietary Blends

The use of these rapid-setting cements allows the fast patching of small areas and requires minimal lane closure times for complete repair. The necessary strength gain of these mixtures is reliable and repeatable for individual bags. The workability, flow, quick hydration, and ease of use of these prepackaged materials make them user friendly and many provide durable and long-lasting repairs.

Chapter 3. Materials

3.1 Introduction

A wide range of cement binders, admixtures, and aggregates were selected for this laboratory testing. Additional cements were added throughout the course of the project as the need arose. The following sections describe the materials used in the study.

3.2 Cements and Supplementary Cementitious Materials

3.2.1 Calcium Aluminate Cements

Two CACs were used in this study, denoted CAC-1 and CAC-2. CAC-1 is a pure CAC containing roughly 60% monocalcium aluminate as the main reactant. By far the most common CAC, it has one of the highest Fe_2O_3 contents of the CACs available; the high iron content provides its dark grey color. Fast setting times and high early strengths can be achieved through the use of lithium-based accelerators. CAC-2 is a blended product that contains CAC and fly ash dosed with proprietary additives to produce high early strengths, increased durability, and manageable setting times for specific projects. No additional admixtures are required for this "all-in-one blend." The chemical composition of these two materials is contained in Table 3.1, based on x-ray fluorescence (XRF) oxide analysis.

3.2.2 Calcium Sulfoaluminate Cements

Three different sources of CSAs were chosen for this study and denoted CSA-1, CSA-2, and CSA-3. CSA-1 is a readily available cement in the United States and is often used for TxDOT projects, while CSA-2 and CSA-3 contain proprietary admixtures and have been developed for specific areas requiring low permeability, long-term durability, and high frost resistance. The oxide analysis of these three products is provided in Table 3.1.

3.2.3 Portland Cement

A single Type III portland cement (as per ASTM C 150) was chosen for this study from a local central Texas source. Type III cements exhibit higher early strengths and heat of hydration compared to other types of portland cement. This cement is not considered fast-setting but with the use of admixtures, higher cement contents, and curing procedures can significantly reduce setting times. A minimum cement content of 700 pounds per cubic yard was used for preliminary testing and adjusted thereafter to achieve better results. Table 3.1 provides the oxide analysis.

3.2.4 Fly Ash

Two different fly ashes were used in the project: one is classified as a Class C fly ash (as per ASTM C 618) from Cason, Texas, and the other is a Class F fly ash from Rockdale, Texas. The Class C ash used contains high amounts of CaO and is highly reactive, often used for flash fill applications. Table 3.1 provides the chemical composition of the fly ash.

3.2.5 Condensed Silica Fume

Used primarily in Phase I to achieve high early strengths in portland cement mixtures, silica fume is nearly 90% amorphous SiO_2 and used as an SCM to reduce the amount of CH through the formation of C-S-H gel. A maximum 8% silica fume by replacement of cement was used for this study. Its properties are listed in Table 3.1.

Table 3.1: XRF oxide analysis for prepackaged materials

Oxides % wt	SiO_2	Al_2O_3	Fe_2O_3	CaO	MgO	SO_3	Na_2O	K_2O	SrO	Mn_2O_3	P_2O_5	TiO_2
CAC-1	4.62	39.71	13.94	37.54	0.64	0.23	0.03	0.14	0.02	0.4	0.11	1.75
CAC-2	13.384	32.507	12.593	43.721	2.127	1.027	0.558	0.219	0.178	0.163	0.403	1.734
CSA-1	14.22	15.58	0.98	49.84	1.46	14.73	0.16	0.47	0.16	0.07	0.11	0.57
CSA-2	14.4	15.01	0.92	49.54	1.34	14.18	0.327	0.55	N/A	N/A	N/A	N/A
CSA-3	14.71	14.8	0.84	48.79	1.26	15.85	0.295	0.54	N/A	N/A	N/A	N/A
Class F fly ash	52.07	23.07	3.96	11.65	2.06	0.48	0.403	0.74	N/A	N/A	N/A	N/A
Class C fly ash	30.78	17.44	5.89	29	6.47	3.83	2.19	0.34	0.47	0.05	0.86	1.37
Silica Fume	90	0.4	0.4	1.6	N/A	0.4	0.5	2.2	N/A	N/A	N/A	N/A
Type III	20.67	4.21	3.6	64.28	0.61	3.63	0.053	0.68	N/A	N/A	N/A	N/A

3.2.6 Prepackaged Products

3.2.6.1 P-AAFA

This binder system is an alkali-activated fly ash blend that comes pre-packaged and consists solely of fly ash, both class C and class F, and a specific dose of alkali activator. This product comes in a ready-to-use bag including 3/8 in. maximum size aggregate and fine graded sand, which is then mixed with a prescribed amount of water. This is a fast-setting mixture with initial set times of around 15 minutes at 73 °F; workability is greatly reduced after only 5 minutes of initial contact with water. Setting time can be delayed by a few minutes with proprietary packets that are added to the water before mixing. XRF analysis for this material as well as the other prepackaged materials is located in Table 3.2.

3.2.6.2 P-2

This proprietary blend is used for horizontal concrete repair for high early-strength. This is a non-gypsum blend containing silica fume with set times between 20–30 minutes at 73 °F for final set. The suppliers of the product state shrinkage compensation and resistance to freezing and thawing are achieved. This ready-to-use pre-packaged blend requires only a prescribed amount of water for use.

3.2.6.3 P-3

This proprietary blend is not rapid-setting but was included in the testing matrix. This polymer modified repair material also contains silica fume. It reaches approximately 2000 psi compressive strengths at 1 day, and provides freezing and thawing resistance according to the manufacturer's specifications. This ready-to-use pre-packaged blend requires only a prescribed amount of water for use.

3.2.6.4 P-4

This proprietary blend is sold as a rapid repair material, reaches high early strengths, and can be open to traffic in as little as 1 hour. This is product is a portland cement and silica fume blend mixed with proprietary admixtures to reach high early strengths. This ready-to-use pre-packaged blend requires only a prescribed amount of water for use.

Table 3.2: XRF oxide analysis for prepackaged materials

Oxides %wt	SiO_2	Al_2O_3	Fe_2O_3	CaO	MgO	SO_3	Na_2O	K_2O
P-AAFA	22.391	17.61	4.35	31.44	9.75	6.49	0.685	0.276
P-2	16.43	11.83	3.56	53.28	1.29	8.46	0.264	0.36
P-3	24.87	4.33	2.78	58.73	1.34	2.24	0.261	0.37
P-4	23.53	10.19	2.26	46.22	0.7	13.29	0.142	0.46

3.3 Admixtures and Additives

3.3.1 Water Reducer

A polycarboxylate high-range water reducer was used to increase the plasticity of these repair mixtures with low w/c. The water reducer is compatible with all the bulk cements used in the study; no admixtures were used for the pre-packaged proprietary blends. This water reducer meets ASTM C 494 Types A and F.

3.3.2 Accelerator

Two liquid accelerators were used in this study. A non-chloride-based accelerator was selected for the portland cement accelerated mixtures. This accelerator meets criteria for ASTM C 494 Types C and E. The maximum dose allowed was used for portland cement mixtures so the total water content was adjusted for these high doses.

A $LiSO_4$-based accelerator was used for the CAC in this study. Doses from 0.5 to 2.5% by cement weight were used to accelerate the mixture and attain the necessary 3-hour compressive strengths.

3.3.3 Retarder

Citric acid was used as a retarder for calcium aluminate and CSAs in doses that did not exceed 0.2% by mass of cement. At higher temperatures, these fast-setting cements can set up in a matter of minutes, so citric acid is used to delay the setting time by 20 minutes or more. This admixture was added as a powder to the mixing water.

3.3.4 Additives

A styrene-butadiene latex polymer was used for calcium aluminate and CSAs to increase bond strength and reduce permeability. Latex-modified concrete has been used for decades for bridge deck overlays to provide a durable repair. The latex-modifier is a suspension of 47.2% solids and 52.8% water by mass. The water in the modifier must be taken into account and reduced from the mixing water to attain the w/c desired.

3.3.5 Air Entrainment

Air-entraining admixtures were used for a subset of the mixtures that were tested for freezing and thawing as well as salt scaling durability properties. Incorporating air entrainers into concrete mixtures at the correct air content and proper air void spacing is the most effective way to provide the required resistance against these durability issues. The selected air-entraining admixture is an aqueous solution of organic materials that provides the necessary air content and spacing factor for scaling and freeze-thaw cycle resistance.

A second method known to increase freeze-thaw durability is to produce concrete with a sufficiently low w/c; a low w/c reduces the capillary porosity and size of pores, which in turn reduces the amount of freezable water that causes distress (Pigeon & Pleau, 1995). Some mixtures tested in Phase I and II contain very low w/c and may exhibit resistance through both mechanisms.

3.4 Aggregates

3.4.1 Coarse Aggregates

Two coarse aggregates were used for this study. Table 3.3 provides the mineralogy and physical properties of the coarse aggregates. A 3/8-in. dolomitic limestone rock (CA1) was used to replicate thin overlay and partial depth repair mixtures. For a subset of mixtures testing ASR, a non-reactive limestone aggregate (CA2) from San Antonio, Texas, was used.

3.4.2 Fine Aggregates

Two fine aggregates were used for this study. Table 3.3 provides the mineralogy and physical properties of the fine aggregates. A siliceous natural river sand (FA1) from the Colorado River in Central Texas was used for the regular mixtures in the study. The second fine aggregate (FA2) tested was for ASR testing. This aggregate is a highly reactive sand from El Paso, Texas.

Table 3.3: Aggregate properties

Aggregates	Absoption	Specific Gravity	Minerology
CA1	0.6	2.8	Siliceous sand
CA2	3	2.57	Dolomitic Limestone
FA1	0.6	2.62	Limestone
FA2	0.69	2.6	Quartz/Chert/Feldspar

3.5 Analytical Procedures

The main laboratory testing for this project was separated into two phases. Phase I involved a screening test to determine the mixture proportions needed to attain a certain compressive strength, typically 3000 psi, at 3 hours or 400 psi flexural strength at 4 hours. Phase II of the study involved a more thorough characterization of the materials selected from Phase I. These test methods are described in this section.

The “all-in-one” bagged products that require only water to use are pre-blended with coarse and fine aggregate, cement, and any admixtures. In order to run analysis on the binders, these materials were subjected to a sieve analysis to determine particle size distribution and approximate binder content. A sample of the binder fraction was used for the chemical analysis.

Most of the binders contain portions of crystalline and amorphous material and thus both x-ray diffraction (XRD) and XRF techniques were implemented to further characterize these materials. XRD techniques were used to qualitatively analyze the crystalline phases of the binders. A Siemens D500 diffractometer with a DacoMP controller was used for the XRD analysis of this project and is shown in Figure 3.1. X-ray beams are rotated from 5° to 70° 2θ with a 0.02° step size and 4-second dwell time for each sample. The incident beam comes from a copper source, and passes through the stationary sample and diffract back to the x-ray detector. Crystalline phases of the sample diffract at specific angles and are detected and recorded to determine the quantity of each phase. The use of an internal standard is commonly used for quantitative Rietveld analysis; zinc oxide was used for this study. The amorphous content of the

materials does not diffract beams, instead showing up as background “noise” as shown in Figure 3.2, but other techniques are available to further analyze the materials.

Figure 3.1: Siemens D500 diffractometer used for XRD

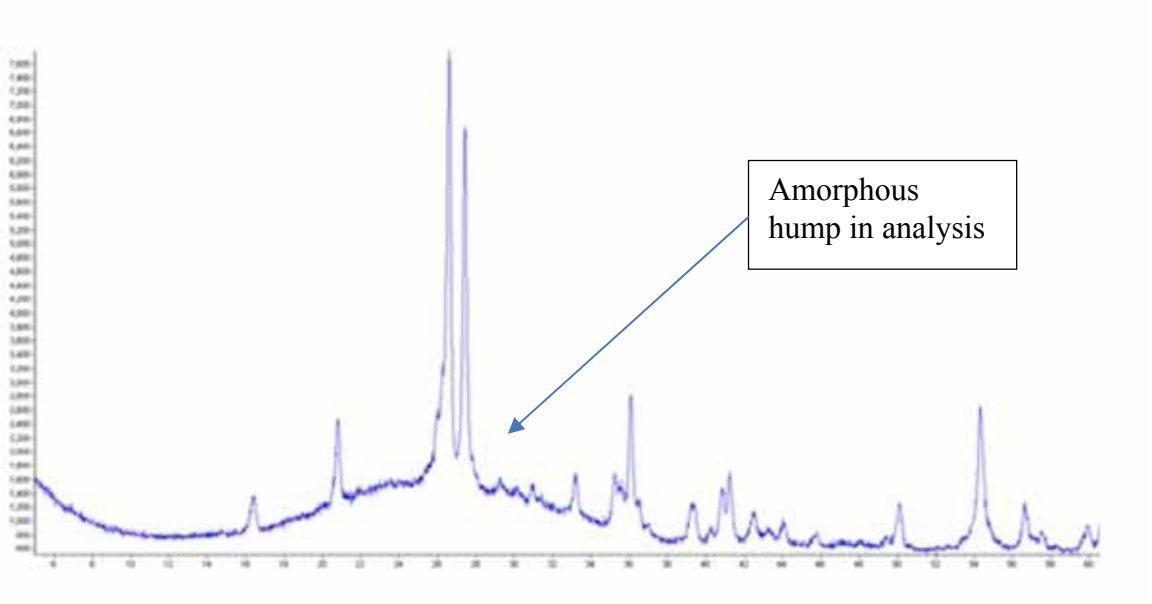

Figure 3.2: Example of amorphous hump in XRD sample

X-ray fluorescence was used to quantify the oxide composition of the materials chosen for the study. The samples were run using a Bruker S4 Explorer, shown in Figure 3.3, at the TxDOT laboratories at Cedar Park, Texas. X-rays are used to excite the innermost electrons of the atoms in a sample, creating vacancies in those electron shells. As these vacancies are filled by electrons in outer shells, light is emitted and detected by the equipment. Since each element emits distinct light waves, the detection and quantification of oxide compositions in the sample can be determined. An example of an XRF spectrum is shown in Figure 3.4.

Figure 3.3: Bruker S4 Explorer used for XRF analysis

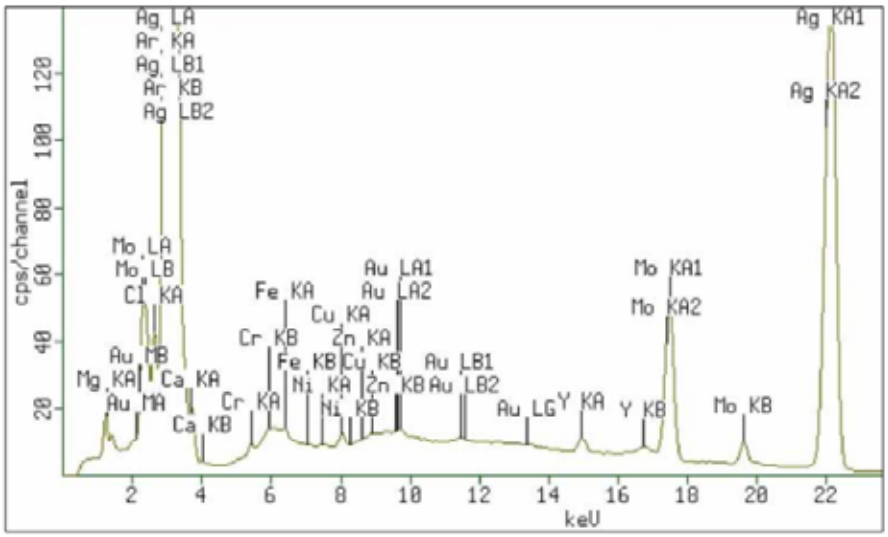

Figure 3.4: Sample of an XRF spectrum analysis

Isothermal calorimetry was used to characterize the heat of hydration of certain binder systems at constant temperature. These temperature-controlled chambers help characterize the behavior of the systems by eliminating the temperature variable. Typical laboratory calorimeters are not capable of accurately testing these high early-strength materials due to the high heats of hydration generated within the sample. For this reason the Grace AdiaCal TC calorimeter, a special calorimeter calibrated at The University of Texas at Austin to evaluate high heats of hydration, was used to test these samples. Samples are placed in individual cells and sensors within the chamber monitor the heat generation within the sample and compare it to a reference sensor that then diverts the energy away from the sample to achieve isothermal conditions (Bentivegna, 2012).

Chapter 4. Phase I Initial Screening Program

4.1 Introduction

A total of six cements and four proprietary mixtures were selected in the initial screening program and subjected to chemical analysis. The proprietary mixtures are available in a "ready-to-use" bag and require only the addition of water, while the other six products require the addition of aggregate, admixtures, and water. For these bulk cements, variations in cement content, w/c, admixture doses, and latex additives were determined to achieve a nominal target compressive strength of 3000 psi at 3 hours as the main criteria for acceptance into Phase II. Some of the parameters measured alongside compression strength included workability, flow, and approximate setting time.

4.2 Material Characterization

4.2.1 X-ray Fluorescence

All the cements selected for this initial screening program were characterized using XRF as described in Chapter 2 and reproduced in Tables 4.1 and 4.2. XRD will occur during Phase II of the project, which is currently ongoing.

4.2.2 Particle Size Distribution

For those pre-packaged all-in-one materials, a sieve analysis was conducted to characterize the particle size distribution and to obtain the binder proportion for XRF analysis. The sieve analyses for the proprietary blends are shown in Figures 4.1 through 4.4. The percentage of cementitious material for each mixture was determined to be around the same amount: 36.2% for P-AAFA, 31.5% for P-2, 32.0% for P-3, and 33.7% for P-4.

Table 4.1: Oxide analysis for bulk material

Oxides % wt	SiO_2	Al_2O_3	Fe_2O_3	CaO	MgO	SO_3	Na_2O	K_2O	SrO	Mn_2O_3	P_2O_5	TiO_2
CAC-1	4.62	39.71	13.94	37.54	0.64	0.23	0.03	0.14	0.02	0.4	0.11	1.75
CAC-2	13.384	32.507	12.593	43.721	2.127	1.027	0.558	0.219	0.178	0.163	0.403	1.734
CSA-1	14.22	15.58	0.98	49.84	1.46	14.73	0.16	0.47	0.16	0.07	0.11	0.57
CSA-2	14.4	15.01	0.92	49.54	1.34	14.18	0.327	0.55	N/A	N/A	N/A	N/A
CSA-3	14.71	14.8	0.84	48.79	1.26	15.85	0.295	0.54	N/A	N/A	N/A	N/A
Class F fly ash	52.07	23.07	3.96	11.65	2.06	0.48	0.403	0.74	N/A	N/A	N/A	N/A
Class C fly ash	30.78	17.44	5.89	29	6.47	3.83	2.19	0.34	0.47	0.05	0.86	1.37
Silica Fume	90	0.4	0.4	1.6	N/A	0.4	0.5	2.2	N/A	N/A	N/A	N/A
Type III	20.67	4.21	3.6	64.28	0.61	3.63	0.053	0.68	N/A	N/A	N/A	N/A

Table 4.2: Oxide analysis for pre-packaged material

Oxides %wt	SiO_2	Al_2O_3	Fe_2O_3	CaO	MgO	SO_3	Na_2O	K_2O
P-AAFA	22.391	17.61	4.35	31.44	9.75	6.49	0.685	0.276
P-2	16.43	11.83	3.56	53.28	1.29	8.46	0.264	0.36
P-3	24.87	4.33	2.78	58.73	1.34	2.24	0.261	0.37
P-4	23.53	10.19	2.26	46.22	0.7	13.29	0.142	0.46

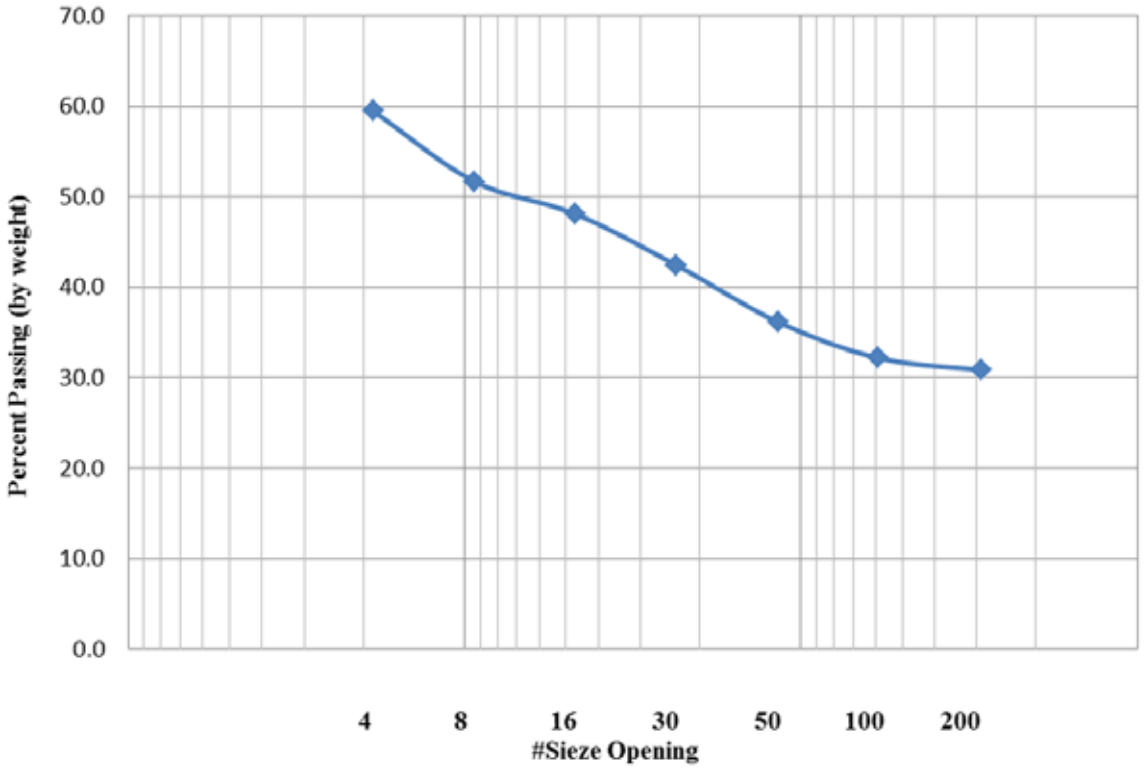

Figure 4.1: Sieve analysis for proprietary blend P-AAFA

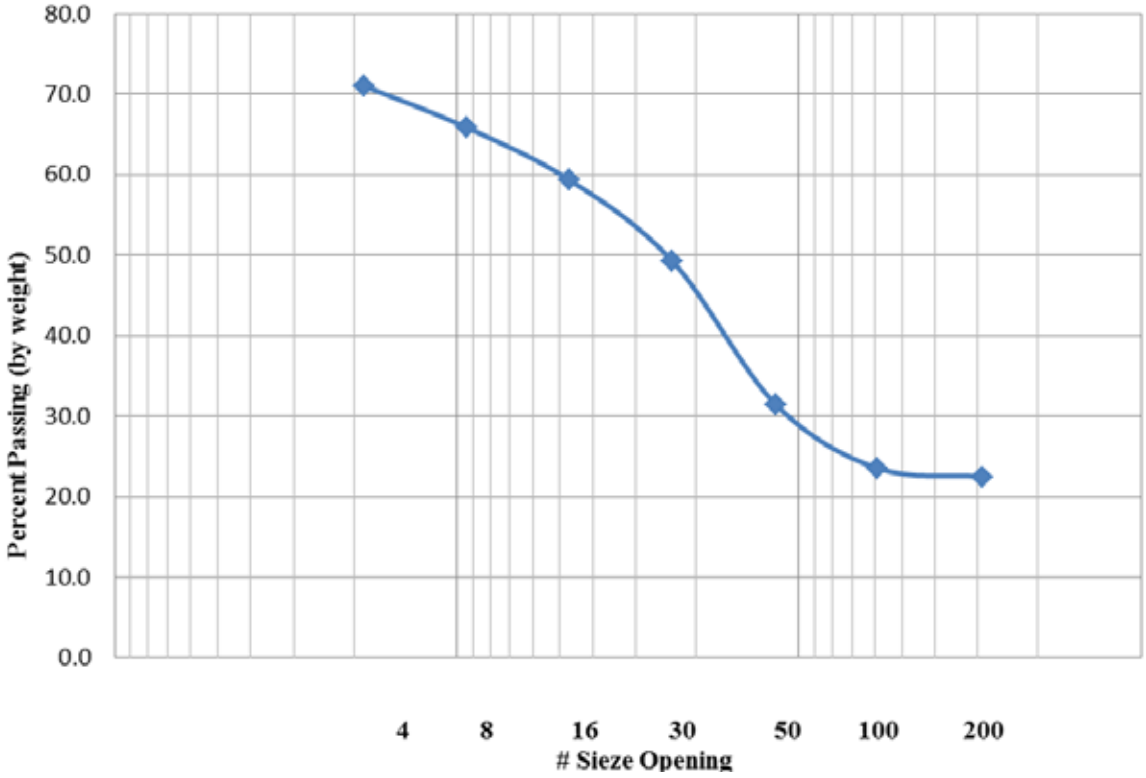

Figure 4.2: Sieve analysis for proprietary blend P-2

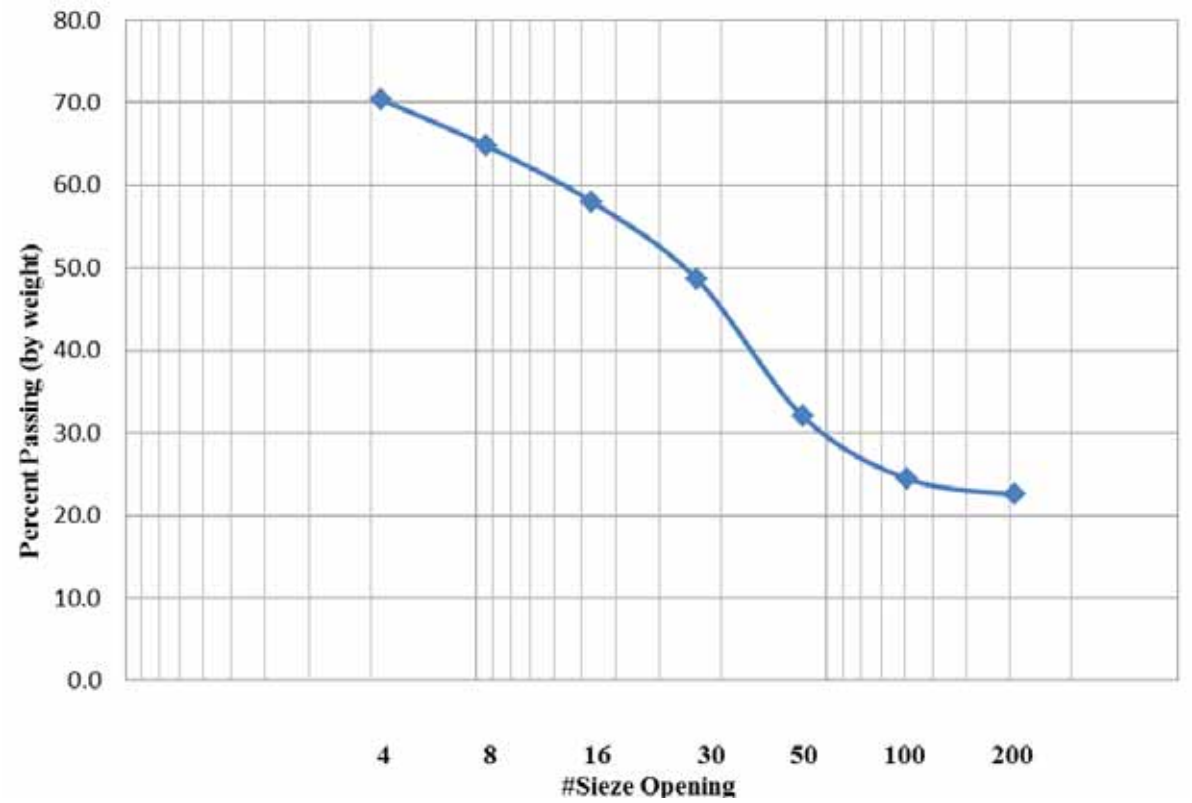

Figure 4.3: Sieve analysis for proprietary blend P-3

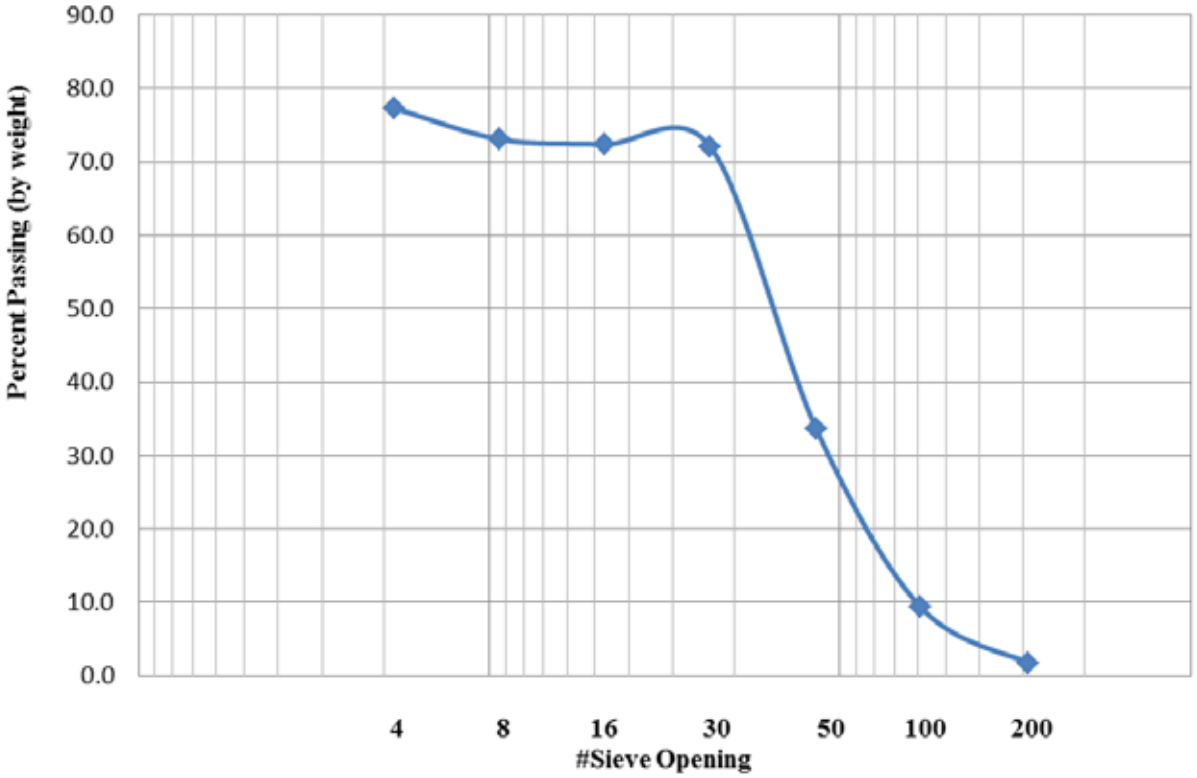

Figure 4.4: Sieve analysis for proprietary blend P-4

4.3 Acceptable Criteria for Repair Materials

Although the specific use for repair materials varies widely, the goal for this study is to create a set of guidelines for the proper placement and selection of durable materials for horizontal applications such as bridge decks and for partial to full depth repairs. Based on prior research, from the experience of TxDOT officials and project managers, this set of criteria for concrete mixtures was selected:

- target strengths, most commonly set to 3000 psi compressive at 3 hours or 400 psi flexural at 4 hours
- minimum required workability time for satisfactory placement
- robustness of the mixture to simulate field experiences
- 28-day design strength
- durability requirements

The initial screening program focused on the fresh properties, including admixture compatibility, flow, water demand, bleeding, and compression strength curves. For the subset of mixtures that met these initial criteria, a more extensive testing regime was developed to test for durability concerns. This ensured that resources were not wasted on mixture designs that are not practical for field application. Figure 4.5 shows the typical properties for any concrete mixture, which provide the basis for the research conducted in this study.

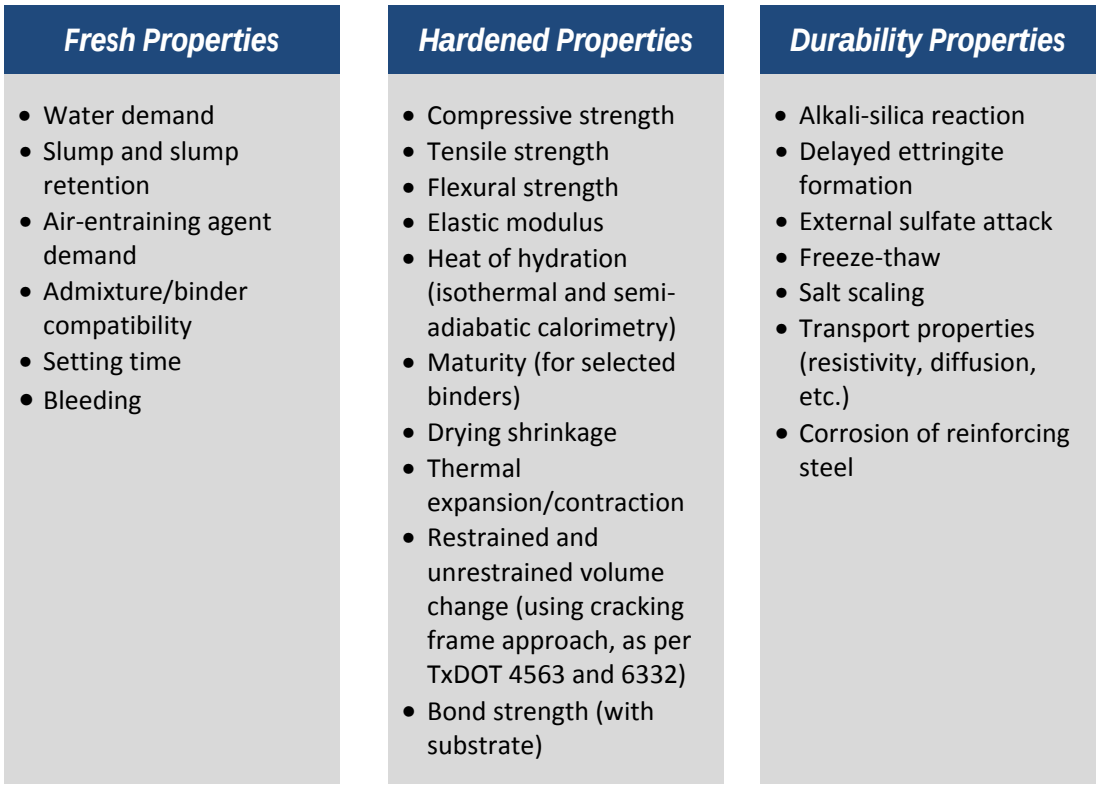

Figure 4.5: Fresh, hardened, and durability properties

4.4 Mixing Procedures

All mixtures in the initial screening program were mixed in a 1.77 cubic feet mixer from Northern Industrial, shown in Figure 4.6. Most of the mixtures followed similar guidelines and any differences are noted below.

Figure 4.6: Northern Industrial mixer used for Phase I

4.4.1 Prepackaged Proprietary Blends

For the all-in-one blends that only require the addition of water, the following mixing procedures were used:

- For P-AAFA the mixer was pre-wet and drained of excess water. A total of 2 ±1/8 quarts of water was needed for each bag. Once the mixer had started, half of the required water and the bagged unit was added and mixing continued for 1 minute. After 1 minute, the remaining water was added and mixed for an additional 5 to 6 minutes, and then the mixture was ready for placement into the specified area.
- For P-2 a total 4.6 pints of water per bag were required, all of which was added to the bagged mix while spinning. A total of 3 to 5 minutes was required for mixing.
- For P-3 all of the water was added to the mixer, 5.5 pints per bag. While the mixer was spinning, the contents of the bag were added and mixed for a maximum of 3 minutes. An additional 0.5 pint was optional if needed.
- For P-4 3.25 quarts of water were required per bag, all of which was added to the mixer prior to the addition of the materials. A total of 3 to 5 minutes was needed to attain the desired consistency and then cast.

4.4.2 Bulk Cement Mixtures

Materials for each mixture were gathered and the moisture content of the aggregates was determined at least 24 hours prior to mixing. The cement, aggregates, water (separated into two approximately equal amounts), and admixtures were weighed prior to mixing. If a latex modifier

was required, it was also added to the total water and mixed thoroughly. With the exception of the accelerated portland cement mixtures, all chemical admixtures were added to one of the water containers and set aside.

The mixer was pre-wetted and drained before the addition of any material. The required fine and coarse aggregate were then added to the mixer along with the mixing water not containing any admixtures and spun for 1 minute. After this initial mixing period, the cement was added to the mixer and continued to spin for 30 seconds, at which point the rest of the water containing admixtures was slowly added over a period of 30 seconds. The mixture was then allowed to mix for an additional 1–2 minutes depending on its consistency.

Portland cement mixtures differed slightly in the addition of admixtures due to the high doses required. The total amount of accelerator was added to the mixing water and mixed thoroughly. The aggregate was added to the mixer along with half of the admixture-water solution and mixed for 1 minute. The cement was then added to the mixer and allowed to mix for 30 seconds. After this, the rest of the water was added to the mixer over a period of 30 seconds and then allowed to mix for an additional minute. At this point the superplasticizer was added to the mixture and allowed to spin for 2 minutes. After that mixing time, the air entrainer was added straight to the cement and allowed to spin for a minimum of 1 minute. This mixture is not fast-setting so the longer mixing time does reduce the available working time of the mix. The casting and curing procedures are discussed in the next section.

4.5 Casting and Curing Procedures

The two types of samples cast in Phase I are shown in Figure 4.7. In order to not waste material for this initial testing, small 0.65 ft^3 size mixtures were cast. This size was enough to cast a set of 18 2-in. cubes and 18 3-in. x 6-in. cylinders to be tested at 2 hours, 3 hours, 4 hours, 5 hours, 6 hours, 12 hours, and 24 hours as well as 3 days, 7 days, and 28 days after mixing. Two cubes and two cylinders were tested at each time interval for compressive strength.

Cubes were cast in two layers and tamped using a nonabsorptive, nonabrasive, nonbrittle tamper per ASTM C 109 requirements in four rounds, as specified in ASTM C 109 and described in Figure 4.8 (ASTM C 109, 2012).

Figure 4.7: Cube and cylinder samples for Phase I mixtures

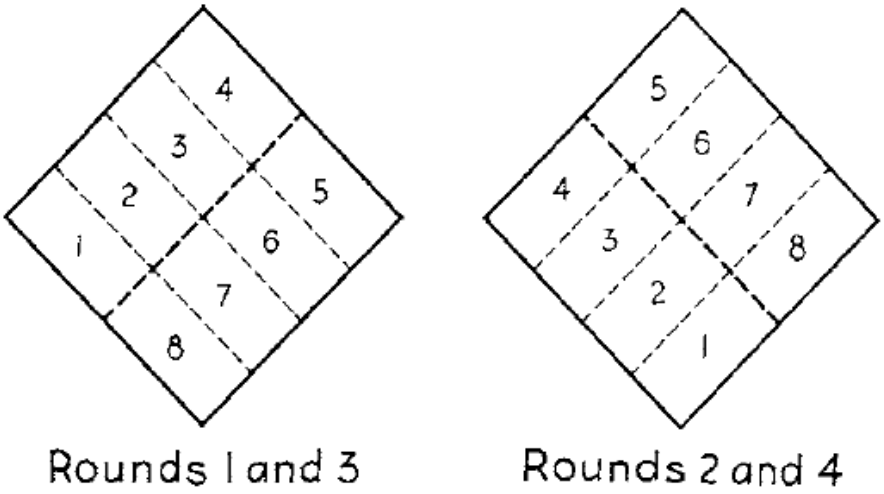

Figure 4.8: Order of tamping in molding of test specimens from ASTM C 109 (2012)

Cylinders were cast in a similar fashion in two layers, rodded 25 times each and struck on the sides to release any entrapped air. After both layers of concrete were rodded, any excess material was struck off with a wood trowel for both cylinders and cubes. Typically final finishing is done after any bleed water has evaporated, but in the case of these rapid-hardening mixtures, final finishing was conducted as soon as possible after finishing with the wood trowel to prevent premature setting with an unfinished surface.

Cubes and cylinders were cast simultaneously for the bulk cement mixtures to compare compressive strengths between the two specimens. The two specimens provided a good correlation, which allowed for less material waste, especially with the pre-bagged mixtures. This

allowed 2-in. cubes to be used as the sole compressive sample. A sample strength gain curve for one of the initial CSA-1 mixtures is shown in Figure 4.9 for cubes and cylinders.

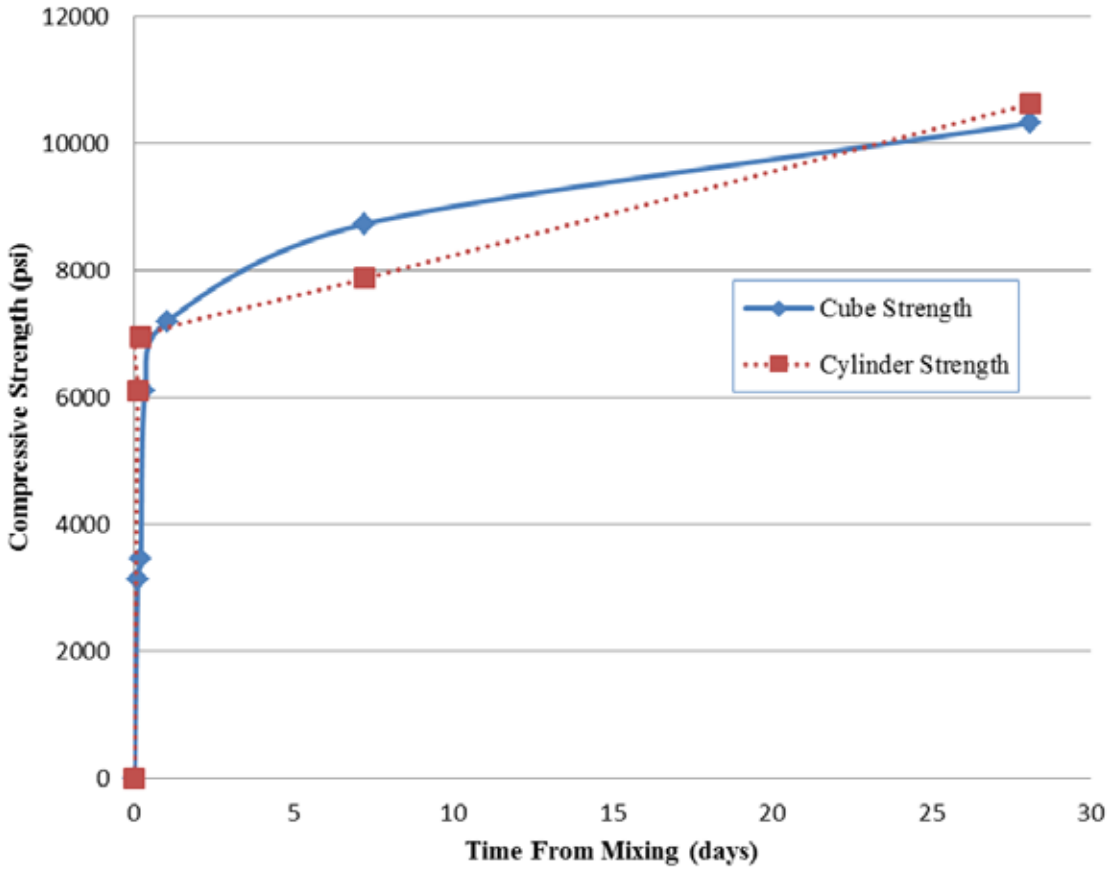

Figure 4.9: Graph showing correlation between cube and cylinder samples

Curing for all samples was done with wet burlap. The burlap was left in a bucket of water for approximately 24 hours prior to mixing to allow the burlap to become completely saturated. The high heat generation tends to evaporate the water on the surface of the sample, so constant rewetting was done for the first 3 to 4 hours until the sample reached 3000 psi compressive strength. Samples were left in a temperature-controlled room until 1 day after mixing and then stripped from the formwork and placed in a 73° F and 100% relative humidity chamber until the end of the testing period. Figure 4.10 shows a typical curing setup.

Figure 4.10: Curing set up for Phase I using damp burlap

4.6 Mix Matrix and Proportions

A series of mixtures involving the six binder systems in combination with admixtures and additives was developed for testing. The series included the following set:

1. Type III portland cement blended with silica fume, high dosages of non-chloride accelerator, and superplasticizers with very low w/c.
2. A straight calcium sulfoaluminate concrete mixture, referred to as *CSA-1*, with and without citric acid as a retarding admixture.
3. A calcium sulfoaluminate latex-modified concrete mixture. This mixture contained 15% latex modifier and is referred to as *CSA-LX*.
4. Two proprietary calcium sulfoaluminate concrete mixtures; these cements were extended using fine and coarse aggregate and citric acid as needed, and are referred to here as *CSA-2* and *CSA-3*.
5. A straight CAC mixture, referred to as *CAC-1*, modified with different $LiSO_4$ accelerator doses and citric acid retarder if needed.
6. A proprietary CAC blend with fly ash termed *CAC-F*; this blend did not require any additional admixtures, and was used as-is.
7. A calcium aluminate latex-modified concrete mixture, *CAC-LX*. Latex content was varied from 10 to 20% for preliminary screening test.
8. Four ready-to-use proprietary blends. These mixtures were mixed as-is with the recommended amount of water from the supplier.

Series 1–7 required modifications in cement content with a minimum of 658 pounds (7-sack) of cement per cubic yard. The w/c, admixture doses, and latex addition were also varied according to the type of concrete mixture. Table 4.3 shows the range of additive doses tested with each series. The four pre-packaged mixtures were unaltered and only water was added. A total of 85 small scale mixtures were cast but only 26 mixtures passed the initial strength requirements for early age strength. Table 4.3 lists those 26 mixtures along with the 3-hour and 28-day compressive strength.

Table 4.3: Mixtures passing Phase I along with admixture doses

Mixes Passing Screening Test	Cement Type/ Content	3 Hour Strength (psi)	28 Day Strength (psi)	w/c	ACC	HRWR % or by cwt	Citric Acid % by cwt	Latex % by cwt
	CSA-1	5070	10779	0.42	N/A	N/A	N/A	N/A
	CSA-1	3176	10318	0.40	N/A	N/A	N/A	N/A
	CSA-1	3171	11250*	0.40	N/A	N/A	0.25	N/A
	CSA-1	5556	11250*	0.40	N/A	0.25%	N/A	N/A
	CSA-1	5975	11250*	0.38	N/A	0.7	N/A	N/A
	CSA-LX	3854	7632	0.38	N/A	N/A	N/A	10
	CSA-LX	3913	8373	0.35	N/A	N/A	N/A	15
	CSA-LX	4219	7726	0.35	N/A	N/A	N/A	10
	CAC	3700	11250*	0.40	0.75	N/A	N/A	N/A
	CAC	4572	11250*	0.40	1	N/A	N/A	N/A
	CAC	3910	11250*	0.40	1.25	N/A	N/A	N/A
	CAC-1	4410	11250*	0.38	1	N/A	N/A	N/A
	CAC-1	3199	11250*	0.38	1	0.25%	N/A	N/A
	CAC-1	3278	11250*	0.38	1.25	0.50%	N/A	N/A
	CAC-1	4182	11250*	0.38	1.25	0.35%	N/A	N/A
	CAC-1	4290	11250*	0.38	2	N/A	0.1	N/A
	CAC-1	2993	9664	0.38	2	0.25%	0.1	N/A
	PC Type III	Not rapid-setting	11200	0.35	10oz / 100lbs cement	13oz / 100lbs cement	N/A	N/A
	CAC-2	3118	7840	0.4	N/A	N/A	N/A	N/A
	CSA-2	3859	6170	0.42	N/A	1oz /100lbs cement	0.2	N/A
	CSA-3	2880	8385	0.4	N/A	N/A	0.2	N/A
	CAC-LX (4 hr strength not 3hr)**	2970**	6280	0.35	2	N/A	N/A	10
	P- 4	3560	7180	N/A	N/A	N/A	N/A	N/A
	P-2	4555	10553	N/A	N/A	N/A	N/A	N/A
	P-1	3287	10536	N/A	N/A	N/A	N/A	N/A
	P -3	Not rapid-setting	10960	N/A	N/A	N/A	N/A	N/A

11250* Maximum peak load of cube compression machine

** 4 hour strength not 3 hour

With the help and input from TxDOT, a subset of these 26 mixtures was selected for a more exhaustive series of testing that focuses on the hardened and durability properties described in Section 4.3, and listed in Figure 4.5. The selected mixtures listed in Table 4.4 have passed into

Phase II. Complete mixture proportions along with strength gain curves for these mixes are included in Appendix A and Appendix B.

Table 4.4: Proportions for selected mixtures passing to Phase II

	Cement Type/ Content(lbs)	3 Hour Strength (psi)	28 Day Strength (psi)	w/c	ACC	HRWR % or by cwt	Citric Acid % by cwt	Latex % by cwt
Mixes Going on to Phase II	P-AAFA	3287	10536	N/A	N/A	N/A	N/A	N/A
	P-2	4555	10553	N/A	N/A	N/A	N/A	N/A
	P -3	Not rapid-setting	10960	N/A	N/A	N/A	N/A	N/A
	P- 4	3560	7180	N/A	N/A	N/A	N/A	N/A
	CSA-1 (700)	5070	10779	0.45	N/A	1.0oz / 100lbs cement	0.2	N/A
	CSA-LX (700)	3500	5800	0.38	N/A	N/A	0.2	15
	CSA-2 (658)	3860	6170	0.42	N/A	1.0oz / 100lbs cement	0.2	N/A
	CSA-3 (658)	2880	8385	0.40	N/A	N/A	0.2	N/A
	CAC-1 (700)	4182	6520	0.38	1.25	0.35%	N/A	N/A
	CAC-2 (752)	3118	7840	0.35	N/A	N/A	N/A	N/A
	CAC-LX (705)	2970**	6280	0.35	2	N/A	N/A	10
	Type III PC (658)	Not rapid-setting	11200	0.35	10oz / 100lbs cement	13oz / 100lbs cement	N/A	N/A

** 4 hour strength not 3 hour

Chapter 5. Engineering Properties

5.1 Introduction and Background

When examining engineering properties for rapid repair materials, one objective is to select repair materials with similar properties as the existing concrete. This will allow for the repair and base concrete to act homogenously which will extend the service life of the repair. The high early-age compressive strengths of rapid repair materials are one of the hallmarks of the technology, but these high early strengths often generate even higher long-term strengths and can cause appreciable mismatch with the base concrete pavement or deck.

Two of the more important engineering properties are the coefficient of thermal expansion (CTE) and modulus of elasticity (MOE). If a repair material has a high CTE, then the expansion and shrinkage of the material due to changes in temperature can cause cracking and break the bond between the base material and repair. The MOE relates to the stiffness of a material and issues can arise when repair materials have higher MOE. The higher the MOE, the more brittle a material becomes, which can lead to problems when transportation structures begin to deflect due to large loads. If the repair material has a higher MOE, then there is a possibility that it will not deflect with the member, which can lead to the bond breaking or spalling of the repair material.

Normally, when following the ASTM standards, these properties are determined at standard temperature 73 °F (23 °C). The team followed these standards but also wanted to simulate climates across Texas to determine how these materials responded to different mixing and curing temperatures. A temperature robustness study was implemented to determine the compressive strength of cylindrical specimens at two different temperatures: 50 °F (10 °C) and 100 °F (38 °C). The team can approximate other engineering properties from these compressive strength values, in order to understand the materials performance under different conditions.

TxDOT has different criteria for concrete repairs, located in their online database. The research team is using TxDOT's Departmental Materials Specification for concrete repair materials, specifically known as DMS-4655, as a guide for classifying the performance of the materials in our testing matrix. This document states minimum and maximum values for most of the engineering properties the team measured, using these criteria to categorize repair materials as non-rapid, rapid, and ultra-rapid repairs. The team selected the criteria for Type A-Rapid Repairs, which are specified for horizontal repairs up to 4 in. in depth.

5.2 Materials and Mixture Proportions

This chapter will include a variety of materials that are included in the 13 mixtures that passed Phase I. These mixtures include materials composed of CACs, CSAs, all fly ash blends, OPC, and proprietary binder blends. All mixtures and proportions, except for the CAC-3 mixture, are located in Table 5.1.

The CAC-3 mixture is composed of the following: a binder content of 752 lb/yd^3 including Type I OPC and a CAC-3 proprietary binder; a .40 w/cm (water-to-cementitious-materials ratio); a dolomitic limestone coarse aggregate (CA1) with a 3/8-in. (9.5 mm) max size aggregate; a siliceous natural river sand (FA1); a superplasticizer dosed at .85% of the amount of CAC-3 binder; and a retarder dosed at 0.35% of the amount of CAC-3 binder.

All of the concrete used to evaluate engineering properties, excluding the temperature robustness study, were obtained from the same batch in order to reduce any variability during mixing. A 2 ft^3 (.06 m^3) concrete mixture was needed to cast enough cylinders, prisms, unit weight, and slump for each mixture. These mixtures were cast in a 4 ft^3 (.11 m^3) steel drum concrete mixer, shown in Figure 5.1.

Figure 5.1: 4 ft^3 (.11 m^3) steel drum concrete mixer

Table 5.1: Fresh state properties for mechanical properties mixtures

Mix ID	Slump (inch)	Unit Weight (lb/ft3)	Air Content (%)
P-1	9	142.0	1.5
P-2	10.5	146.0	3.9
P-3	10	144.0	3.0
P-AAFA	8.5	150.6	3.0
CSA-1	4	147.2	2.8
CSA-2	9	137.6	10.0
CSA-3	11	144.8	3.4
CSA-Latex	9	142.4	6.5
CAC-1	9.5	138.5	8.0
CAC-2	10	143.7	7.5
CAC-3	6.5	148.0	5.0
CAC-Latex	10	144.4	4.5
PC Type III	0.5	153.6	5.0

Note: Measured from the 2 ft^3 (.06 m^3) concrete mix mentioned previously.

The research team followed these standards for slump, unit weight, and air content, respectively:

- ASTM C 143 (2012)
- ASTM C 138 (2013)
- ASTM C 231 (2010)

5.3 Mechanical Properties at Standard Temperature

Table 5.2 provides the information on the mixtures cast at standard temperature, which is considered 73 °F (23 °C). The compressive strength was measured at 3 hours because TxDOT wants to allow traffic onto the repaired section as soon as possible. Two of the mixtures, CAC-1 and CAC-Latex, have two values under the 3-hour compressive strengths designation. The second value, 4-hour compressive strength, was presented due to the lower compressive strength at 3 hours. The other properties are all measured following their respective standards at 28 days after casting.

Table 5.2: Mechanical properties for all mixtures

Mix ID	3 Hour Compressive Strength (psi)	28 Day Compressive Strength (psi)	Flexural Strength (psi)	Modulus of Elasticity (ksi)	Tensile Strength (psi)
P-1	3560	7190	560	4410	520
P-2	4720	10540	1530	5140	790
P-3	--	8220	1410	5510	720
P-AAFA	3040	8910	870	5000	670
CSA-1	5040	8440	770	5290	620
CSA-2	4000	6170	700	4650	550
CSA-3	4680	7900	870	5850	660
CSA-Latex	3500	5800	790	4500	490
CAC-1	570 (4210)	6520	1190	6140	580
CAC-2	3080	7860	880	5900	690
CAC-3	3010	6760	1110	5410	640
CAC-Latex	480 (2970)	6280	1190	4680	600
PC Type III	--	11740	1230	7670	870

5.3.1 Compressive Strength

Compressive strength is an important property to report for repair materials because the repair must be as strong, if not stronger than, the existing material to carry the designated load. Since the research team is focusing on repairs for bridge decks, there is not a need for high compressive strengths in the repair material because typical strengths for the concrete in bridge decks at 28 days are in the 4000 to 6000 psi (27.6 to 41.4 MPa) range (NCHRP, 2004). The focus of these repairs is on rapid strength gain to reduce the amount of time needed to block traffic.

5.3.1.1 Experimental Procedures

For this section, the research team followed ASTM C 39, *Standard Test for Compressive Strength of Cylindrical Concrete Specimen*. Compressive strength values were measured at 2 hours, 3 hours, 4 hours, 6 hours, 12 hours, 1 day, 3 days, and 28 days after mixing. This provided a strength gain curve for each of the materials. The team also followed ASTM C 1231 when unbonded neoprene end caps were used on the cylinders during testing (2013).

Due to the rapid setting time, the team decided to reduce the mixture size by casting 3-in. x 6-in. (76.2 mm x 152.4 mm) cylindrical specimens for determining compressive strength. Previous research states that below a compressive strength of 7250 psi (50 MPa) there is a statistical equivalence between 6-in. x 12-in. (152.4 mm x 304.8 mm) cylinders and 3-in. x 6-in. (76.2 mm x 152.4 mm) cylinders (Day & Haque, 1993). As previously mentioned, typical bridge decks do not require high compressive strengths; therefore, when the 3-in. x 6-in. (76.2 mm x 152.4 mm) and 6-in. x 12-in. (152.4 mm x 304.8 mm) cylinders can have discrepancies beyond 7250 psi (50 MPa), there is adequate strength for these applications.

5.3.1.2 Results and Discussion

The results of compressive strength tests for 12 of the mixtures were previously discussed in Chapter 5; the strength curve for mixture CAC-3, which was added into the initial Phase I mixtures, is shown in Figure 5.2 out to an age of 28 days.

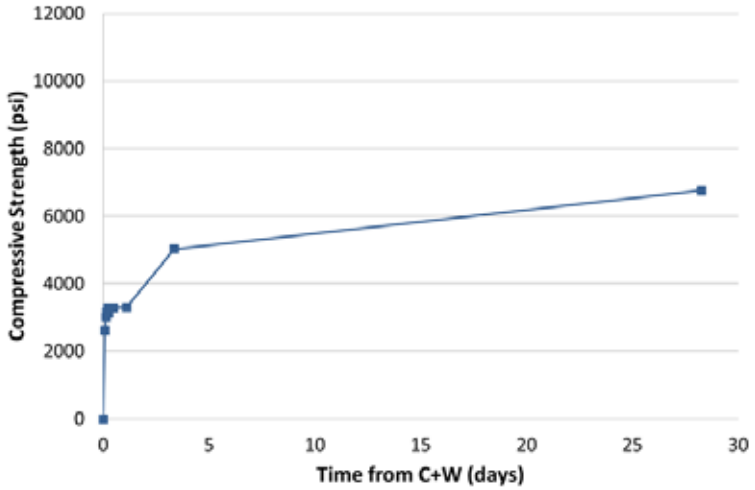

Figure 5.2: Compressive strength for CAC-3 mixture

Referring back to Table 5.2, it is evident that the P-3 and PC Type III mixtures have a slower strength gain compared to the other mixtures because there is a negligible compressive strength at 3 hours. This is due to the composition of these mixtures. Both P-3 and PC Type III are mainly composed of portland cement, which does not gain strength as quickly as the other binder systems. CAC-1 and CAC-Latex mixtures also gained strength slower than most of the other rapid repair mixtures; however, the 4-hour compressive strength of each mixture was 4210 and 2970 psi (29 and 20.5 MPa), respectively. These CAC mixtures were slightly "sluggish" at 3 hours after mixing, but once calcium aluminate mixtures start to hydrate, the strength gain is very rapid.

The 28-day compressive strengths range from 5800 to 11742 psi (40 to 81 MPa). Ironically, the PC Type III mixture had the slowest strength gain, as well as the highest 28-day compressive strength. This mixture contained a very high cement content, accelerator, and low w/cm, thus contributing to a high compressive strength. It can be seen that the CSA mixtures have rapid strength gain but their 28-day strength is weaker than the rest as a whole. Overall, the P-2 mixture performed the best for both early (3 hour) and later (28 day) compressive strengths.

5.3.2 Flexural Strength

The flexural strength, also known as modulus of rupture, is the bending strength of unreinforced concrete beams. This bending strength is important for repairs that are larger in size on roadways and bridge decks because the force from the swelling of soils or heavy traffic loads can cause flexure in either direction. TxDOT has a current minimum specification of 620 psi (4.3 MPa) for the 28-day modulus of rupture of concrete pavements.

The 28-day flexural strength of normal-weight portland cement concrete can be approximated as 10–15% of the 28-day compressive strength according to the ACI 318 Building Code (2011). The flexural strength of rapid repair materials, which generally have higher compressive strengths, is typically higher than normal-weight portland cement concrete.

5.3.3.1 Experimental Procedures

The flexural strength of each mixture was measured following ASTM C 78, *Standard Test Method for Flexural Strength of Concrete*. The test specimens were wet-cured for 28 days before testing began. The flexural strength for this test is calculated using the simple beam third-point loading, which ensures a constant bending moment without any shear force being applied in the middle third section (Mamlouk & Zaniewski, 2006).

5.3.3.2 Results and Discussion

The results from Table 5.2 range from 562 psi (3.9 MPa) for the P-1 mixture to 1531 psi (10.6 MPa) for the P-2 mixture. All of the mixtures, except for P-1, passed the minimum criteria for 28-day flexural strength in concrete pavements. When examining each binder system as a group, their flexural strengths were very similar.

The mixtures containing mostly portland cement have high modulus of rupture, while the CSA binders portrayed significantly lower flexural strengths. The tensile strength for the CSA mixtures averaged 11% of their respective compressive strengths, while the CAC mixtures averaged above the range suggested by the ACI Building Code at 16% of their respective compressive strengths. All of the calcium aluminate mixtures, except for the CAC-2 mixture, have relatively high flexural strengths.

5.3.3 Modulus of Elasticity

The MOE of concrete is an important property in the design of concrete structures and is commonly referred to as the stiffness of the desired material. Mamlouk and Zaniewski define the MOE or Young's modulus (E) as the proportional constant between normal stress and normal strain of a homogenous and linear elastic axially loaded member (2006). Concrete is not a homogenous material but composed of aggregate and cement paste, thus negating the use of the classic relationship of Young's modulus.

One objective when making a decision on a certain repair material is to try to match the MOE to the existing concrete. If the repair has a significantly higher or lower modulus, there could compatibility issues with the existing structure. It is evident that the MOE for concrete repairs is an area of concern for TxDOT because of the specified maximum modulus value in their Departmental Materials Specification (TxDOT, 2011). The maximum MOE value is 5000 ksi (34.5 GPa) for rapid repair materials. While the ACI 318 Building Code suggests that the MOE for normal-weight can be assumed to be $Wc^{1.5}$*33*sqrt(*f'c*), for this equation, the *Wc* value refers to the unit weight of the concrete in lb/ft^3 and the *f'c* is the compressive strength value in psi (2011). The modulus value of concrete is highly dependent on the coarse aggregate in the mixture, such that siliceous aggregates tend to significantly increase MOE values compared to limestone aggregates.

5.3.3.1 Experimental Procedures

The research team followed ASTM C 469, *Standard Test Method for Static Modulus of Elasticity and Poisson's Ratio of Concrete in Compression* (2010). This standard measures the chord modulus of the concrete specimen in the working stress range of 0 to 40% of the ultimate concrete strength. Neoprene pads were used following the unbonded end caps standard mentioned previously in the compressive strength section. Figure 5.3 shows the setup used to determine the modulus.

Figure 5.3: MOE setup

5.3.3.2 Results and Discussion

Because the MOE is typically related to compressive strength, the mixtures researched portrayed relatively higher modulus values due to their higher compressive strengths. In the previous chapter, Table 4.4 showed that only 7 of the 13 mixtures passed TxDOT's criteria. Of

the four proprietary mixtures, which are composed of different aggregates, only two were below the 5000 ksi (34.5 GPa) specified modulus. The non-proprietary mixtures were composed of dolomitic limestone for coarse aggregate and siliceous river gravel for fine aggregate. The P-1 mixture presented the lowest modulus value at 4410 ksi (30.4 GPa), while the PC Type III mixture had the highest at 7670 ksi (52.9 GPa). When the ACI 318 equation was used to approximate the MOE from the compressive strength, the approximation underestimated the modulus measured. Thus, this equation should not be used to approximate the MOE of rapid repair materials because it was 5% lower than the measured modulus.

5.3.4 Splitting Tensile Strength

The splitting tensile strength of concrete is another important property of concrete repair materials. Again, TxDOT has a designated minimum splitting tensile strength of 400 psi (2.8 MPa) for rapid repair materials following a 28-day curing period (TxDOT, 2011). According to Neville, splitting (indirect) tensile strength values for portland cement concrete vary from 2.5 MPa to 3.1 MPa (360 psi to 450 psi) (1981). This splitting tensile strength is typically lower than the direct tensile strength of the specimen, which is about 10% of the specimen's compressive strength.

5.3.4.1 Experimental Procedures

To evaluate the splitting tensile strength, the research team followed ASTM C 496, *Standard Test Method for Splitting Tensile Strength of Cylindrical Concrete Specimens* (2011).

5.3.4.2 Results and Discussion

Each of the 13 mixtures tested passed the minimum criteria set by TxDOT. The CSA-Latex mixture had the lowest splitting tensile strength at 490 psi (3.4 MPa), while the PC Type III mixture had the largest splitting tensile strength at 870 psi (6 MPa). When comparing the value of 10% of each mixture's 28-day compressive strength to its respective splitting tensile strength, it is evident that the 10% value is greater for every mixture. The CAC mixtures tensile strength values averaged 9% of the 28-day compressive strength values; the CSA mixtures, on the other hand, averaged about 8% of the 28-day strength values. This result possibly arose because the compressive strengths were calculated with 3-in. x 6-in. (76.2 mm x 152.4 mm) cylinders while 4-in. x 8-in. (101.6 mm x 203.2 mm) cylinders were used to measure tensile strength. According to Mehta and Monterio, when the compressive strength of concrete increases, the 10% assumption of the tensile strength decreases; tensile values of 7 or 8% of the compressive strength have been seen for high strength concrete (1993). Thus, as the compressive strength increases, the concrete becomes more brittle, which impacts the tensile strength of the specimen more than the compressive strength. This could be applicable to rapid repair materials since higher compressive strengths were observed at 28 days.

5.4 Temperature Robustness

The temperature robustness study was implemented to examine the sensitivity of temperature for each binder. Some binders, such as calcium sulfoaluminate, have been known to be more sensitive to temperature than other binder systems. The research team elected to test all 13 mixtures at temperatures of 50 °F (10 °C) and 100 °F (38 °C). Previous literature suggests

that due to its rapid hardening ability, CAC can be placed at low temperatures with little reduction in strength gain (Bentivegna, 2012), but there are scarce data for many of these rapid repair mixtures for testing at varying temperature extremes.

5.4.1 Experimental Procedures

For this experiment, all the mixing materials were measured and stored in an environmental chamber at the specified temperature for 24 hours before mixing time. This step ensured that all of the materials were at the specified temperature before mixing and casting. The specimens were mixed and cast in the mixing room, which is kept at standard temperature of 73 °F (23 °C), and immediately following were placed back into the environmental chamber for 24 hours after the time of mixing. The team cast a total of 18 3-in. x 6-in. (76.2 mm x 152.4 mm) cylinders, which were capped following placement, for compressive strength measurements. Each mixture's compressive strength was measured at 2, 3, 4, 6, 12, and 24-hour intervals for comparison to the compressive strengths measured at standard temperature.

The cylindrical specimens were tested in accordance with ASTM C 39 as well as ASTM C 1231 due to the use of neoprene end caps. Figure 5.4 presents the environmental chamber used to heat and cool the specimens.

Figure 5.4: Environmental chamber for temperature robustness study

5.4.2 Results and Discussion

This section discussed the results of each mixture, with Figures 5.5 through 5.17 illustrating the results. For ease of reference, the research team has grouped the following mixtures into proprietary, CSA, CAC, and portland cement mixtures. The first three proprietary blends were significantly affected by the cooler temperature, while the alkali-activated fly ash blend had a higher compressive strength at 24 hours at 50 °F (10 °C) compared to 73 °F (23 °C). The P-3 mixture is technically not a rapid repair material, according to TxDOT criteria, which is made apparent by the strength curve in Figure 5.7.

The straight CSA blend in Figure 5.9 and the CSA-Latex Mixture in Figure 5.12 showed a significant drop in compressive strength of 2000 psi (13.8 MPa) from the standard temperature to the cooler temperature. The four CSA mixtures do not show a significant difference when

heating the material, and the CSA-3 mixture is the only mixture with a higher compressive strength at 50 °F (10 °C) than at 73 °F (23 °C).

As a whole, CAC mixtures do not seem to be affected by temperature change as expected. The CAC-3 mixture is the only one to show reduced strengths at 50 °F (10 °C), where this mixture had less than 500 psi (3.4 MPa) at 24 hours. For the most part, the standard temperature mixtures had the highest compressive strengths at 24 hours.

The temperature robustness study did affect the portland cement mixture, which was expected. The 100 °F (38 °C) mixture is 4000 psi (27.6 MPa) stronger than the 50 °F (10 °C) mixture at 24 hours.

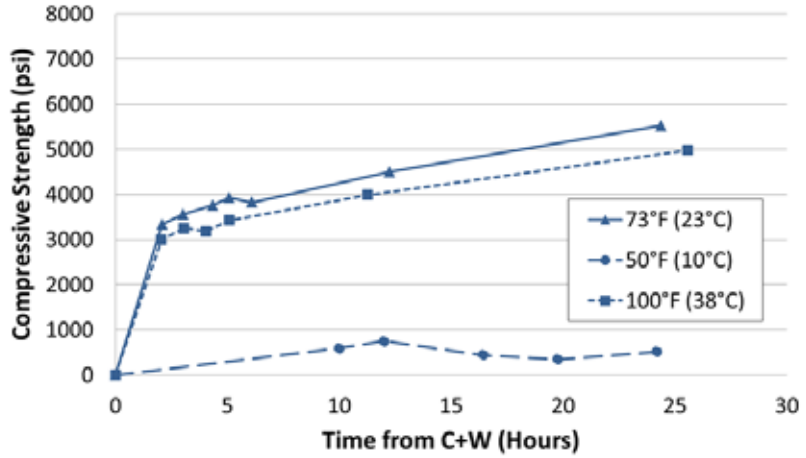

Figure 5.5: Compressive strength comparison for mixture P-1

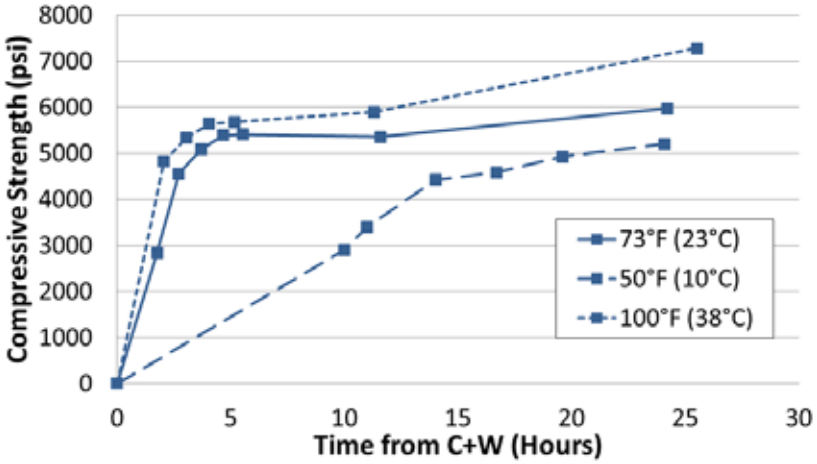

Figure 5.6: Compressive strength comparison for mixture P-2

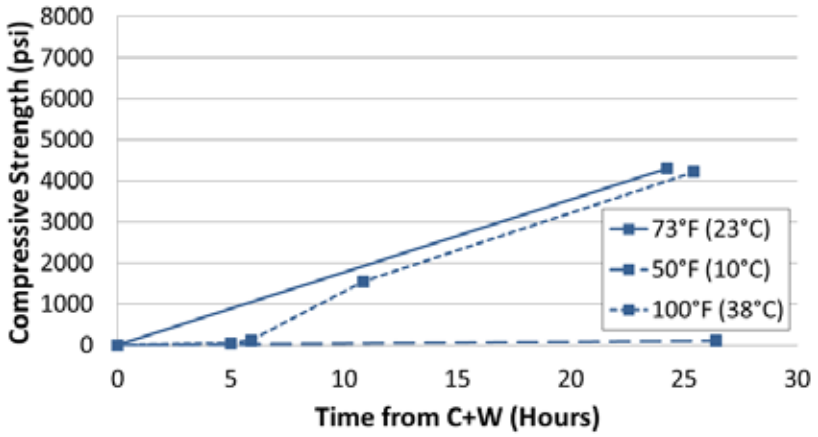

Figure 5.7: Compressive strength comparison for mixture P-3

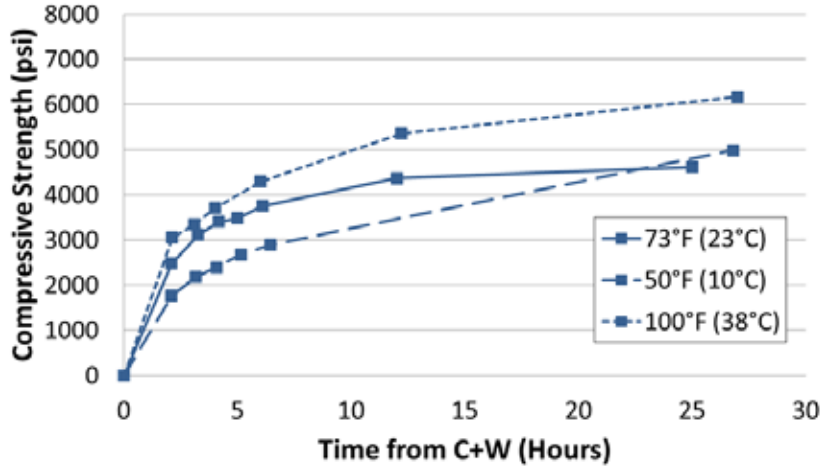

Figure 5.8: Compressive strength comparison for mixture P-AAFA

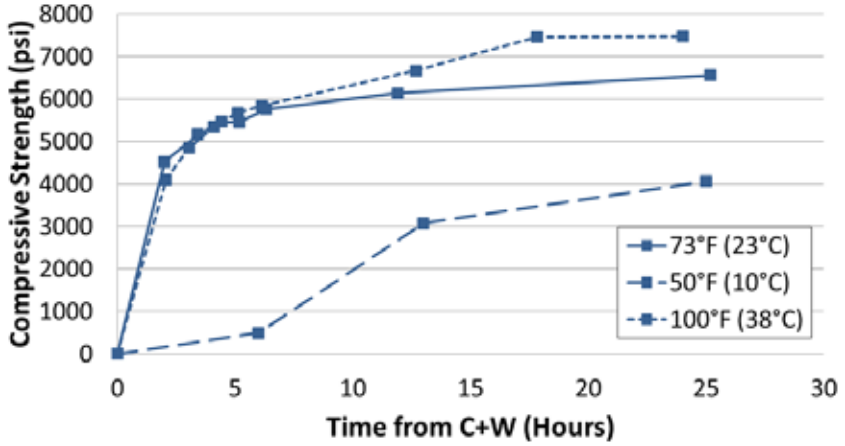

Figure 5.9: Compressive strength comparison for mixture CSA-1

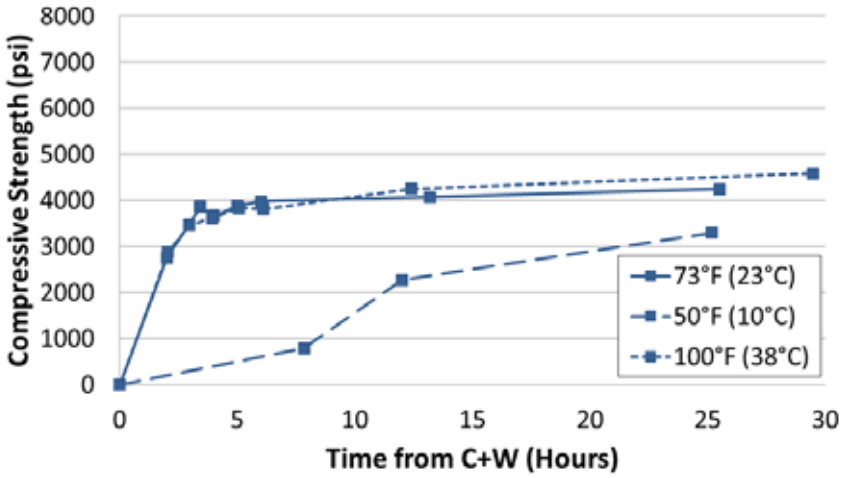

Figure 5.10: Compressive strength comparison for mixture CSA-2

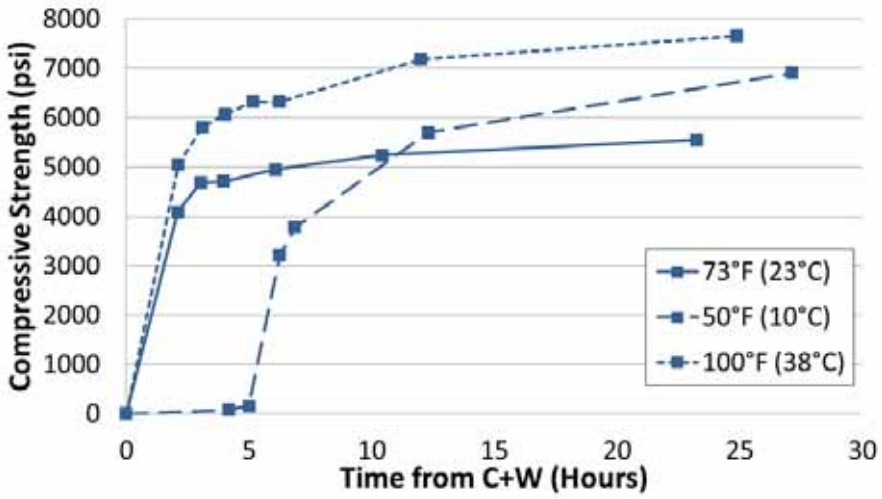

Figure 5.11: Compressive strength comparison for mixture CSA-3

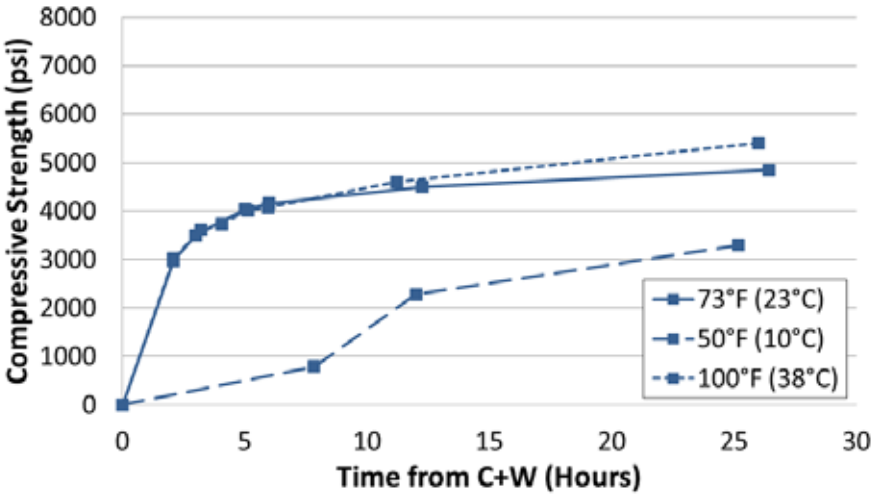

Figure 5.12: Compressive strength comparison for mixture CSA-Latex

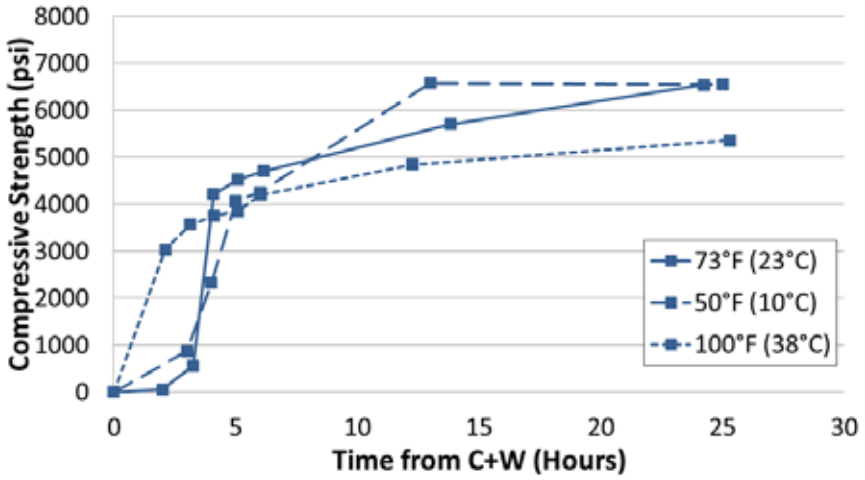

Figure 5.13: Compressive strength comparison for mixture CAC-1

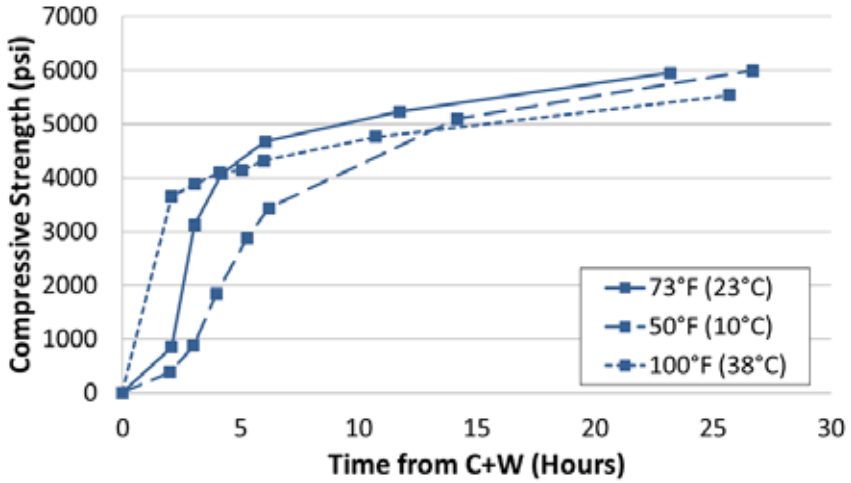

Figure 5.14: Compressive strength comparison for mixture CAC-2

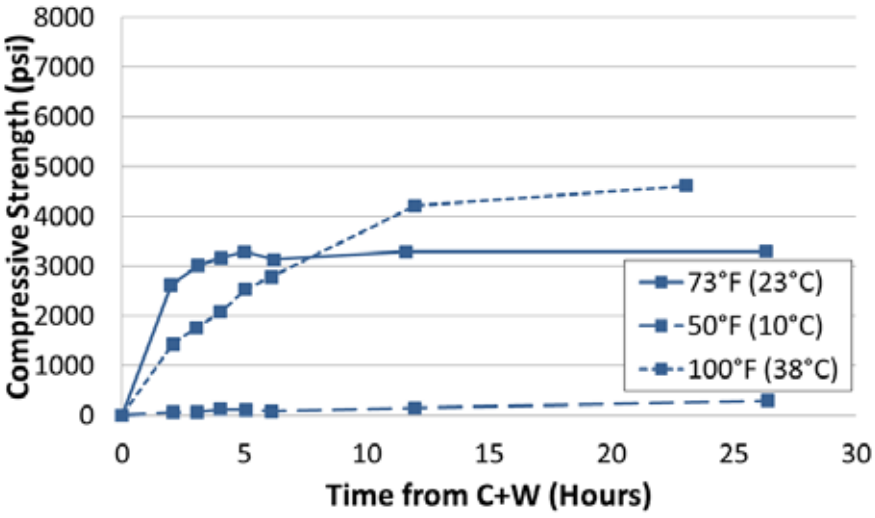

Figure 5.15: Compressive strength comparison for mixture CAC-3

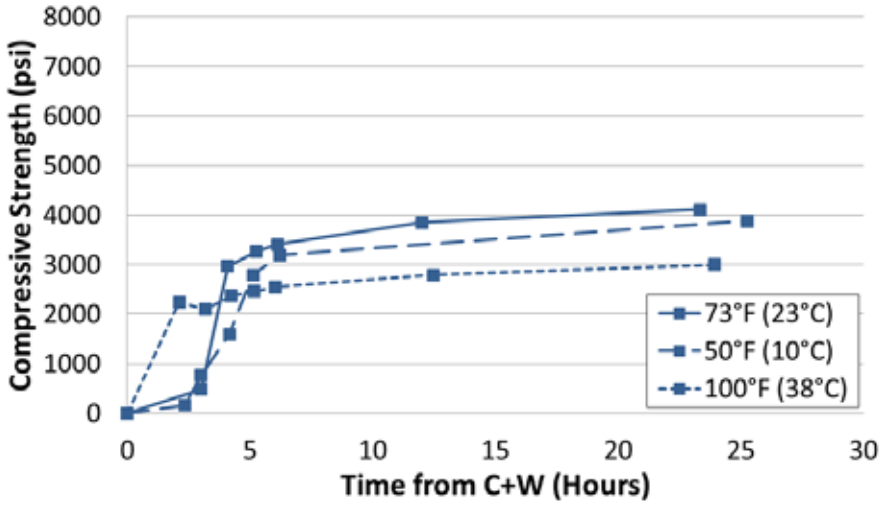

Figure 5.16: Compressive strength comparison for mixture CAC-Latex

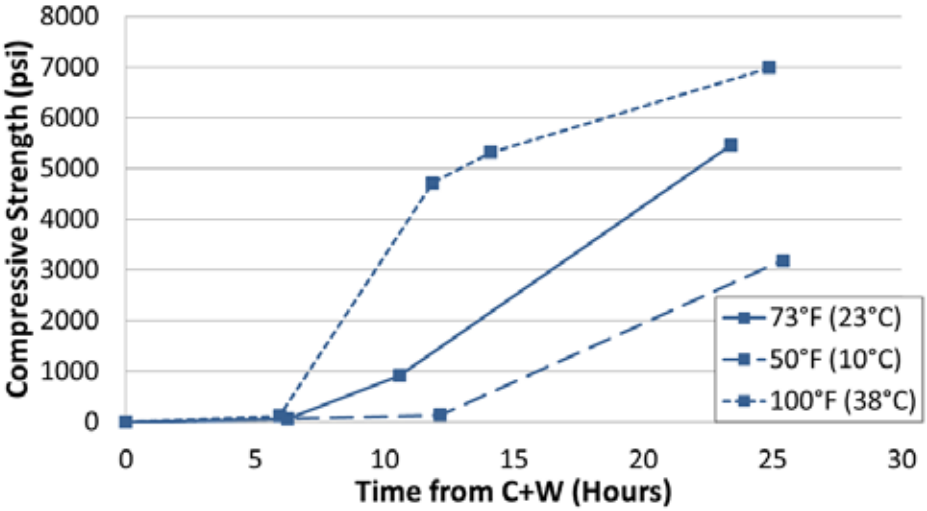

Figure 5.17: Compressive strength comparison for mixture PC Type III

5.5 Coefficient of Thermal Expansion

The CTE is the measure of a material's ability to expand and contract due to various temperatures. As previously mentioned, it is imperative to select repair materials that have CTE values similar to those of the existing concrete. OPC concrete has CTE values ranging from 4 to 7 με/°F (8 to 12 με /°C) and TxDOT's criteria for rapid repair materials is a maximum CTE value of 6 micro strain/°F following a 28-day cure.

Typically, the type of aggregate used is the largest contributing factor towards the CTE of concrete. Limestone aggregates yield lower CTE values when compared to siliceous aggregates. Of the 13 mixtures tested, 9 of the mixtures contained a dolomitic limestone used for the coarse aggregate and siliceous river sand for the fine aggregate. Cement paste also affects the CTE, but since it composes less than 30% of the volume in concrete, the paste has less influence on the CTE.

5.5.1 Experimental Procedures

The research team followed AASHTO T 336, *Standard Method of Test for Coefficient of Thermal Expansion of Hydraulic Cement Concrete* (2011). This method involves measuring the length deformation of a 4-in. x 8-in. (101.6 mm x 203.2 mm) cylindrical specimen submerged in a water bath that ranges in temperature from 50 °F to 122 °F (10 °C to 50 °C). Figure 5.18 is an image of the setup the research team used to evaluate the CTE of each mixture.

Figure 5.18: CTE setup

5.5.2 Results and Discussion

All 13 mixtures underwent CTE testing and the results are presented in Table 5.3. The proprietary mixtures contained various aggregates not selected by the research team, which, in turn, possibly contributed to higher CTE values. The only mixtures satisfying TxDOT's criteria were P-2, the three CAC mixtures, and PC Type III mixture. The CAC mixtures' values were not within tolerance of the AASHTO T 336 standard but the data are included in the table for completeness (2011). The tolerances for the CTE standard include CTE values of less than or 0.2 με/°F or 0.3 με/°C when the specimen is ramping up to 122 °F (50 °C) and down to 50 °F (10 °C). The CAC-1 and CAC-2 mixtures would not fall within the tolerances set by AASHTO T 336 standard. Overall, the P-2 and PC Type III exhibited the lowest CTE values, attributed most likely to the aggregates used in P-2 and the PC binder used in the PC Type III. Interestingly, latex significantly increased the CTE compared to straight CAC mixtures. This finding deserves more attention and additional testing in the future to confirm this behavior; if this is a repeatable trend, studying the underlying mechanisms would be worthwhile.

Table 5.3: CTE for all mixtures

	COTE	
Mix ID	(με/°F)	(με/°C)
P-1	8.23	14.81
P-2	4.78	8.61
P-3	6.63	11.94
P-AAFA	6.57	11.83
CSA-1	6.75	12.15
CSA-2	6.71	12.07
CSA-3	6.68	12.03
CSA-Latex	6.49	11.69
CAC-1	5.58	10.05
CAC-2	5.31	9.55
CAC-3	5.18	9.33
CAC-Latex	7.1	12.78
PC Type III	5.41	9.73

5.6 Bond Strength

Bond strength can be described as a material's ability to adhere to its surroundings. Repair materials must have relatively high bond strengths because concrete repairs normally consist of multiple contact surfaces with the existing concrete. If the bond breaks at the contact surface, the gap formed can be a passageway for water and chlorides to reach the reinforcing steel and cause corrosion. A few ways to increase the bond strength of concrete materials are with the addition of SCM or SBR latex polymer. The addition of SCM to the concrete allows for more hydration and generates more C-S-H, which is considered the "glue" that binds concrete together. Latex-modified concrete is often selected with the goal of producing a lower permeability, more flexible concrete, and as an additional effect, providing better adhesion to the base material.

5.6.1 Experimental Procedures

Multiple bond strength tests for concrete repair materials exist but two of these tests are more widely used. These two tests are the pull-off method and the slant-shear bond test. TxDOT prefers the slant-shear bond test for rapid repair materials that follows ASTM C 882, *Standard Test Method for Bond Strength of Epoxy-Resin Systems Used with Concrete by Slant Shear* (2012). The research team followed this standard with the assistance of TxDOT's concrete materials lab. TxDOT provided the base specimens for these slant shear tests, which contain the specifications of DMS-4655 (2011). The base specimen must be at saturated surface dry condition before casting the repair materials on top. Figure 5.19 presents a substrate specimen provided by TxDOT.

Figure 5.19: Substrate for slant shear bond strength study

The specimens were cast in 3-in. x 6-in. (76.2 mm x 152.4 mm) cylinders and were capped immediately after casting. The cylinders were removed from the molds at 24 hours to be cured for an additional 48 hours. TxDOT has criteria for the slant-shear bond strength of rapid repair materials of 2000 psi (13.8 MPa) at 3 days, which is when the research team elected to measure bond strength as well (TxDOT, 2011).

5.6.2 Results and Discussion

Table 5.4 presents the bond strength data for all 13 mixtures, along with the compressive strength data at 3 days for comparison. The CSA mixtures, as a whole, had higher bond strengths than the CAC mixtures and proprietary mixtures. The latex-modified mixtures did not seem to have higher bond strengths as literature has suggested, and in fact, bond strengths were reduced when using latex with either CSA or CAC. There was not as strong of a correlation between compressive strength and bond strength measured at the same time. Lastly, only 5 of the 13 mixtures would have been deemed acceptable by TxDOT's standards for rapid repairs at 2000 psi (13.8 MPa).

Table 5.4: Three-day compressive and bond strengths for all mixtures

Mix ID	Compresssive Strength (psi)	Bond Strength (psi)
P-1	6190	1820
P-2	7220	2290
P-3	6820	1050
P-AAFA	5660	1540
CSA-1	6870	2050
CSA-2	4940	2020
CSA-3	5720	2800
CSA-Latex	4810	1700
CAC-1	6550	2010
CAC-2	6360	1710
CAC-3	5020	1810
CAC-Latex	4510	1710
PC Type III	7590	1790

5.7 Summary and Conclusions

Table 5.5 summarizes the performance of the Phase II mixtures compared to the limits set by TxDOT for the engineering properties of rapid repair materials. The boxes with check symbols suggest that the designated mixture passed the requirements set by TxDOT, while unmarked boxes suggest that the designated material did not meet the requirements.

Table 5.5: TxDOT's criteria for rapid repair materials (TxDOT, 2011)

Mix ID	Compressive Strength	Modulus of Elasticity	Splitting Tensile Strength	Coefficient of Thermal Expansion	Bond Strength
P-1	✓		✓		
P-2	✓	✓	✓	✓	✓
P-3		✓	✓		
P-AAFA	✓	✓	✓		
CSA-1	✓	✓	✓		✓
CSA-2	✓		✓		✓
CSA-3	✓	✓	✓		✓
CSA-Latex	✓		✓		
CAC-1		✓	✓	✓	✓
CAC-2	✓	✓	✓	✓	
CAC-3	✓	✓	✓	✓	
CAC-Latex	✓		✓		
PC Type III		✓	✓	✓	

The following conclusions can be drawn from the information provided in the chapter:

- The selection of the repair materials should not be focused on the material with the strongest or highest values for the engineering properties, but on selecting a repair material with similar properties to those of the existing substrate. Selecting repair materials in this manner will increase the service life on any repair.

- The P-2 mixture satisfied the most criteria when considering all of the properties measured at standard temperatures.
- The CAC mixtures presented the best behavior during the temperature robustness study but did not fall within the tolerances set by the AASHTO T 336 standard (2011).
- Combining latex with either CSA or CAC had significant impact on the engineering properties, reducing compressive strength, MOE, tensile strength (for CSA mixture only), and bond strength and increasing the flexural strength. According to Bentivegna's field study, the latex-modified CAC overlays showed worse signs of deterioration when compared to plain CAC mixtures (2011).

Chapter 6. Early-Age Volume Change

6.1 Introduction and Background

Early-age volume change is an important topic for rapid repair materials due to the restrained nature of a repair. When a partial, half depth, or full depth repair is performed on a bridge deck, there is restraint from all directions excluding the surface. This restraint can cause cracking when there is a significant volume change, thus leading to a shortened service life of the repair and existing structure. This can be exacerbated when the mechanical and thermal properties of the repair material are significantly different than the base concrete.

The research team evaluated multiple forms of volume change, including drying shrinkage, autogenous deformation, and thermal volume changes. Drying shrinkage is caused when concrete is placed in a dry or unsaturated environment, which allows for the water from the surface of the concrete to evaporate. This causes the surface pores to shrink due to the surface tension created by capillary action.

Autogenous shrinkage occurs in concrete with low w/c due to the lack of water during cement hydration. This causes some of the pores to be filled with a water-vapor mix that creates surface tension. The surface tension places tensile forces on the concrete matrix, which in turn forces the paste to shrink around the aggregate (Riding, 2007). Autogenous shrinkage, known as "external" volume reduction, is only a factor up until setting time, where the concrete develops enough tensile strength to restrain the shrinkage. Although chemical shrinkage and autogenous shrinkage are similar, differences exist within each of their mechanisms. The respective volumes of cement and water when separate are greater than when they are combined, and this reduction in volume is referred to as *chemical shrinkage*. Chemical shrinkage occurs as a result of hydration throughout the life of the concrete and is considered "internal" volume reduction (Ideker, 2008).

A miniature rigid cracking frame (RCF) and free shrinkage frame (FSF) are two instruments that were used to monitor autogenous deformation and thermal volume changes. The devices typically used by researchers at UT for portland cement concrete are much larger than those used in this study; miniature frames were developed at UT for evaluating rapid repair materials in order to maintain temperature control during rapid heat generation. The miniature frames are roughly one-third the size of the larger frames and the dimensions of each frame are noted in Sections 6.4 and 6.5. The RCF restricts movement in the concrete and measures the stress generated from thermal effects, autogenous deformation, and strength development. The FSF allows for unrestrained (free) movement under controlled temperature, which gives us the autogenous deformation of a concrete or mortar mixture.

6.2 Materials and Mixture Proportions

This drying shrinkage portion of this chapter includes all 13 mixtures passing Phase I. Because calcium aluminate and calcium sulfoaluminate binders (CSA-1 and CAC-2) were evaluated using the miniature RCF and FSF, these mixtures were also evaluated for drying shrinkage.

6.3 Drying Shrinkage

The underlying mechanism for drying shrinkage is related the movement of water out of the pore structure of the concrete matrix (Ideker, 2008). Drying shrinkage occurs when the concrete is stored in unsaturated air, which causes the water at the surface to evaporate. The rate of water loss on concrete surfaces is highly dependent upon environmental factors such as wind, relative humidity, and ambient temperature (Whigham, 2005). Normally, drying shrinkage is not an issue for OPC concrete as long as the proper curing procedures are followed. This is not always the case for rapid repair materials, which tend to have high thermal effects that can drive water to the surface more frequently. TxDOT has drying shrinkage criteria for rapid repair materials that require the concrete to have less than 0.07% expansion at 28 days from mixing (TxDOT, 2011).

6.3.1 Experimental Procedures

The research team followed the ASTM C 157, *Standard Test Method for Length Change of Hardened Hydraulic-Cement Mortar and Concrete*. This standard was modified due to the interest in early age properties. Instead of curing the specimens to 28 days, the team removed the specimens from molds when a compressive strength of 3000 psi (20.7 MPa) was obtained, and initial drying shrinkage measurements were recorded. These specimens were measured according to ASTM C 157, along with additional measurements at 3, 6, 12, 24, 48, and 72 hours if 3000 psi (20.7 MPa) was reached at 3 hours. Figure 6.1 presents the specimens in a room kept at 73 °F (23 °C) and 50% relative humidity.

Figure 6.1: Drying shrinkage prisms

6.3.2 Results and Discussion

The drying shrinkage values for all 13 mixtures are presented in Table 6.1. When comparing the drying shrinkage values of the 13 mixtures to the criteria set by TxDOT, only 4 of the 13 mixtures have greater than 0.07% expansion. The CAC mixtures exhibited the higher shrinkage values at 28 days; three of the four mixtures did not pass TxDOT's criteria. The mixtures containing fly ash performed worse than mixtures without fly ash. The CSA-1 mixture

had the lowest percent expansion at 28 days, while the CAC-Latex mixture had the highest at .094% expansion.

Table 6.1: Drying shrinkage values for all 13 mixtures

Mix ID	28-Day Drying Shrinkage (με)	28-Day Drying Shrinkage (%)	64-Week Drying Shrinkage (με)	64-Week Drying Shrinkage (%)
P-1	57	0.006	133	0.013
P-2	410	0.041	633	0.063
P-3	550	0.055	733	0.073
P-AAFA	867	0.087	813	0.081
CSA-1	33	0.003	140	0.014
CSA-2	263	0.026	433	0.043
CSA-3	237	0.024	323	0.032
CSA-Latex	193	0.019	177	0.018
CAC-1	297	0.030	543	0.054
CAC-2	880	0.088	1153	0.115
CAC-3	840	0.084	1303	0.130
CAC-Latex	943	0.094	1070	0.107
PC Type III	290	0.029	427	0.043

6.4 Restrained Stress Development

The RCF was invented in Munich, Germany, when portland cement concrete began to crack on the autobahn in Austria. This frame was designed to incorporate testing of autogenous deformation, thermal effects, creep, relaxation, and strength development (Ideker, 2008). The RCF is composed of copper tubing and insulation to control the internal temperature of the concrete. The frame measures stress in a passive manner: when the concrete tries to expand, compressive stresses are formed within the mixture, which causes tensile stresses in the two Invar steel bars shown in Figure 6.2. Strain gauges are mounted on the Invar side bars to measure the strain, convert it to stress with the properties of the Invar, and then reverse the stress due to the passive nature of the system.

Figure 6.2 shows a top view of the RCF. The Invar side bars run along the sides of the concrete. The crossheads provide restraint with metal "teeth" to ensure there is no slipping of the concrete. The miniature RCF is one-third the size of the original frame and has dimensions of 2 in. x 2 in. x 21.5 in. (50.8 mm x 50.8 mm x 546 mm).

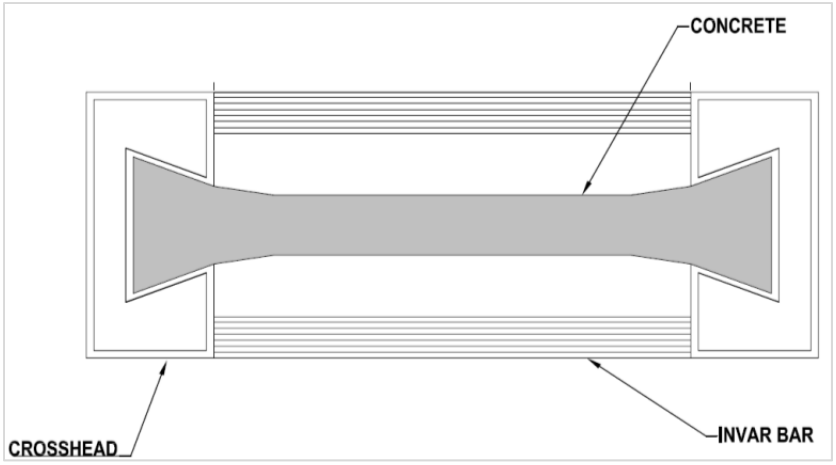

Figure 6.2: Top view schematic of RCF (Ideker, 2008)

Thermal effects, autogenous deformation, and strength development can be measured by the stresses in the concrete when the frame follows a time temperature history; however, rapid repair materials have high early heat generation, which causes difficulties when trying to control the temperature of the concrete within certain tolerances. For this reason, the research team decided to test the RCF isothermally at 73 °F (23 °C), thus eliminating the thermal effects of the mixture. The stresses measured in the frame will provide the team with valuable information on the autogenous behavior of the binder.

6.4.1 Experimental Procedures

The CAC-2 and CSA-1 mixtures were mixed in a 1.75 ft^3 (.05 m^3) drum mixer described in Zuniga (2013). The research team needed 0.35 ft^3 (.01 m^3) of concrete to cast specimens in the RCF, FSF, and time of set can. The setting time was measured by penetration resistance in accordance with ASTM C 403 for the FSF (2008).

Before mixing could begin, the RCF was cleaned and sealed to prevent drying, thus ensuring autogenous shrinkage only when testing is done at a fixed temperature. Plastic sheeting was placed in the center section of the frame and was taped down with waterproof HVAC aluminum foil tape. The plastic sheeting was not used in the crossheads because the team wanted to ensure sufficient bonding for restraint. Then, silicone was applied to seal and smooth the gaps between the bottom crossbars, crossheads, and center section of the frame.

One water bath was used to control the temperature of the RCF, FSF, and time of set can. A T-valve was connected to the output of the water bath, such that both frames would receive equal amounts of water simultaneously. The team placed one thermocouple in the crosshead section of the frame and another in the center of the specimen to record the temperature throughout the frame and drive the water bath temperature.

The mixture was cast into the RCF in two layers where consolidation was achieved with plastic tamping rods. After the excess concrete was removed, the two thermocouples were placed in the specimen and a piece of plastic sheeting cut to the "dog-bone" shape of the RCF was taped down with the foil tape. The top section of the frame was then attached, thus creating an autogenous system where no water was permitted to enter or leave the specimen. The water bath was connected to begin the isothermal temperature control of the frame and the setting time was

measured immediately. The research team selected to run the isothermal conditions to 72 hours after mixing since a cracking temperature was not the objective of the experiment.

6.4.2 Results and Discussion

The following two figures contain the results of the isothermal stress development for both a CSA and CAC mixture. These binder systems were chosen due to their vastly different early-age characteristics, which are evidenced in the stress development figures.

The CSA binder system generates early-age strength development with an ettringite-based system, which is typically, but not always, expansive. Thus, CSA concrete has been known as shrinkage-compensating or shrinkage-reducing concrete. This is evident in Figure 6.3 where the CSA-2 mixture witnesses compressive stresses up to 190 psi (1.3 MPa). This mixture also has tensile stresses at 2.5 hours from mixing due to a temperature drop of 3 °C while the research team monitored the specimen. This drop was caused when ice was added to the water bath to cool the bath, as the specimen was generating heat during the final setting of the concrete.

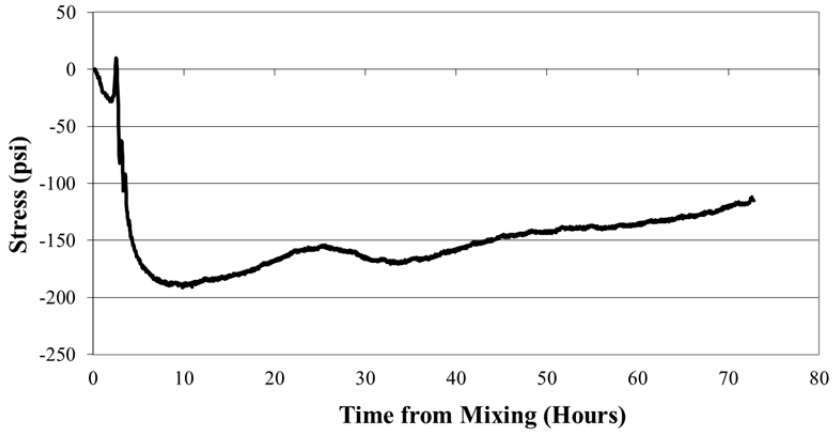

Figure 6.3: Restrained stress development for CSA-1 mixture

Figure 6.4 presents the stress development for the CAC-2 mixture. This mixture tries to expand while the repair material is still plastic, but once final setting occurs the mixture attempts to shrink, causing tensile stresses. These tensile stresses increase over the 72 hours up to 270 psi (1.9 MPa) and seem to still increase after the research team had completed their testing. The CAC-2 mixture generates tensile stresses similar to that of a typical portland cement concrete mixture under a 73 °F (23 °C) environment.

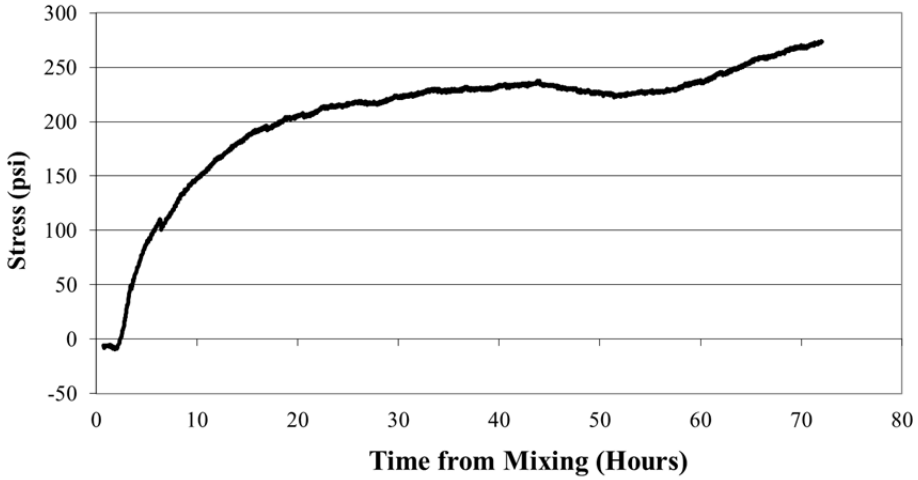

Figure 6.4: Restrained stress development for CAC-2 mixture

6.5 Unrestrained (Free) Deformation

The unrestrained deformation of a concrete mixture can be measured with an FSF. This frame measures the linear movement of a concrete specimen in a sealed, temperature-controlled environment; this linear movement is used to calculate autogenous shrinkage. As with the RCF, a smaller version of the FSF is necessary to control the temperature for rapid repair materials. Figure 6.5 presents a side view of the FSF.

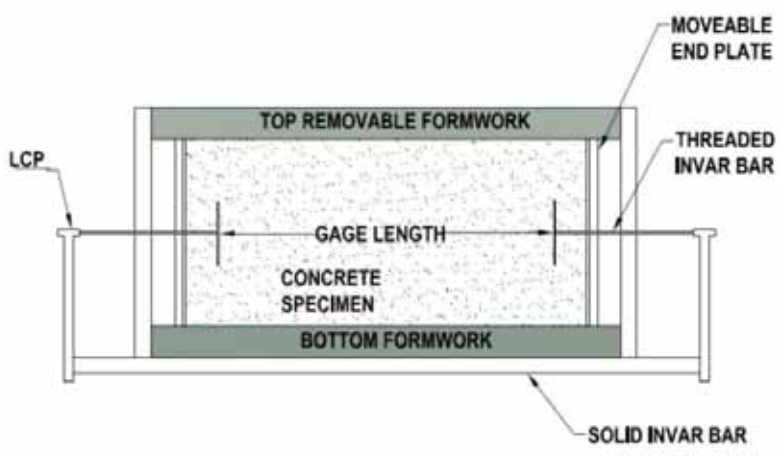

Figure 6.5: Side view schematic of FSF (Ideker, 2008)

The cross section of the FSF and the RCF are the same at 2 in. x 2 in. (50.8 mm x 50.8 mm), but the total length of the FSF is 6.9 in. (175 mm) with a 5.3 in. (135 mm) gage length between Invar bars. The solid Invar bars below the frame and the threaded Invar bars were selected due to their resistance to thermal deformations. Each of the threaded Invar bars are screwed onto a linear control potentiometer at both ends, which measures changes in voltage resulting in length change. Aluminum end squares were constructed in order to reduce slippage between the concrete and the small threaded Invar rods. These end squares are 0.5 in. x 0.5 in.

(13 mm x 13 mm) and have been tapped in the center to allow for the threaded Invar rod to screw into them.

As mentioned earlier, both the RCF and the FSF run off of the same water bath. The FSF is composed of copper pipes within the formwork, as well as with insulation to keep the specimen controlled at a specific temperature. At both ends of the frame are two moveable steel plates bolted to sides the frame. These end plates are in contact with the concrete specimen until the final setting of the concrete, when the end plates are released, thus allowing for unrestrained deformation.

6.5.1 Experimental Procedures

Before mixing began, the FSF was cleaned and prepped. First, the steel end plates needed to be bolted to the frame and extended to allow for a smooth release at final setting of the concrete. The frame was oiled and plastic sheeting was then taped carefully inside the frame to make certain that the cross section of the frame was not being reduced. A second layer of plastic and oil was added to the body of the frame, while the steel end plates were coated in thick grease to prevent friction during release. After the aluminum end squares were screwed onto the threaded Invar rods, the linear control potentiometers were adjusted until they were at mid-stroke so that the specimen would not deform out of the range of the equipment.

The same mixing procedure and batch were used for both the RCF and FSF specimens. The concrete was mechanically vibrated into the frame with plastic tamping rods until the mixture was consolidated. Once the excess concrete was removed, two thermocouples were placed at third points along the length of the specimen to get a uniform temperature profile. Finally, the top piece of plastic sheeting was placed using aluminum foil tape before the top of the frame was put in place. The water bath tubes were connected to the frame to begin temperature control while the setting time was monitored with the penetration resistance test following ASTM C 403 (2008). Both of the steel plates were released once final setting had occurred to allow for free deformation.

6.5.2 Results and Discussion

Figures 6.6 and 6.7 present the unrestrained deformation of the CSA-1 and CAC-2 mixtures from initial setting to 72 hours from the setting time. The CSA-1 mixture in Figure 6.6 presents atypical results when compared to portland cement concrete. Portland cement concrete at low w/cm usually witness autogenous shrinkage, while the CSA-1 mixture exhibits autogenous expansion due to the expansive products formed during hydration. This autogenous expansion confirms the compressive stresses generated in the RCF with expansive strains up to 700 $\mu\varepsilon$. The CAC-2 mixture results (Figure 6.7) show the typical trends of a portland cement concrete mixture where an initial expansion occurred, followed by a steady shrinkage out to 72 hours. This also confirms the behavior witnessed in the RCF, where the mixture generated tensile stresses under the isothermal conditions.

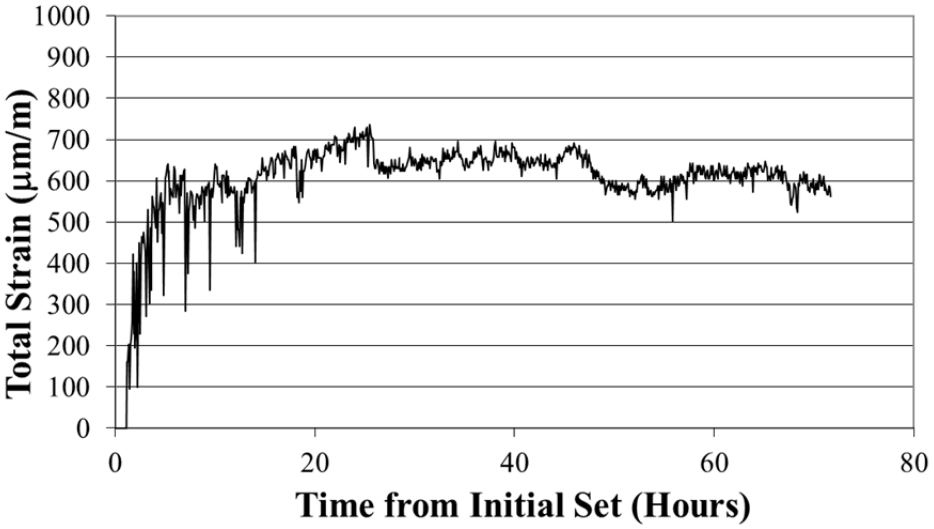

Figure 6.6: Unrestrained (free) deformation for CSA-1 mixture

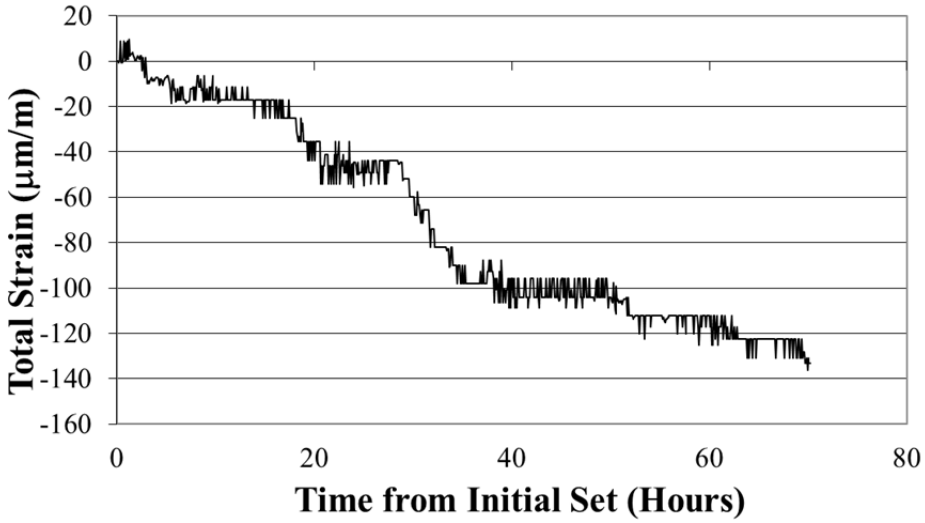

Figure 6.7: Unrestrained (free) deformation for CAC-2 mixture

6.6 Summary and Conclusions

The research team reached the following conclusions based on the results provided in this chapter:

- The CSA binder system had less drying shrinkage than did the CAC binder system at both 28 days and 64 weeks. Three of the four CAC mixtures did not meet TxDOT criteria at 28 days from mixing.
- Mixtures containing fly ash contained more drying shrinkage than mixtures not containing fly ash.
- The CSA-1 mixture presented autogenous expansion and compressive stresses in both the FSF and RCF, confirming the shrinkage compensating property for this binder.
- The CAC-2 mixture presented autogenous shrinkage and tensile stresses in both the FSF and RCF—behavior that is similar to that of a typical portland cement concrete with low w/cm.

Chapter 7. Calorimetry

7.1 Introduction and Background

Calorimetry or heat evolution is an important property to obtain for both portland cement and rapid repair materials. Heat evolution and heat flow are measured with methods such as isothermal calorimetry, semi-adiabatic calorimetry, and gradient calorimetry; these methods of temperature evaluation can assist in the understanding of early-age performance issues for rapid repair materials. For portland-cement-based systems, investigating material combinations at different isothermal temperatures allows calculation of an apparent activation energy, which can be combined with data/information from semi-adiabatic calorimetry to predict thermal distributions in mass concrete applications (Poole, 2007) (Riding, 2007). Unfortunately, a similar analysis of activation energy is not possible for rapid repair materials, such as CAC, due to the different hydration products that form at different temperatures.

Isothermal calorimetry is obtained by controlling the designated material's temperature to desired conditions with thermostats, heating fans, and cooling fans, while measuring the heat generated from the material with heat flow sensors. For portland cement the heat evolution generally continues for several days or even weeks, depending on whether SCMs are added to the mixture, while the heat evolution for most rapid repair materials is complete by 24 hours. Rapid repair materials exhibit an initial peak due to the dissolution of materials, which is neglected in the calculation of heat of hydration properties. The different mixtures were compared based on a relationship involving heat flow and time, the amount of time to the peak heat flow, the peak heat flow for a mixture, and a cumulative heat flow for a mixture.

The semi-adiabatic calorimeter, or *Q-drum*, was created to measure the heat generated from a cylindrical concrete specimen to determine different hydration parameters. Generally, these hydration parameters are combined with the apparent activation energy calculated from isothermal calorimetry, along with other properties from the cementitious material used in the mixtures, to develop an adiabatic temperature curve. This temperature curve was used to model different mass concrete elements commonly used in the field and was combined with different climates from across the state. This information was imported into a program called ConcreteWorks, which can provide heat generation and transfer for different mass concrete elements if the properties of the concrete and specifics of construction are known.

Thermal gradients exist in every concrete structure but are a larger issue in mass concrete members for portland cement, as well as in any rapid repair materials member where there is high heat generation. Many jobs in Texas are now requiring contractors to measure and monitor these temperature gradients in mass concrete elements; thus, formwork insulation may be used to control the temperature gradients in concrete (Riding, 2007). The issue with thermal gradients in mass concrete elements is that the exothermic reaction generated by cement hydration is still occurring in the center of these structures, while the concrete at the surface is dissipating heat into the environment. This difference in temperature causes different expansion and shrinkage, which lead to stresses developing between the interior and exterior of the element. For rapid repair materials, the issue is related to how quickly their heat evolution occurs since the elements are still gaining strength as high amount of heat are generated. The smaller repair elements can dissipate heat more easily at the surface, which causes the same thermal stresses at an earlier age.

7.2 Materials and Mixture Proportions

The 13 mixtures passing Phase I of the project were studied using isothermal, semi-adiabatic, and cylindrical calorimetry. Only the Phase III mixtures were included in the temperature gradient slabs study. All of the concrete mixture proportions and mixing procedures are described in Zuniga (2013). The team tested each of the 13 mixtures as concrete, mortar, and paste for isothermal calorimetry, where only the paste materials were preheated and precooled for the samples tested at 50 °F (10 °C) and 100 °F (38 °C). For the remaining tests, each material was stored at 73 °F (23 °C) 24 hours before mixing. The 3-in. x 6-in. (76.2 mm x 152.4 mm) calorimetry cylinders were cast from the large mechanical properties at standard temperature because the team desired to see the peak temperature generated for each mixture at this time. The remaining mixtures were cast as standalone mixtures due to the different applications of each.

7.3 Isothermal Calorimetry

Isothermal calorimetry measures the heat flow from cement hydration reactions by differential heat flow sensors that allow for comparison of different mixtures and provide time-lapsed understanding of the hydration mechanisms. The timing and shape of heat flow curves can provide an understanding of the performance of different cementitious systems (Bentivegna, 2012). The excess heat release of rapid repair materials inspired the research group at The University of Texas at Austin to design and construct a new isothermal calorimeter. This task was assumed by Anthony Bentivegna in 2012 and he was able to construct and calibrate a new calorimeter tailored to the heat generation of calcium aluminate. Because the rapid repair materials used in this project behave similarly to CAC, the calorimeter Bentivegna constructed was used in this project. More information on the design, construction, calibration, and properties of the calorimeter can be found in Bentivegna's dissertation (2012). Figure 7.1 presents the insulated chamber for the Bentivegna's calorimeter.

Figure 7.1: Stainless steel calorimeter chamber

The isothermal calorimetry study was performed on concrete, mortar, and paste at 50 °F, 73 °F, and 100 °F (10 °C, 23 °C, and 38 °C); due to constructability issues only the paste mixtures materials were cooled or preheated. This approach allows for less "noise" in the beginning of the data acquisition while the sample holder and the material itself are acclimating to the calorimeter temperature. Thus, this chapter's results section will focus on the paste samples but the concrete and mortar data can be found in Appendix C and Appendix D.

Heat flow (mW/g), one of the means cited earlier for comparing different mixtures, is measured by heat flow sensors within each channel, which indicates voltage changes. The differences in voltage can produce a power output when the proper calibration factors are applied. The power is then normalized per gram of cementitious material and plotted against time of mixing to generate the relationships presented in the results and discussion section. Table 7.1 presents the time to peak heat flow, as well as the peak heat for each mixture. The time to peak heat flow provides the research team with a comparison method for the hydration rates of different mixtures, while the peak heat value can give insight as to which mixtures are more likely to have internal thermal effects.

The cumulative heat release (J/g) provides a comparison method involving the amount of energy release per gram of cementitious material. The cumulative heat release can provide a comparison of the total hydration for each mixture. This value includes the area under the heat flow curve up to 48 hours but neglects the initial drop or rise in heat flow when the specimen are placed into the calorimeter. The research team used Simpson's rule for numerical integration to calculate the cumulative heat release.

7.3.1 Experimental Procedures

The cement, admixtures, and water for each mixture were weighed out prior to mixing and the total mass of each paste specimen was approximately 15 grams. The paste sample mass was selected based on Bentivegna's previous work with CAC given its high early heat release. The mixing procedure for the paste specimen were as follows: add the cement to the water in the sample holder and tap the cup on the counter for 30 seconds; place on the ultrasonic mixer for 30 seconds; place the lid on the sample holder; set into appropriate calorimetry channel and start the program. An ultrasonic mixer was used to mix the paste samples and was set on the highest vibration setting to achieve sufficient hydration of all cement grains. The average time from mixing cement and water to starting the calorimeter was 1.5 minutes. Figure 7.2 presents the sample holders suggested by Grace Construction Products and the ultrasonic mixer used for paste samples.

Figure 7.2: A) Grace AdiaCal TC Calorimetry Sample Holder (Bentivegna, 2012)
B) Ultrasonic Mixer used for Paste Samples

After the concrete was mixed, a portion of the mixture was wet sieved through a No. 4 sieve on a vibrating table. This allowed the research team to remove some variability that occurs during mixing because both concrete and mortar would be sampled from the same mixture. The concrete samples were measured to approximately 100 grams for the 73 °F and 50 °F (23 °C and 10 °C) calorimetry mixtures, but due to the acceleration of hydration at 100 °F (38 °C), smaller sample sizes were weighed out to 50 grams. The mortar samples were measured to 30 grams for the 73 °F and 50 °F (23 °C and 10 °C) calorimetry mixtures, and 20 grams for the 100 °F (38 °C) mixtures. Again, all of these masses were selected based upon Bentivegna's results in 2012. The average time from mixing until the sample was placed into the calorimeter was 6 minutes; this time was taken into account for the time to peak heat value.

7.3.2 Results and Discussion

As mention previously, the analysis of calorimetry will focus on the paste specimen but the concrete and mortar data are provided in Appendix C and Appendix D. Appendix C contains tables displaying the time to peak heat, peak heat, and cumulative heat for each mixture, while Appendix D includes graphs of concrete, mortar, and paste behaviors at different temperatures. In Appendix D, the P-AAFA mixture's 50 °F (10 °C) graph does not appear to have a hydration peak. The calorimeter was cooling the specimen down to 50 °F (10 °C) as it was generating heat; therefore, the hydration peak was overlapped with the cooling curve. This is the only mixture to have this issue because of the P-AAFA mixture's rapid heat evolution.

Table 7.1 presents all of properties of the isothermal calorimetry curves for the paste specimen and Figures 7.3–7.11 provide the calorimetry curves. The proprietary mixtures are excluded from this table because the research team could not construct adequate paste samples from "all-in-one" packages. When focusing on time to peak heat, the CSA mixtures seem to retard more at 50 °F (10 °C) than the CAC mixtures. Another trend to highlight is the time to peak heat for the CAC-1 and CAC-Latex mixtures is slower at 73 °F (23 °C) than 50 °F (10 °C). Overall, the PC Type III mixture, as to be expected, has the longest time to peak heat. For the peak heat flow, the CAC-1 and CAC-Latex mixtures have the largest variability between 73 °F (23 °C) and 100 °F (38 °C) as well as the highest peak heat of 97 and 100 mW/g, respectively. The CAC-3 mixture had the lowest peak heat flow value for the 50 °F (10 °C) mixtures. The CAC and CSA mixtures with and without latex have higher cumulative heat at 50 °F (10 °C) than at 73 °F (23 °C), which is the opposite of the other mixtures' behavior. The CSA-1 mixture has the highest cumulative heat; however, the CAC mixtures have a higher cumulative heat as a binder system.

Table 7.1: Paste summary table for isothermal calorimetry

Mix ID	Temperature °F (°C)	Time to Peak Heat (Hours)	Peak Heat Flow (mW/g cement)	Cumulative Heat (J/g)
CSA-1	50 (10)	7.65	21	225
	73 (23)	1.62	29	132
	100 (38)	1.02	60	346
CSA-2	50 (10)	9.22	15	165
	73 (23)	2.12	30	180
	100 (38)	0.77	62	214
CSA-3	50 (10)	8.75	20	153
	73 (23)	2.43	26	167
	100 (38)	1.25	57	207
CSA-Latex	50 (10)	7.98	29	221
	73 (23)	1.92	54	211
	100 (38)	0.63	84	202
CAC-1	50 (10)	1.48	23	242
	73 (23)	2.53	23	196
	100 (38)	0.27	97	249
CAC-2	50 (10)	7.95	7	189
	73 (23)	3.70	15	235
	100 (38)	0.38	59	242
CAC-3	50 (10)	1.82	2	138
	73 (23)	1.12	8	215
	100 (38)	0.90	26	223
CAC-Latex	50 (10)	1.45	22	261
	73 (23)	3.53	30	302
	100 (38)	0.28	100	267
PC Type III	50 (10)	16.82	2	179
	73 (23)	10.35	4	206
	100 (38)	5.92	8	237

The CSA mixtures were influenced the most when varying the temperature, specifically the mixture at 50 °F (10 °C). There is a delay of 6 to 8 hours when the materials were cooled prior to mixing and placed in a 50 °F (10 °C) calorimeter. Of the CSA mixtures, the CSA-Latex mixture had the largest peak heat flow values at each temperature.

The CAC-1 and CAC-Latex mixtures performed similarly under all three temperatures, which was expected because both mixtures contain the same components, except for the latex. This suggests that latex does not affect the heat evolution of CACs, although results shown earlier in this report exhibited a lower rate of strength gain when latex was combined with CAC. These two mixtures also had faster heat evolution at 50 °F (10 °C) than 73 °F (23 °C), which is different than all other mixtures and suggests temperature has a more significant effect on CAC mixtures than previously thought. The CAC-2 mixture performed about as expected, with descending and slower heat flows as the temperature decreased. The CAC-3 mixture performed poorly at 50 °F (10 °C) where there was virtually no peak heat flow. This mixture did show a

second peak beginning at 24 hours after mixing for the other two temperatures, which suggests that the portland cement in the mixture begins to hydrate and generate heat later.

Figure 7.11 presents the heat evolution of the PC Type III mixture, which exhibits the type of heat generation expected with portland cement mixtures. The higher the temperature, the faster the heat generation and higher the peak heat flow.

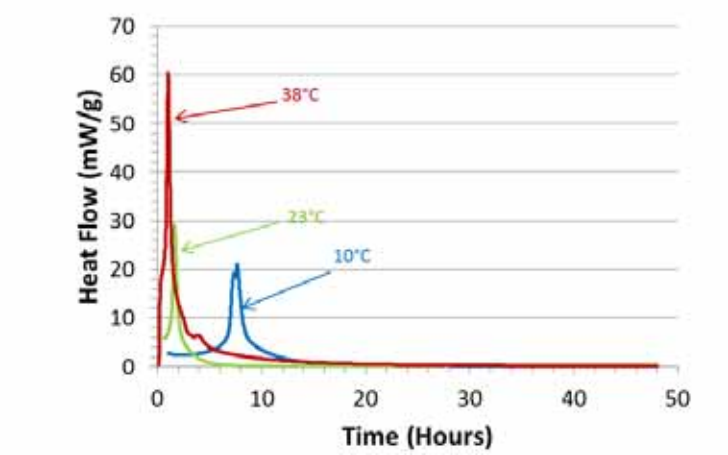

Figure 7.3: Isothermal calorimetry for CSA-1 paste mixture

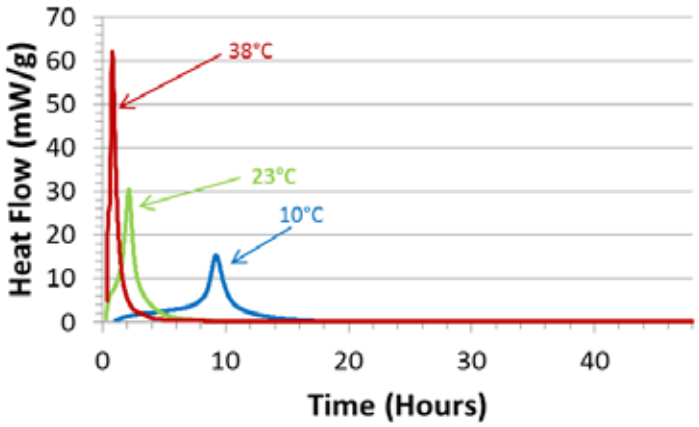

Figure 7.4: Isothermal calorimetry for CSA-2 paste mixture

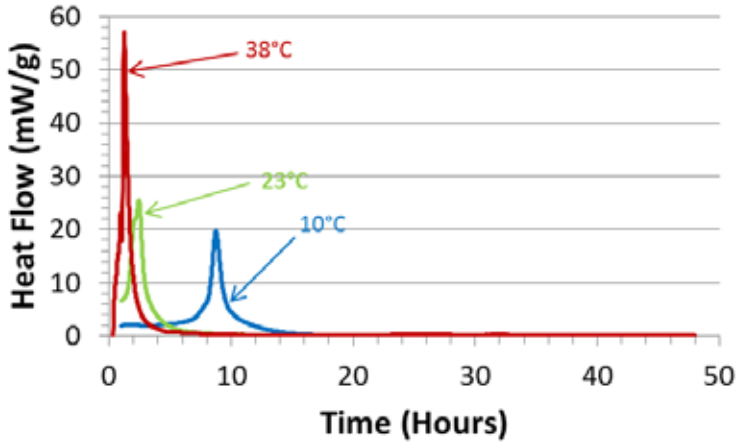

Figure 7.5: Isothermal calorimetry for CSA-3 paste mixture

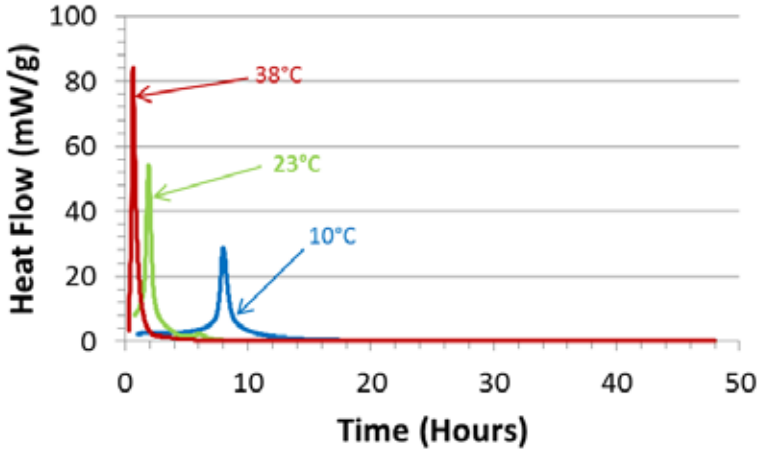

Figure 7.6: Isothermal calorimetry for CSA-Latex paste mixture

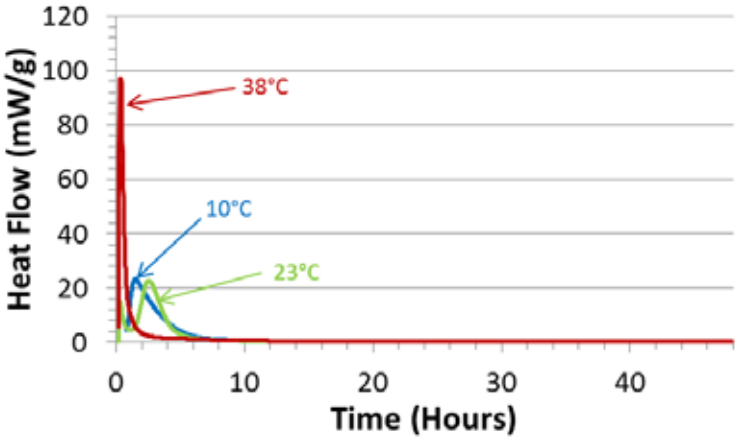

Figure 7.7: Isothermal calorimetry for CAC-1 paste mixture

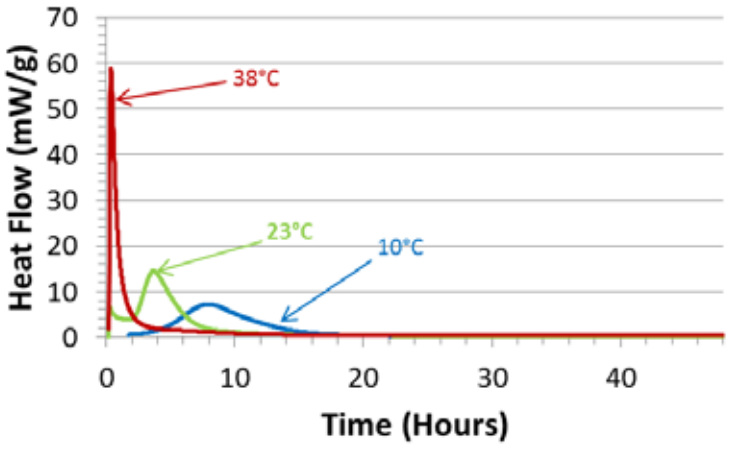

Figure 7.8: Isothermal calorimetry for CAC-2 paste mixture

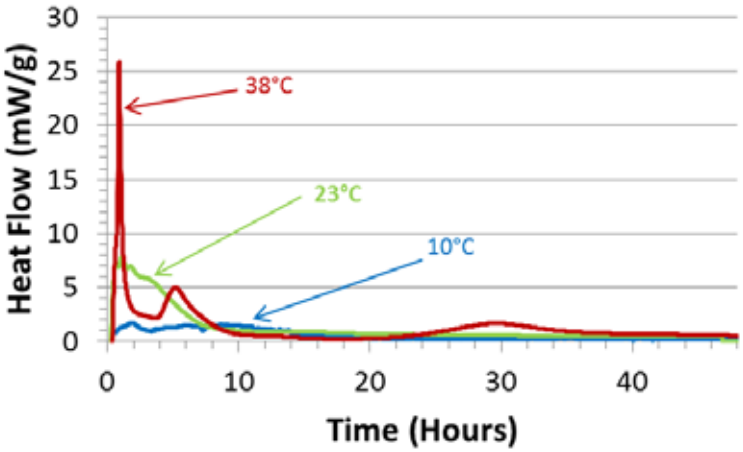

Figure 7.9: Isothermal calorimetry for CAC-3 paste mixture

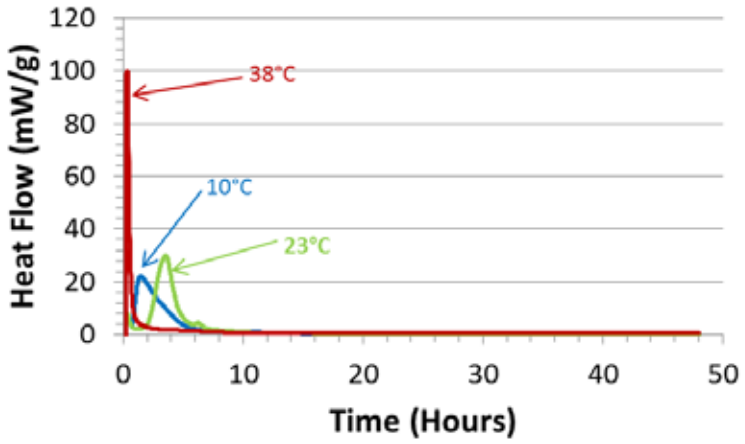

Figure 7.10: Isothermal calorimetry for CAC-Latex paste mixture

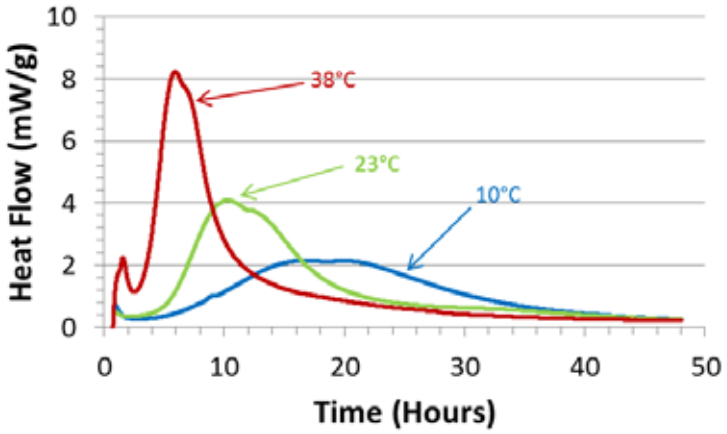

Figure 7.11: Isothermal calorimetry for PC Type III paste mixture

7.4 Semi-Adiabatic Calorimetry and Calorimetry Cylinders

When semi-adiabatic calorimetry is tested on portland cement concrete, hydration parameters such as, α_u, β, and τ can be computed from different sections of the temperature curve. These hydration parameters can be combined with the apparent activation energy from isothermal calorimetry to model the thermal distributions in a hydrating concrete element. This, however, cannot be computed for the rapid repair materials at hand because these materials contain different hydration products than portland cement, which prevents the calculation of hydration parameters.

The semi-adiabatic calorimeter can still generate a temperature evolution and key temperature related properties for rapid repair materials. Some of the same properties from isothermal calorimetry can be computed for semi-adiabatic, such as the time to peak heat, the peak heat, and the cumulative heat. Another property added to this section is related to the T_{off} value for CAC. Bentivegna describes T_{off} as the time at which CAC increases in temperature by 1 °C from the initial temperature (2012). The research team wanted to use the same concept but for an increase of 3 °C from initial temperature due to the variability in temperature in the semi-adiabatic calorimeters. The notation for this temperature property is $T_{\Delta 3°C}$.

The semi-adiabatic calorimeter (or Q-drum) measures the temperature of a mixture with a thermocouple placed in the center of a 6-in. x 12-in. (152.4 mm x 304.8 mm) concrete cylinder. The heat flux escaping the drum is also measured, in order to capture all of the heat generated by this concrete specimen. Another method the research team used to monitor the heat generation of a mixture was by placing a thermocouple in a 3-in. x 6-in. (76.2 mm x 152.4 mm) cylinder. This cylinder was cast as a part of the mechanical properties mixture at standard temperature to correlate the temporary heat profile with the mechanical properties of a mixture. The same temperature properties applied to the Q-drum specimen are applied to 3-in. x 6-in. (76.2 mm x 152.4 mm) specimen as well.

7.4.1 Experimental Procedures

The 6-in. x 12-in. (152.4 mm x 304.8 mm) cylinder for the Q-drum was mixed in the 1.75ft^3 (.01 m^3) mixer mentioned previously. Three lifts of concrete were placed and rodded in the Q-drum cylinder. The specimen was weighed and a Type K thermocouple was placed in the

center of the cylinder at mid-depth to record the temperature of the concrete. The heat flux was measured at the control box located on the side of the metal 30 gallon drum, which was filled with insulation to prevent heat loss. Any heat that did escape the insulation was measured by the sensors picking up the heat flux. The cylinder was placed in the Q-drum, where time was recorded from the time of mixing until the start of the program; on average, this time was 6 minutes, which was included in the calculation of the heat evolution properties. The heat generation was measured from 120 to 160 hours depending on how long it took for the heat to dissipate from the specimen.

The 3-in. x 6-in. (76.2 mm x 152.4 mm) calorimetry cylinder was cast in two lifts, which were consolidated on a vibrating table. Then, a Type J thermocouple was placed in the center of the cylinder at mid-depth; the cylinder was capped immediately after and temperature was recorded out to 24 hours when the cylinder was removed from the mold to continue the curing process.

7.4.2 Results and Discussion

This section presents plots (Figures 7.12–7.24) of the semi-adiabatic calorimetry on the left and the 3-in. x 6-in. (76.2 mm x 152.4 mm) calorimetry cylinders on the right for one mixture. Also, all of these temperature plots are in degree Celsius due to the nature of calorimetry.

Some of the trends presented for the proprietary mixtures are that the time to peak and time to 3 °C are slower for the Q-drum mixtures than for the 3-in. x 6-in. (76.2 mm x 152.4 mm) calorimetry cylinders. The P-3 mixture took the longest to reach peak heat at almost 30 hours for the Q-drum cylinders, while the P-AAFA mixture was the quickest to peak heat in 0.8 hours for the calorimetry cylinders. The P-AAFA and P-1 mixtures each had very similar times to 3 °C for the Q-drum and calorimetry cylinders. P-AAFA mixture was the only mixture to have very similar peak temperatures for the Q-drum and the calorimetry cylinders.

The CSA mixtures had the most repeatability of any binder system for all of the properties. The time to peak heat for this binder system was very quick and the peak temperatures were high as well. The CSA-1 and CSA-Latex mixtures performed very similar on all of the calorimetry properties just as with the isothermal calorimetry. The heat curve for CSA-2 mixture has a second peak, a behavior not replicated by any of the other CSA mixtures.

The CAC-1 mixture has the highest peak temperature of any mixture for the Q-drum and calorimetry cylinders, while the CAC-3 has the lowest peak temperature of any mixture for the Q-drum. Similarly to isothermal calorimetry, the CAC-1 and CAC-Latex mixtures generated the same amount of heat, which further proves that latex does not reduce the amount of heat generated in a mixture. The CAC-3 mixture was slower to gain heat due to it being mostly composed of portland cement. The CAC-2 mixture seemed to slow the time to peak heat, as well as reduce the peak temperature.

The PC Type III mixture's calorimetry cylinders had the lowest peak temperature, which is to be expected because it is not a rapid repair material. This mixture also has a slower time to peak than the other mixtures. When the PC Type III mixture was tested in the Q-drum, a higher peak heat was reached than expected and the P-3 mixture had a slower time to peak heat than this mixture.

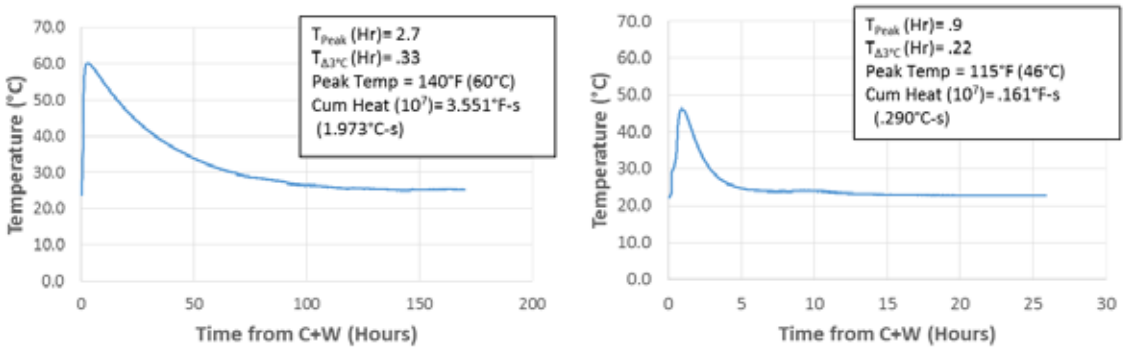

Figure 7.12: Mixture P-1 Q-drum and cylinder calorimetry

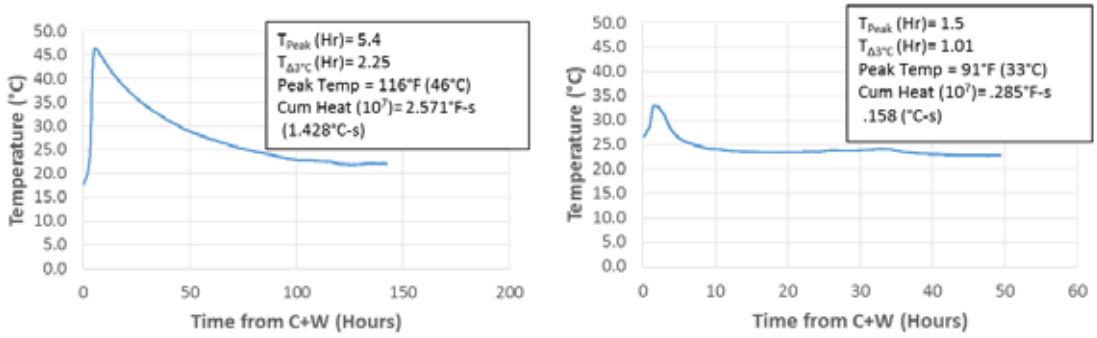

Figure 7.13: Mixture P-2 Q-drum and cylinder calorimetry

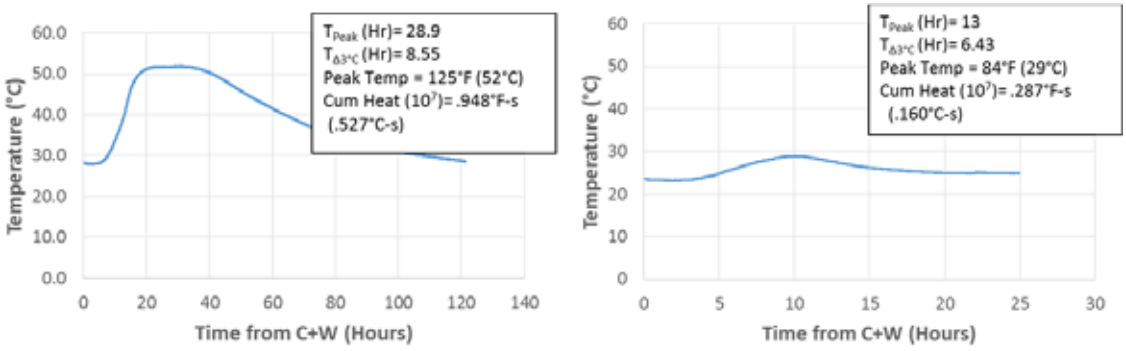

Figure 7.14: Mixture P-3 Q-drum and cylinder calorimetry

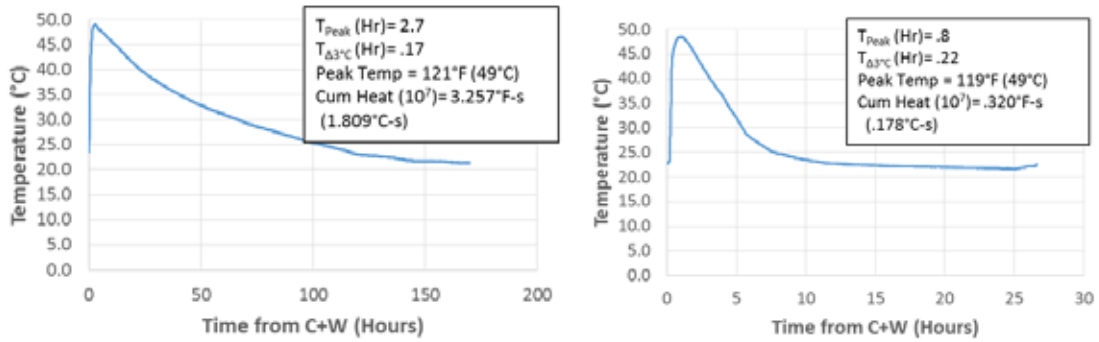

Figure 7.15: Mixture P-AAFA Q-drum and cylinder calorimetry

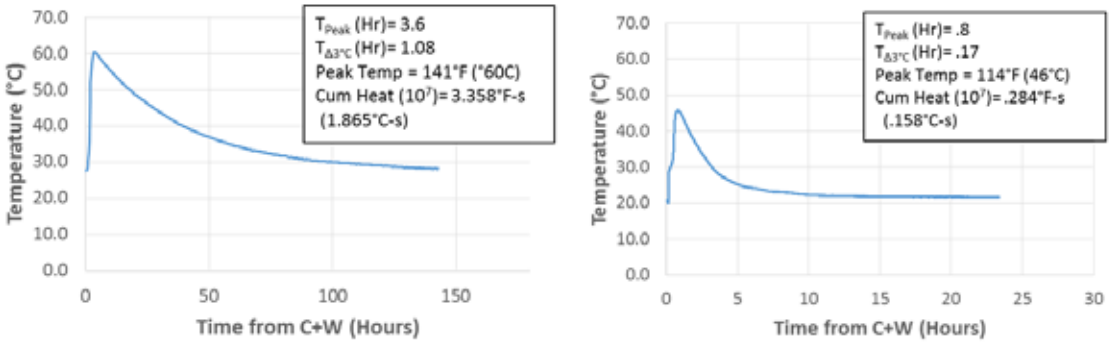

Figure 7.16: Mixture CSA-1 Q-drum and cylinder calorimetry

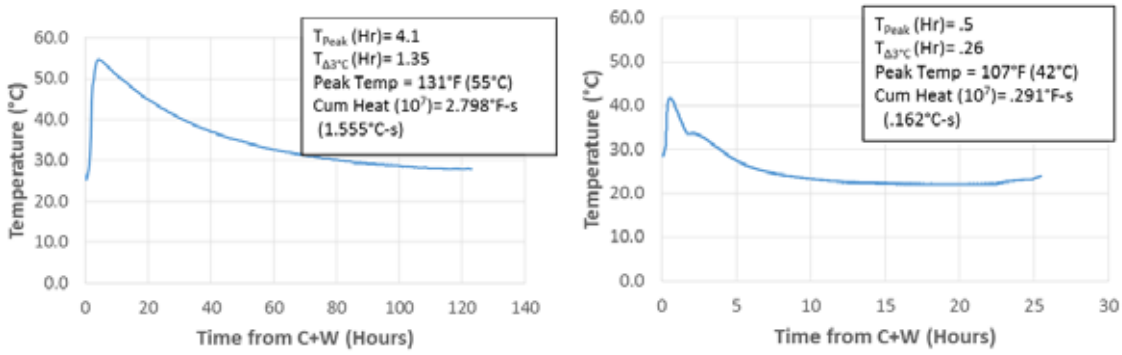

Figure 7.17: Mixture CSA-2 Q-drum and cylinder calorimetry

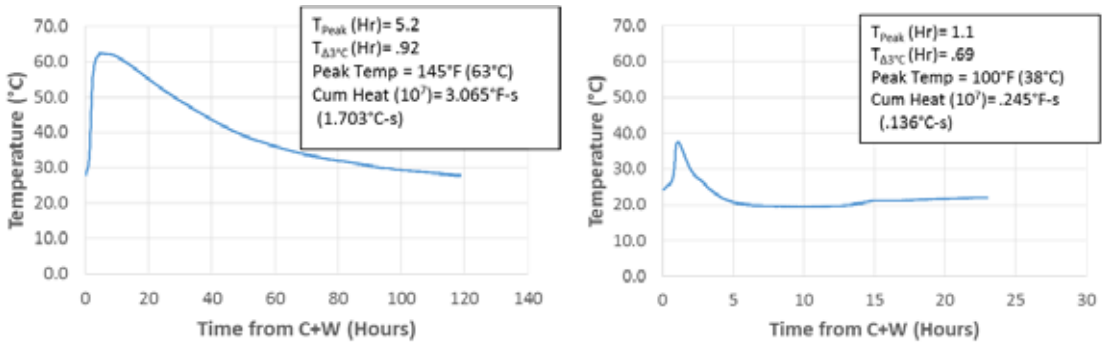

Figure 7.18: Mixture CSA-3 Q-drum and cylinder calorimetry

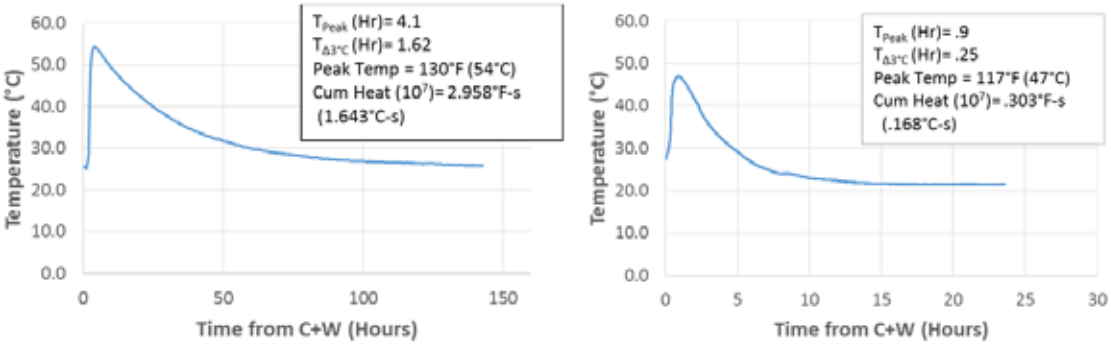

Figure 7.19: Mixture CSA-Latex Q-drum and cylinder calorimetry

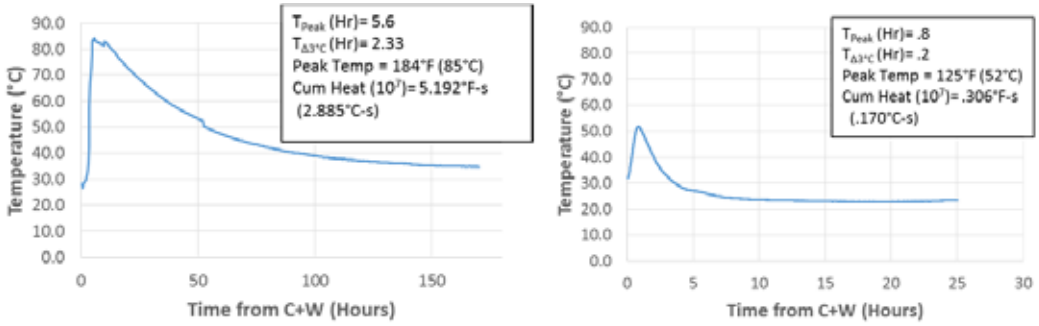

Figure 7.20: Mixture CAC-1 Q-drum and cylinder calorimetry

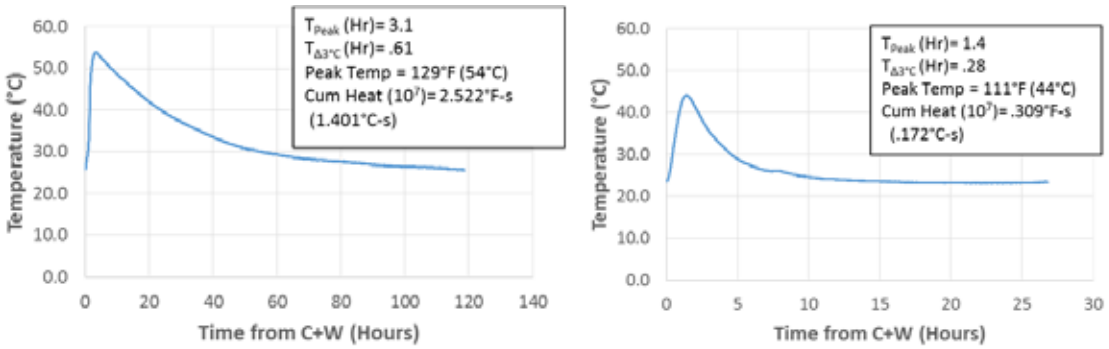

Figure 7.21: Mixture CAC-2 Q-drum and cylinder calorimetry

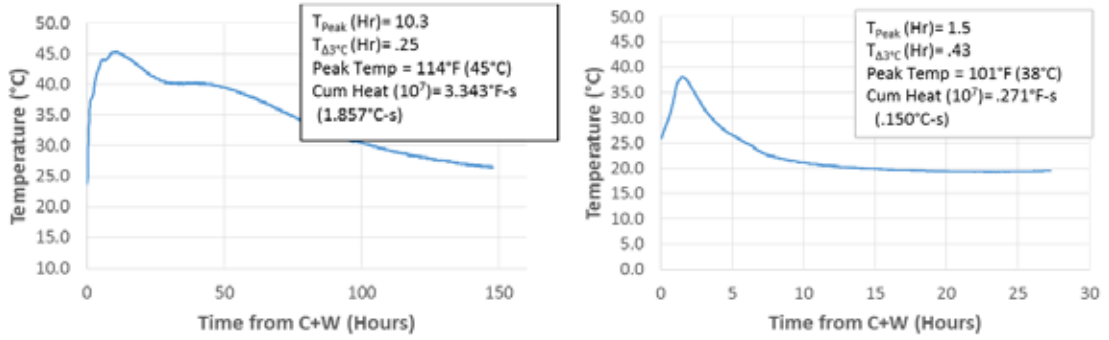

Figure 7.22: Mixture CAC-3 Q-drum and cylinder calorimetry

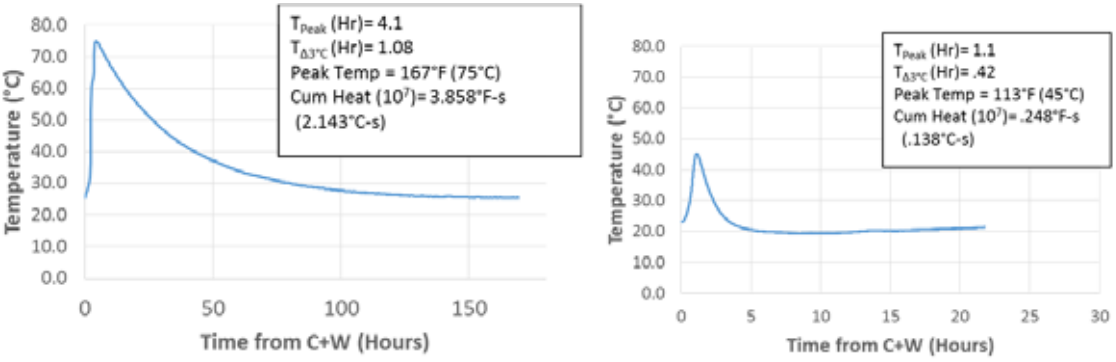

Figure 7.23: Mixture CAC-Latex Q-drum and cylinder calorimetry

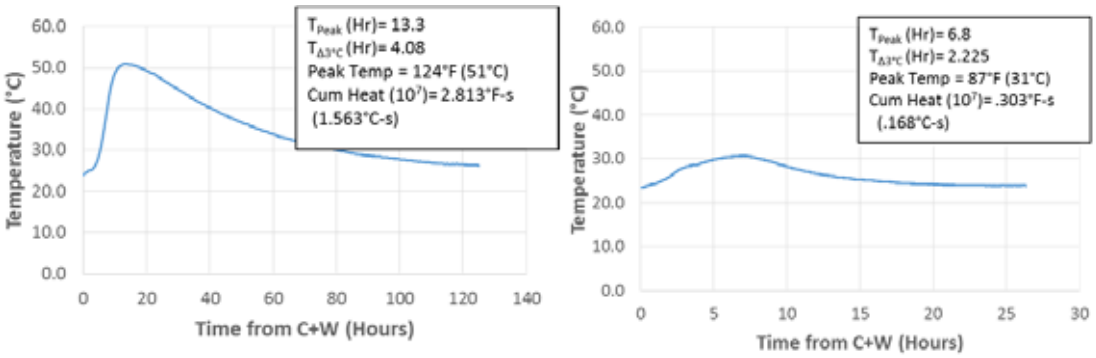

Figure 7.24: Mixture PC Type III Q-drum and cylinder calorimetry

7.5 Temperature Gradient Slabs

As mentioned previously, thermal gradients can present problems for rapid repair materials when the exothermic reaction, occurring during cement hydration, produces high early-age heat generation before the repair generates sufficient strength. The temperature differential between the center of the element and the surface causes thermal stresses to be formed; these stresses can cause thermal cracking if the stress exceeds the tensile strength of the concrete. This is normally an issue when there is a cooler environment and the rapid repair material generates a high early-age heat even at this lower temperature. The CAC mixtures presented this behavior during the isothermal calorimetry study at 50 °F (10 °C) where the heat evolution was more rapid and higher than at 73 °F (23 °C).

For this study the team cast three different temperature gradient slabs with varied depths. The dimensions for these slabs were chosen to simulate the common depths for rapid repair materials and each temperature slab remained in their respective wooden formwork for the entire test. The goal was to measure the temperature differential from the center of a slab at 1-in. (25.4 mm) increments for the Phase III mixtures. The research team wanted to examine the time to peak heat, the time to a 3 °C increase, the peak temperature, and the cumulative heat generated, as well as the temperature differential of 1 in. (25.4 mm) from the top surface and the mid-depth of the slab in a 73 °F (23 °C) environment. If this temperature differential is large enough and occurs early in the hydration of the repair materials, then thermal cracking may be of concern.

7.5.1 Experimental Procedures

The temperature gradient slabs were mixed in a 9 ft^3 (.25 m^3) steel drum mixer per the mixing procedure laid out by Zuniga (2013). The dimensions for these slabs were a 2.5 ft x 2.5 ft cross section with depths of 2, 4, and 6 in. Before mixing, the formwork was constructed of common lumber and plywood, while plastic rods were cut to 1, 3, and 5 in. and epoxied to the center of the formwork. Then, Type J thermocouples were tied to the plastic rods at 1-in. (25.4 mm) increments, starting from the bottom of the formwork, to record the temperature.

On the mixing day, the wooden formwork was lubricated with form oil to preserve the formwork and the data logger was initiated. The mixing time was recorded so that the time to peak heat could be calculated. The three temperature slabs required 4.8 ft^3 (.14 m^3) of concrete and a mechanical vibrator was carefully used to consolidate the concrete without moving the thermocouples. Each of the mixtures was measured out to 120 hours from mixing time in a 73 °F (23 °C) environment. Figure 7.25 presents the three temperature gradient slab formworks.

Figure 7.25: The three temperature gradient slabs formwork

7.5.2 Results and Discussion

Figures 7.26 through 7.31 contain a maximum temperature gradient value from their respective 6-in. (152.4mm) deep slabs. The other properties were selected from the 4-in. (101.6mm) deep slab because this is a typical depth repair for bridge decks. The temperatures were recorded at every inch; however, for presentation purposes the data plotted is from the thermocouple at mid-depth for each of the slabs.

The two proprietary mixtures had a temperature differential of around 4 °F (2.2 °C) through 3 in. of concrete. The P-AAFA mixture had a faster heat generation, higher peak temperature, and more uniform temperature curves for each depth. The P-2 mixture seems to generate much less heat for the 2-in. (50.8mm) depth slab and all of the slabs seemed to take longer to dissipate the heat from the center of the member, thus resulting in larger cumulative heat values.

Both of these mixtures generated the highest temperatures and temperature gradients, which could be problematic if these mixtures were cast in cooler temperatures. The team observed no thermal cracking on any of the temperature slabs. A 10.13 °F (5.63 °C) temperature gradient through 3 in. of concrete is a significant difference. The CSA-1 mixture reached its peak temperature faster than the CAC-2 mixture; however, the CAC mixture seemed to present a more uniform heat evolution when altering the depth of the member.

The PC Type III mixture presented the slowest time to peak heat and highest cumulative heat among all of the mixtures, which was expected due to the nature of portland cement. Both of these mixtures were composed of mostly portland cement but the CAC-3 mixture had a 30% replacement of a rapid-setting blend to speed up heat evolution and strength gain triggered by ettringite formation. These two mixtures also have an interesting trend for the 2-in. (50.8mm) slab where the temperature curve dips below the ambient temperature immediately following the decrease of the hydration curve.

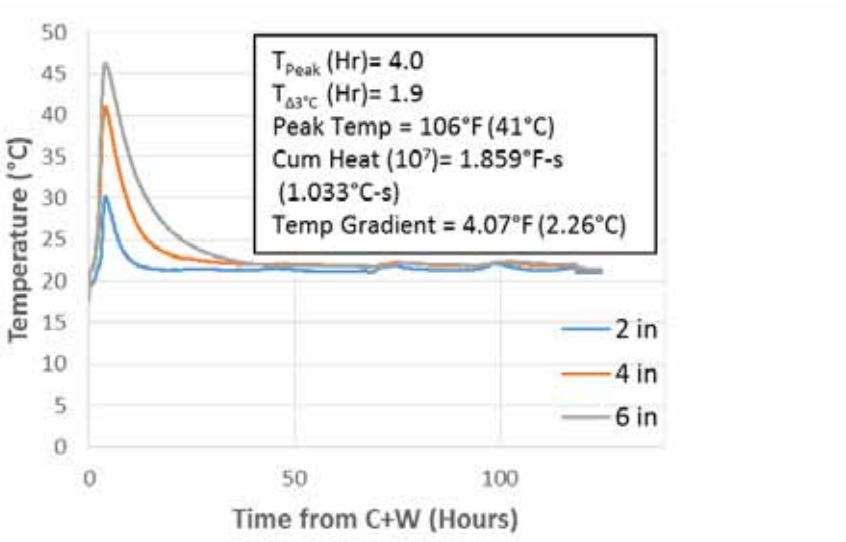

Figure 7.26: Mid-depth temperature for each of temperature gradient slabs for P-2 mixture

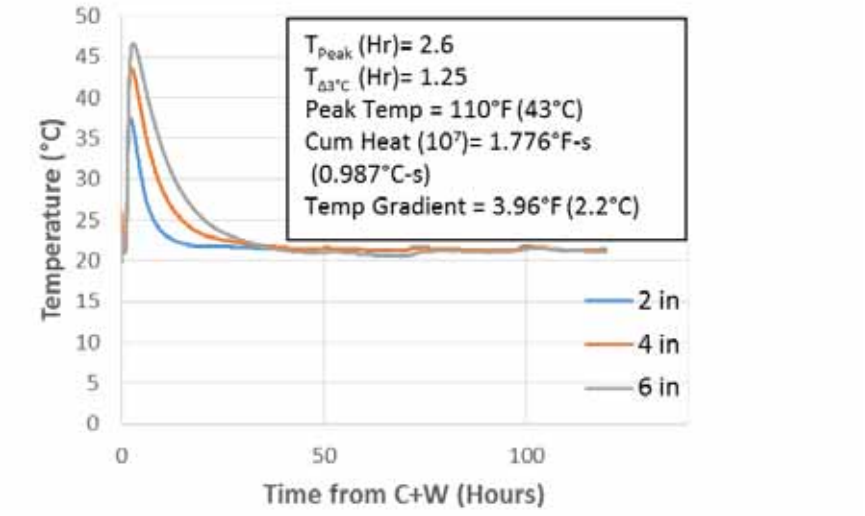

Figure 7.27: Mid-depth temperature for each of temperature gradient slabs for P-AAFA mixture

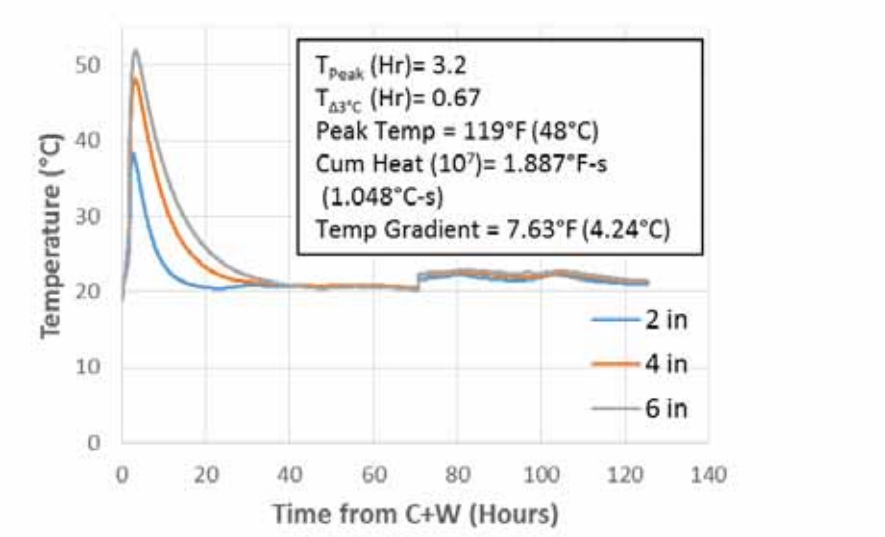

Figure 7.28: Mid-depth temperature for each of temperature gradient slabs for CSA-1 mixture

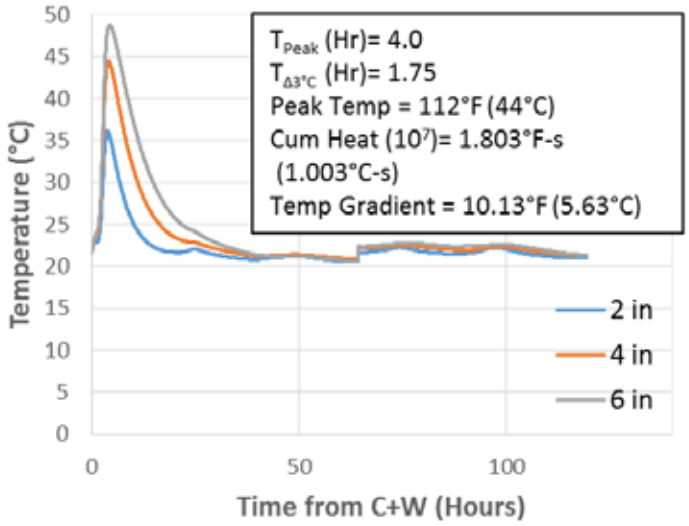

Figure 7.29: Mid-depth temperature for each of temperature gradient slabs for CAC-2 mixture

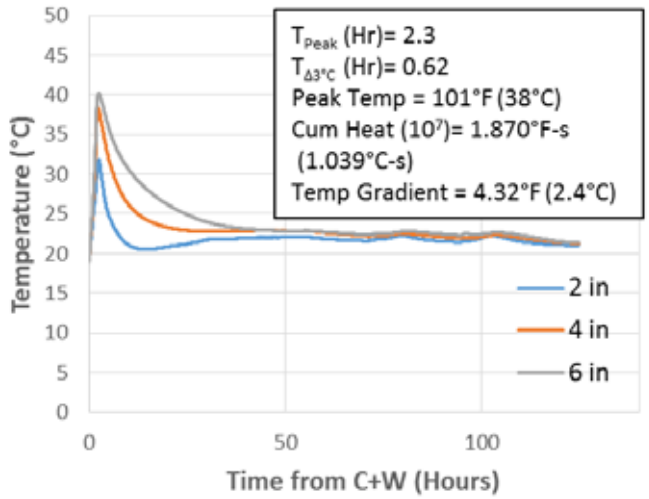

Figure 7.30: Mid-depth temperature for each of temperature gradient slabs for CAC-3 mixture

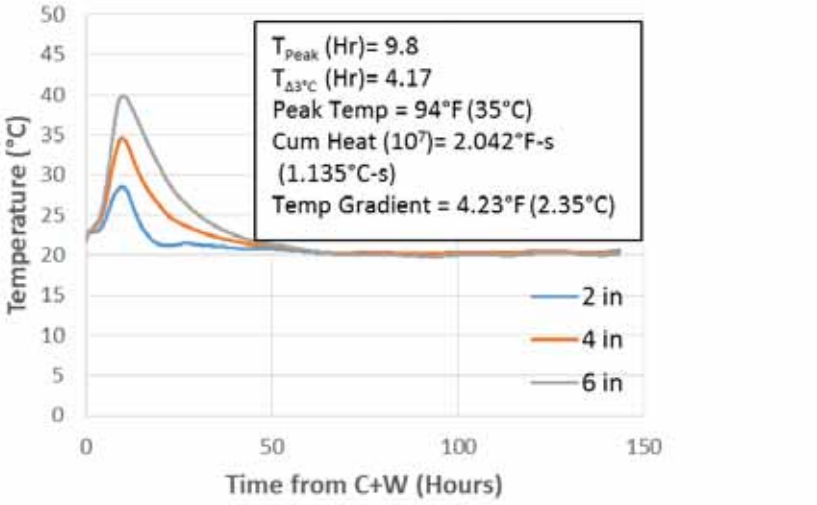

Figure 7.31: Mid-depth temperature for each of temperature gradient slabs for PC Type III mixture

7.6 Summary and Conclusions

The summary of the calorimetry performances of each binder system is as follows:

- The P-AAFA mixture has a rapid time to peak heat and generates about the same peak temperature when studied at 50 °F, 73 °F, and 100 °F (10 °C, 23 °C, and 38 °C).
- The CAC mixtures were the most variable as a whole, with the CAC-3 mixture having very slow heat generation, lower peak temperatures, and relatively no heat generation at 50 °F (10 °C) compared to the other three mixtures. Unlike the CAC-3 mixture, the remaining CAC mixtures had very rapid heat generation, highest peak temperatures, largest temperature gradient, and the best performance at 50 °F (10 °C) of any mixture.

- The CSA mixtures were retarded by the cooler temperatures at 50 °F (10 °C) but had a high temperature gradient at 7.63 °F (4.24 °C) when cured at 73 °F (23 °C). For semi-adiabatic calorimetry, these mixtures had around the same calorimetry properties and temperature curves.
- The mixtures containing mostly portland cement, P-3, and PC Type III had slower heat generation and lower peak temperature values than did the other rapid repair materials.

Chapter 8. Field Testing

8.1 Introduction and Background

The field performance of these rapid repair materials is a crucial aspect in this project. One of the biggest challenges in research is to overcome the disconnect between laboratory results and results in the field. The most practical method of correlating the two results is to implement the mixtures tested in the laboratory in the field. It is rather difficult to simulate live traffic loads and exposure conditions on rapid repair materials due to the size and nature of repairs; thus, the best method for measuring a material's service life is with implementation in the field.

As mentioned, the research team had an opportunity to use an existing series of bridge deck sections from a previously funded TxDOT project for applying a subset of repair materials. Sections of the decks were saw-cut and removed, so that the Phase III mixtures could be cast into six different repair sections, which are 2 ft x 12 ft (0.61 m x 3.66 m) in cross section and 4 in. (101.6 mm) in depth. The team measured fresh state properties, compressive strength, temperature gradients, and a complete visual inspection for cracking. These repair sections will provide the team with certain performance properties not witnessed in the laboratory.

TxDOT has an ongoing in-house research project evaluating pavement repairs using different rapid setting materials, including some of the rapid repair materials studied by the research team. One of the key objectives for the research team was to perform a visual survey of selected repair jobs performed by TxDOT prior to or during this project. To meet this objective, the team accompanied different TxDOT employees to a previous repair site in Cotulla, Texas. This site contained 12 highway pavement repairs cast with different repair materials; six of these materials were a part of the team's mixture matrix.

8.2 Materials and Mixture Proportions

The site visit mixture identifications are listed in Table 8.1; however, the proportions for the non-proprietary mixtures are unknown because the cast date was completed prior to the site visit. TxDOT followed instructions listed on the proprietary mixtures' bags, which are what the team followed for the P-1, P-2, and P-AAFA mixtures.

8.3 Simulated Bridge Deck Repairs

The simulated bridge deck repairs implemented at the research campus allowed for a multitude of tests on these repair materials in real-world exposure conditions. The repair section dimensions were chosen at long aspect ratios to promote transverse cracking due to large volume changes in the longitudinal direction. The team did not use reinforcement in order to examine which mix would resist cracking. Visual inspections for cracking were monitored daily for the first week and then the team examined the sections weekly; however, the majority of the cracking was generated in the first week following casting. The fresh state properties and compressive strength were measured at 73 °F (23 °C) for quality control and comparisons to previous mixes. Six cylinders were cast from the outdoor mixtures, which were left on the bridge decks for a comparison of compressive strengths at ambient and standard temperature. The

temperature of the repair sections was also recorded with thermocouples out to 5 days at different depths, in order to generate a temperature gradient profile for each repair section.

These bridge deck repairs were cast on three different dates grouped into two casting periods. The P-2, PC Type III, and P-AAFA mixtures were cast on August 13, 2013. The CAC-3 mixture was cast on the following day. Figure 8.1 is an image of one of the bridge deck sections and schematic of these bridge decks.

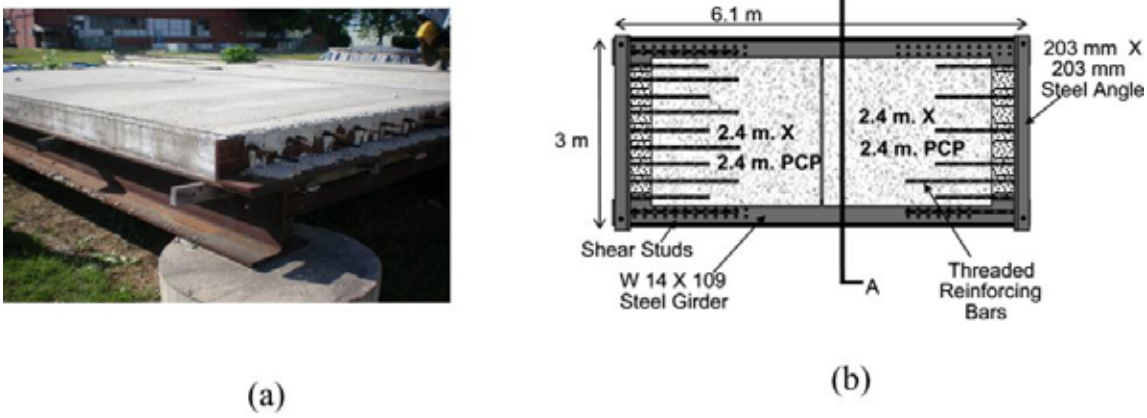

Figure 8.1: Large-scale bridge deck elements: A) Photo; B) Schematic

8.3.2 Experimental Procedures

Prior to mixing, the repair section needed to be construction, prepped, and instrumented. The first task was the removal of concrete by a concrete wet-saw, two 90-pound pneumatic jackhammers, and sandblasting equipment. Once the deteriorated concrete and excess blast sand had been removed, a hammer drill was used to create a hole for plastic rods cut to 4 in. (101.6mm). These plastic rods were epoxied into the holes and thermocouples were attached at 1, 2, and 3 in. (25.4mm, 50.8mm, and 76.2mm) depths with zip ties to be monitored by a datalogger.

All of the mixture materials were placed in a 73 °F (23 °C) environment 24 hours before mixing. Each repair material was cast indoors for the fresh state properties and the majority of the compressive cylinders, as well as outdoors for the repair section and six compression cylinders for comparison. The indoor mixture was produced in a 4 ft^3 (.11 m^3) steel drum concrete mixer where the slump, unit weight, air content, and 18 4-in. x 8-in. (101.6 mm x 203.2 mm) compression cylinders were cast. The 4-in. x 8-in. (101.6 mm x 203.2 mm) cylinders were consolidated on a vibrating table and immediately capped for a 24-hour curing period.

The outdoor mixture required 10 ft^3 (.28 m^3) of concrete to fill the repair section. Mixing this large amount of concrete required two 9 ft^3 (.25 m^3) concrete drum mixers, which were placed on top of the bridge decks to allow for a direct pour from the mixer to the repair slot. On the morning of each cast date, the repair section was lightly sprayed with water to pre-wet the concrete to prevent the existing substrate from pulling water from the repair mixture. After the concrete was poured into the repair sections, the mixture was vibrated, finished, and cured with wet burlap. The P-AAFA mixture was the only repair section not wet-cured per the manufacturer's instructions. Six 4-in. x 8-in. (101.6 mm x 203.2 mm) cylinders were also cast,

rodded, and left on the decks for an ambient temperature cure to simulate compressive strength of the repair.

8.3.3 Results and Discussion

Images of these experimental procedures previously described, along with tables for fresh state properties and a cracking log for the Phase III mixtures, can be found in Appendix E. This section will include discussion on the compressive strength generation, heat evolution analysis, and crack mapping for the Phase III mixtures.

Figure 8.2 presents the compressive strength data of the six Phase III mixtures measured out to 12 hours. The compressive cylinders were tested to 28 days but the team focused on the early-age strengths. All of the mixtures (excluding the PC Type III mixture) reached 3000 psi (20.7 MPa) compressive strength by 3 hours, which was one of the criteria TxDOT established for these repair materials. The CSA-1 and P-2 mixtures presented the most rapid strength gain of the repair materials, while the CAC-2, CAC-3, and P-AAFA mixtures had similar strength gains up to 6 hours.

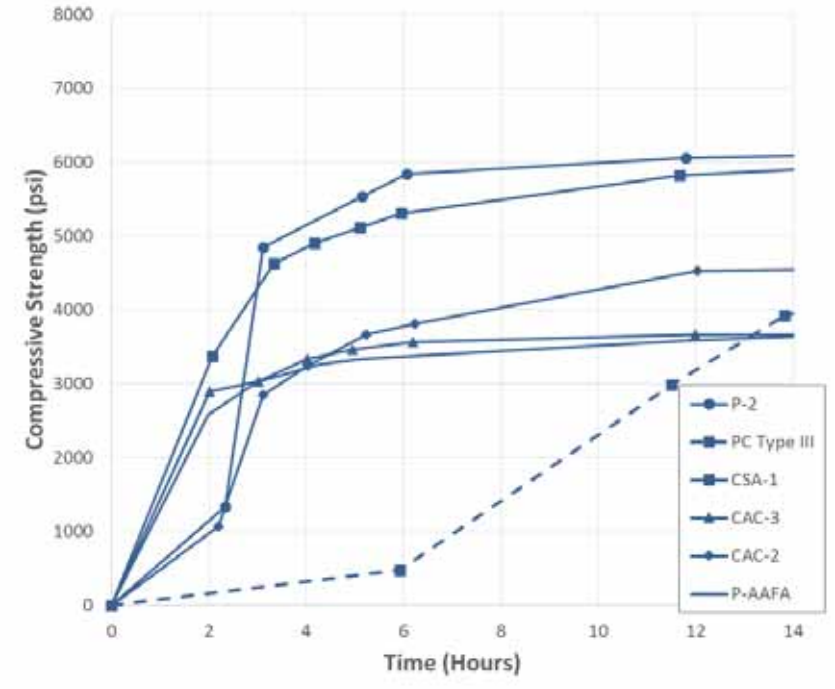

Figure 8.2: Compressive strength curves for Phase III mixtures

Figures 8.3 and 8.4 represent the temperature analysis for the thermocouple placed at mid-depth for all six mixtures included in the simulated bridge deck study. Of the four mixtures in the first cast period, the CAC-3 mixture generated the highest temperature, which occurred on a day with a cooler ambient temperature. The CAC-3 mixture also presented an early small peak that represents the ettringite system responsible for early strength gain, as well as a higher peak about 12 hours later that could represent the portland cement hydration. After the first 24 hours for each mixture, the heat generation is complete as seen in isothermal calorimetry; therefore,

any discrepancies in temperature past the first day are related to the amount of heat absorbed from direct sunlight for darker shades of concrete.

The second cast period compared the CAC-2 and P-AAFA mixtures, indicating that the CAC mixture generates more heat than the proprietary mixture. An interesting trend for the P-AAFA mixture is that by the fourth day the concrete was generating only as much heat as the ambient temperature. This development did not occur in any of the other mixtures.

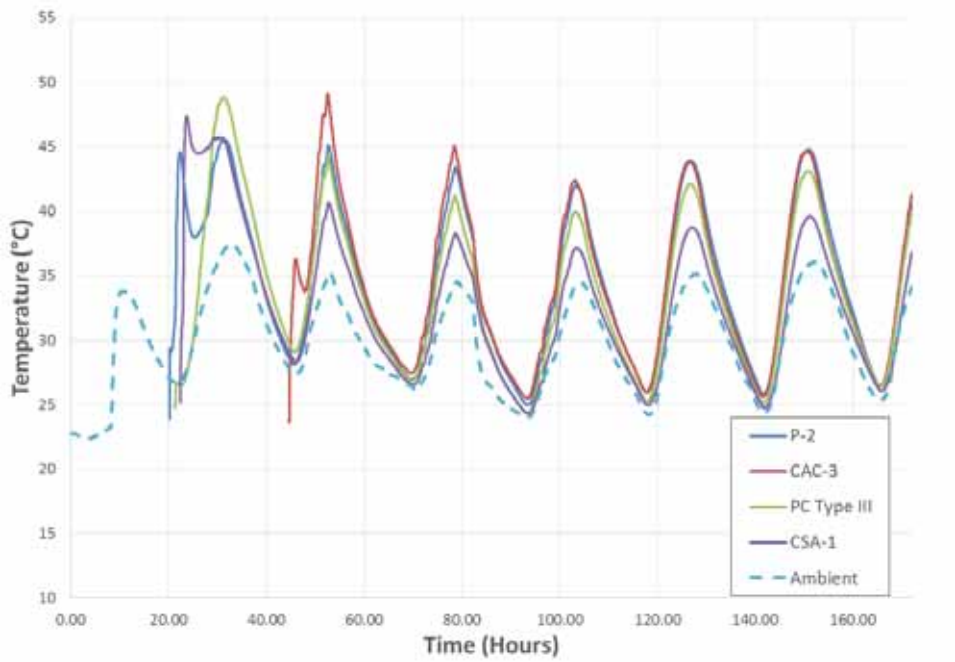

Figure 8.3: Temperature analysis for first cast period

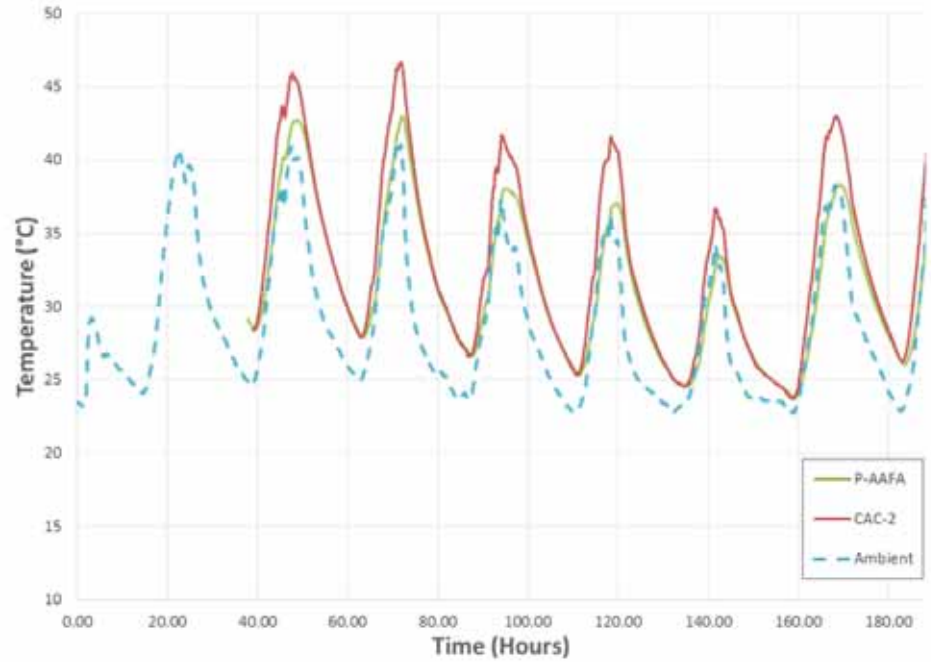

Figure 8.4: Temperature analysis for second cast period

Figures 8.5 and 8.6 represent the temperature gradients measured for all six of the Phase III mixtures. The gradients were measured from top and bottom thermocouple and the largest gradients for each mixture were within the first 24 hours. After the first 24 hours, the slab is heating and cooling with the ambient temperatures with an average peak differential of 6 °C. The CAC-3 mixture exhibited the highest temperature differential of all the Phase III mixtures. However, the second cast period ambient temperature was lower, so a fair comparison cannot be made. Just as before, after the fourth day the only difference between the temperatures measured in each mixture was based on how much heat is absorbed from the environment.

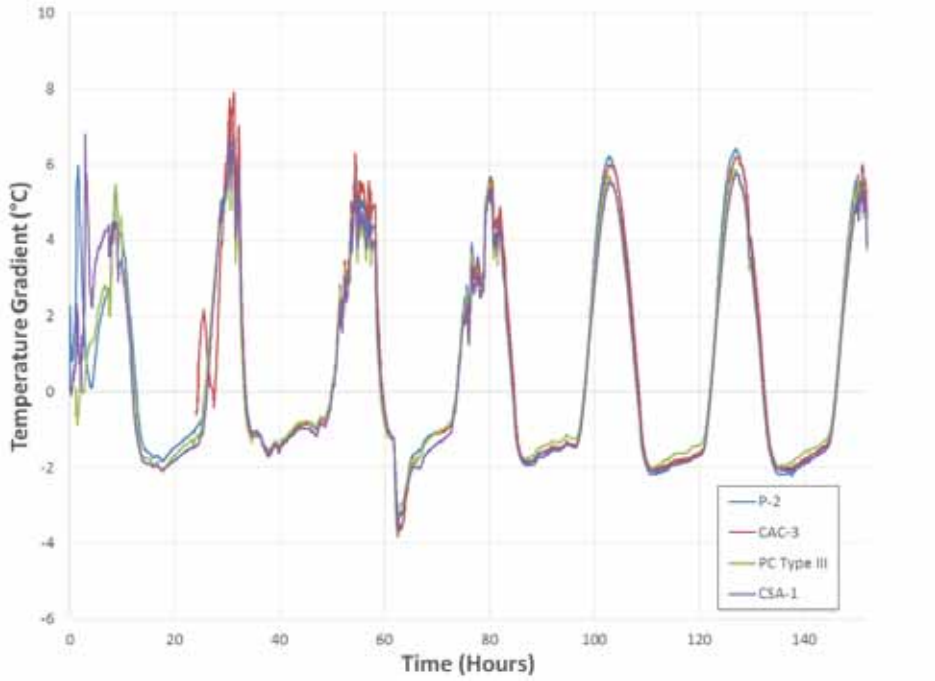

Figure 8.5: Temperature gradients for first cast period

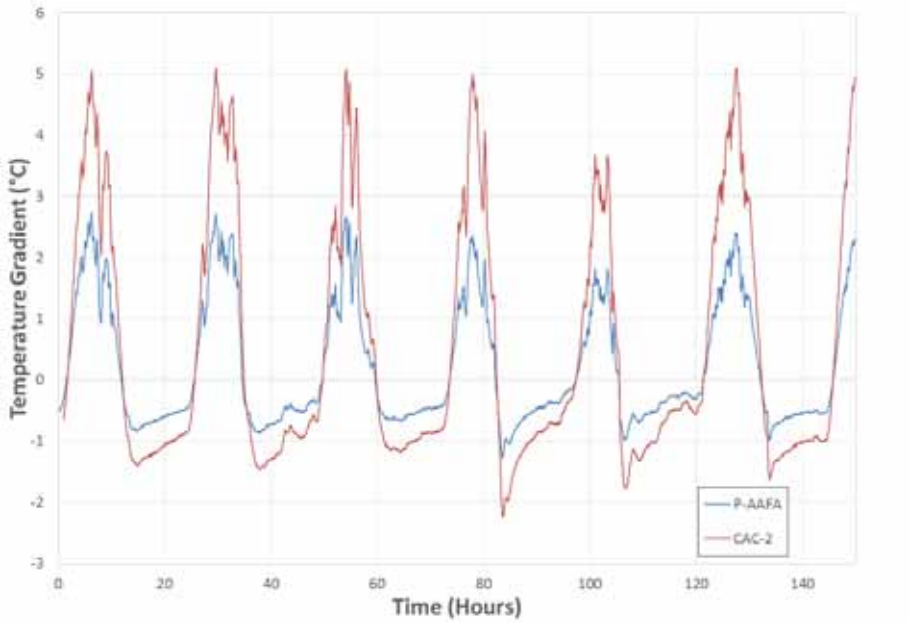

Figure 8.6: Temperature gradients for second cast period

Figure 8.7 presents a crack map of the all six repairs at 6 months from each cast period. It is important to note that all of the cracking occurred in the first 7 days, except for the crack in the center of the P-AAFA repair. All of the other mixtures obtained a crack in the center of the repair within 72 hours. The P-2 and CAC-3 mixtures were cast into a bridge deck with fibers in the existing concrete, which could have resisted movement during temperature changes, thus causing stresses and cracking when the repairs were trying to expand and shrink with changes in temperature. The CAC-2 mixture seemed to have excess water on the casting day, which could have contributed to drying shrinkage cracking when the concrete was acclimating to the environment.

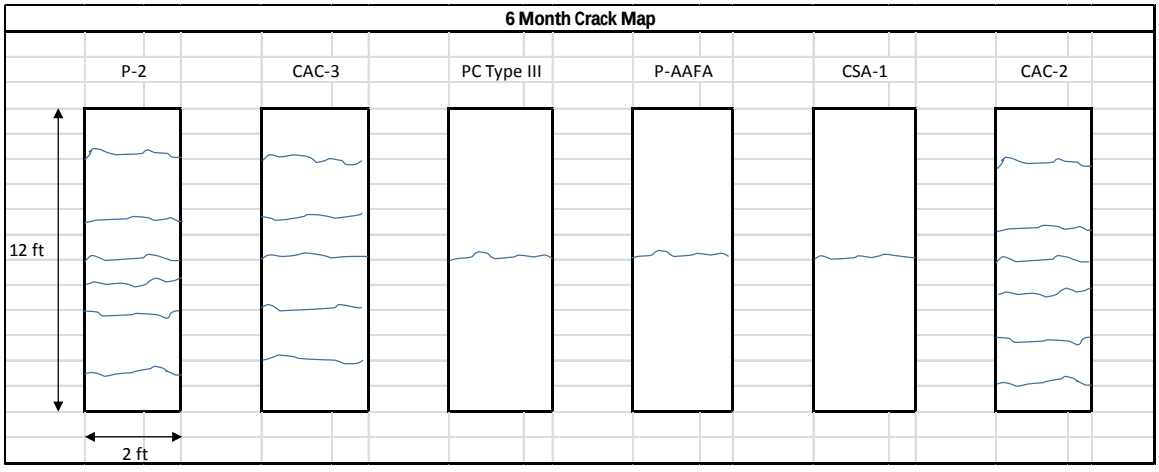

Figure 8.7: Crack map of bridge deck repairs

8.4 Highway Repair Evaluation

The highway repair evaluation was a part of the key objectives selected by the research team because of the importance of field performance data. Unfortunately, the casting date occurred before the team was notified about the repair site but some details were given from the mixing day. TxDOT had the producers of each repair material tested come to the site on the casting date and place their respective material. This plan was implemented in order to have each material placed in the correct fashion, so that the mixing variable could be removed, allowing testing of only the durability and service life of the repair.

The site visited was just outside of Cotulla on a divided four-lane highway. The site was composed of 12 repair sections; 6 of these sections contained materials tested by the research team. The six mixtures implemented were P-1, P-2, P-AAFA, CSA-1, CSA-2, and CSA-3. All of these mixtures were cast in November of 2012 and the research team inspected the site 8 months later in July of 2013. The team focused on a visual inspection, crack mapping, measurement of crack width, and soundness testing.

8.4.1 Experimental Procedures

First, the traffic control crew blocked off the highway lane containing all 12 repair sections. The research team, along with a TxDOT team, began examining each of the repairs. The dimensions of each repair were reported, along with the distance between transverse cracking, any crack width, notation of longitudinal cracking if occurred, delamination, spalling, and any visual details. Pictures were taken of each repair to note any interesting characteristics and one of the TxDOT engineers checked the bond of the repair by tapping the repair with a hammer and listening for a dull sound.

After the site investigation, the research team and TxDOT engineers shared reports and resources to allow for a more detailed evaluation of the repair sites.

8.4.2 Results and Discussion

This section will discuss the results from Table 8.1 for each mixture implemented at the Cotulla site.

Table 8.1: Cotulla site visit cracking information

	Repair Dimensions (inches)		Cracks			Cast Date Information		
Material	Length	Width	Transverse (No or Spacing)	Longitudinal	Max (inches)	Date	Temperature (°F)	Weather Conditions
P-1	48	20	No	Yes	0.008	11/1/2012	90	Foggy Morning
P-2	60	20	No	No		11/13/2012	70	Cloudy, light wind
P-AAFA	137	21	20 to 34"	No		11/14/2012	50	Cloudy, light rain
CSA-1	57	18	(1) @ 17" from outside	No	0.03	11/14/2012	50	Cloudy, light rain
CSA-2	79	21	8 to 15"	No	0.03	11/14/2012	50	Cloudy, light rain
CSA-3	138	28	No	No		11/1/2012	90	Foggy Morning

Of the proprietary mixtures at the repair site, only the P-1 mixture was not strong enough to resist the previous longitudinal crack and the surface was slightly worn with a brown coloration. The P-2 mixture performed very well, and did not show any transverse or longitudinal cracking, which indicates the repair material is both compatible with the existing concrete and strong enough to resist the original crack. The P-AAFA mixture proved to have a very rapid setting time because the material formed a cold joint where one of the batches set up.

This caused some delamination, which was observed when tapping the hammer on the repair, but the material resisted the original crack. There were transverse cracks about every 2 ft but the surface showed little degradation from traffic.

All of the CSA mixtures were strong enough to resist the previous longitudinal crack; however, the CSA-1 and CSA-2 mixtures had transverse cracks. The CSA-2 mixture had multiple cracks at about every 12 in. (304.8mm), which could suggest that the repair was not compatible with the existing pavement. The surface of the CSA-2 mixture was in good condition and showed little degradation due to traffic loads and friction. Only one transverse crack appeared in the CSA-1 mixture, on the wheel path; there was some plastic cracking. The CSA-3 mixture performed very well and showed no cracking or surface deterioration.

8.5 Summary and Conclusions

The summary of the field performance of selected mixtures is as follows:

- All of the Phase III mixtures, excluding the PC Type III mixture, reached 3000 psi (20.7 MPa) at 3 hours after mixing for the simulated bridge deck repair.
- After the first 24 hours of the temperature gradient analysis, the heat evolution for each mixture had dissipated and the fluctuation in temperatures was due to the fluctuation in the ambient temperature.
- The CAC-3 mixture generated the highest heat and heat differential of all the other Phase III mixtures. It also presented a quicker ettringite-induced peak followed by a larger delayed peak approximately 8 hours later, which could be the portland cement hydrating.
- The P-AAFA mixture emitted as much heat as the ambient temperature 4 days after mixing, while the other mixtures experienced slightly elevated temperatures.
- All of the cracking in the repair sections occurred within the first 7 days after casting, except for the P-AAFA mixture.
- The CAC-2 mixture seemed to have excess water that could have contributed to drying shrinkage or plastic cracking.
- The P-2 and CSA-3 mixtures performed the best at the Cotulla site; neither showed cracking or surface defects after 8 months of frequent and high axle loads.
- All three CSA mixtures have performed well, so far. The only issue is the transverse cracking with the CSA-2 mixture but this could suggest that it is not compatible with the existing pavement.

Chapter 9. Freezing-and-Thawing Cycles and Salt Scaling Resistance

9.1 Introduction and Background

Although Texas is generally considered a hot weather state, parts of Texas, primarily north of Interstate 20, can be subject to harsh freezing-and-thawing cycles during the winter months. These cycles may cause damage within the concrete's structure as water within the pores changes phase from liquid to solid.

The specific mechanisms relating to individual tests will be discussed later, but a well-distributed matrix of fine air bubbles allows for relief of the osmotic and hydraulic pressures and helps prevent damage from freezing-and-thawing cycles. To accomplish this, an air-entraining admixture must be added to the concrete during mixing in order to produce the desired air-void system.

9.2 Materials and Mixture Proportions

A 4 ft^3 steel drum concrete mixer was used to produce the concrete that was used to measure air in fresh concrete, hardened air, and materials subjected to freezing, thawing, and salt scaling. It should be noted that the mixing procedure is further described in Zuniga (2013). When making use of proprietary and premanufactured concrete blends, the research team followed the provided manufacturers mixing instructions.

A synthetic air-entraining admixture complying with ASTM C 260 was used in mixtures CAC-1, CAC-2, CAC-3, and PC Type III. Individual dosage varied between materials due to previous tests performed in Zuniga (2013). During Phase I testing, each material was tested approximately three times with a goal of a stable fresh air content between 5 and 7%. This percentage is widely accepted as reducing or eliminating the damage from freezing and thawing for small-sized aggregate due to the relative air content in the paste. The final dosages of the air-entraining admixture are shown in Table 9.1

Table 9.1: Final dosage of air-entrainment admixture for Phase II and III testing

Material	AEA (oz/cwt)
P-1	--
P-2	--
P-3	--
P-AAFA	--
CSA-1	--
CSA-2	--
CSA-3	--
CSA-Latex	--
CAC-1	0.25
CAC-2	0.25
CAC-3	1
CAC-Latex	--
PC Type III	0.15

A subset of the Phase II and III materials did not receive any air-entraining admixture due to various constraints. These constraints are listed as follows:

- P-1, P-2, P-3, P-AAFA: These materials are pre-manufactured bags with all required materials. Since the contents of these materials are not completely known, it is assumed that an air-entrainment admixture or other mechanism making it resistant to freezing-and-thawing damage is included.
- CSA-Latex, CAC-Latex: With the addition of styrene-butadiene latex, the manufacturer recommends not using an air-entraining admixture.
- CSA-1, CSA-2, CSA-3, CSA-Latex: The manufacturer stated that materials composed of CSA would not require additional air-entraining admixtures to maintain resistance to freezing-and-thawing damage.

9.3 Air Void Analysis

An air-entrainment admixture stabilizes a system of evenly distributed small and stable air bubbles throughout the concrete by introducing surface-acting molecules into the concrete. These molecules have two ends: one hydrophobic and one hydrophilic (Mindess, Young, & Darwin, 2003). The hydrophobic end repels water as the hydrophilic end attracts it, creating bubbles as schematically shown in Figure 9.1.

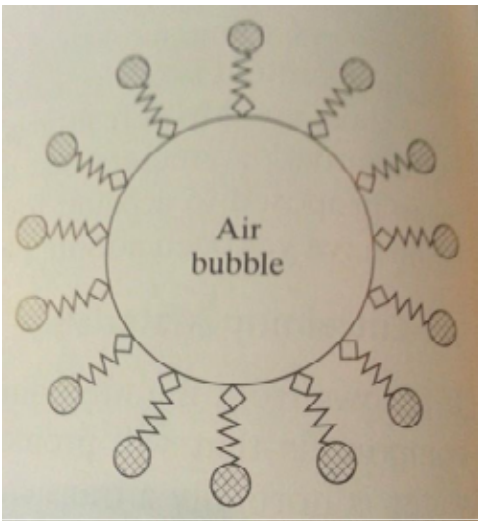

Figure 9.1: Schematic of air-entrained air bubble displaying the admixtures hydrophobic and hydrophilic ends (Mindess, Young, & Darwin, 2003)

It is important to note that air-entraining admixtures are specifically formulated to allow a uniform spacing of these bubbles. Various factors can affect the actual amount of entrained air, so each material was tested separately in Phase I, as shown in Zuniga (2013), to determine an appropriate amount of air-entrainment admixture.

To quantify the effectiveness of air-entraining agents or the entrapped air content of a concrete material, two forms of air void analyses were performed. First, a fresh air analysis was performed using an air chamber and following ASTM C 231. This procedure produces a value for the air present during the fresh state. Although this closely correlates to the hardened air that actually protects from freezing-and-thawing damage, it does not provide any information regarding the size and spacing of bubbles, just the total volume of air.

To analyze the hardened air content, hardware and software for RapidAir 457 was used. This combination allows a statistical analysis of filled air voids to determine not only the air content as a percentage, but also other significant values. These values include, but are not limited to, the specific surface and spacing factor, which, in combination with the air content allows the quality of the air to be more completely determined. This apparatus employs image analysis as a method of evaluating the air-void system.

9.3.1 Experimental Procedure

9.3.1.1 Air Entrainment

The concrete mixing procedure followed is outlined in Zuniga (2013). When using an air-entraining admixture, it is important to add liquid admixtures as a solution in the mixing water because the water is normally added per ASTM C 192. This mixing procedure allows for full engagement of the air-entraining agent and distribution of the air matrix throughout the concrete.

9.3.1.2 Fresh Air Analysis

The fresh air analysis was performed along with casting of hardened air samples, salt scaling specimens, and freeze-thaw specimens. The amount of air entrainment was established during the initial Phase I testing. Fresh air content was measured in accordance to ASTM C 231 using a Type B pressure meter. Despite the rapid-setting nature of the majority of Phase II and III materials, the material was rodded in the pressure chamber (versus vibration) and ASTM C 231 was performed normally.

9.3.1.3 Hardened Air Void Analysis

To perform a hardened air void analysis, 4-in. (102 mm) diameter cylinders were cast simultaneously with fresh concrete used for fresh air analysis. These cylinders were then moist cured for 28 days and then frozen until the hardened air void analysis could be completed.

First, specimens were cut twice along the length using a wet saw, as shown in Figure 9.2, to approximately 0.5 in. (13 mm) thickness. The sawing must be done carefully to give as uniform a surface as possible and to prevent burrs or other breakage deformities along the edges (Ley, 2007).

Figure 9.2: Wet saw used for cutting hardened air specimens

After cutting, specimens were allowed to dry for approximately 24 hours. The following steps were performed in accordance to Appendix B of Ley (2007), with special consideration of the thoroughness of the procedure. Polishing of the specimens was done with the table and nickel-plated diamond discs with magnetic backing obtained from ASW Diamond (shown in Figure 9.3) with various grits.

Figure 9.3: Polishing table and various grit plates for polishing hardened air specimens

Upon drying, specimens were blackened with the use of permanent rounded-tip Sharpie markers with strokes in one direction and left to dry for another 24 hours. After this time had passed, specimens were blackened in the direction perpendicular to the original strokes to create a more uniform dark appearance. They were then allowed to dry for another 24 hours.

Next, the voids were filled with barium sulfate ($BaSO_a$) powder to create contrast in the specimen. This powder is shown in Figure 9.4:

Figure 9.4: Barium sulfate to fill air voids in colored concrete section

To apply the powder, it was gathered onto the specimen using a small metal lab spoon. These piles were then pressed into the voids with the use of a large rubber stamp. Next, the specimen was shaken to remove any loose powder and a bare, dry palm passed over the surface to clean any material not trapped in the voids. The process of applying powder and removing excess was then repeated until all voids were filled satisfactorily. The objective is to generate a dark background upon which the white air voids can be easily identified by the image analysis program.

After filling the voids, care must be taken so only voids within the past fraction of the concrete is "read" by the program. To do this, any voids within the coarse aggregate portion of the sample were blackened using Sharpie markers. The final sample, as shown in Figure 9.5, was ready for analysis.

Figure 9.5: Example of final concrete specimen ready for use in RapidAir system

After the sample preparation, the specimens are mounted in the RapidAir hardware shown in Figure 9.6. The hardware and software allow a computerized version of the modified point count given in ASTM C 457, with each sample only taking a few minutes.

Figure 9.6: RapidAir system used for performing hardened air void analysis

9.3.2 Results and Discussion

The hardened air void analysis and comparison of fresh and hardened properties of the various materials yielded the results shown in Table 9.2.

Table 9.2: Comparison of fresh & hardened air void analyses for Phase II & III materials

Material	Additional AE (oz/cwt)	Fresh Air Content (%)	Hardened Air Content (%)	Specific Surface	Spacing Factor
P-1	--	1.5	2.83	1063.0 1/in	0.0053 in
				41.9 1/mm	0.1346 mm
P-2	--	3.9	5.09	466.2 1/in	0.0104 in
				18.4 1/mm	0.26416 mm
P-3	--	3.5	4.5	629.7 1/in	0.009 in
				24.8 1/mm	0.2286 mm
P-AAFA	--	3	2.63	714.1 1/in	0.01 in
				28.1 1/mm	0.2540 mm
CSA-1	--	2.75	10.5	772.6 1/in	0.0043 in
				30.4 1/mm	0.1092 mm
CSA-2	--	10	18.72	571.7 1/in	0.0036 in
				22.5 1/mm	0.0914 mm
CSA-3	--	3.5	3.75	767.3 1/in	0.0076 in
				30.2 1/mm	0.1930 mm
CSA-Latex	--	3.9	5.18	646.4 1/in	0.0079 in
				25.4 1/mm	0.2006 mm
CAC-1	0.25	8	14.1	463.8 1/in	0.0054 in
				18.3 1/mm	0.1372 mm
CAC-2	0.25	7.5	12.66	477.7 1/in	0.0051 in
				18.8 1/mm	0.1295 mm
CAC-3	1	5	5.4	605.8 1/in	0.0085 in
				23.9 1/mm	0.2159 mm
CAC-Latex	--	4.5	3.79	423.7 1/in	0.0136 in
				16.7 1/mm	0.3454 mm
PC Type III	0.15	5	2.395	726.9 1/in	0.0101 in
				28.6 1/mm	0.2565 mm

In most situations, fresh air content is used to determine the appropriateness of concrete for freezing-and-thawing conditions in the field. As previously stated, a fresh air content of 5 to 7% is appropriate for most conditions. Based on this value, all materials except CSA-2, CAC-1, CAC-2, CAC-3, and PC Type III were below the lower bound for use when using the ASTM C 231 test. Various materials, including CSA-2 and CAC-2, were above this 7% value, with 10% and 7.5% air respectively.

According to ASTM C 457, the spacing factor is the most important factor in determining theoretical freezing-and-thawing resistance of a particular cement paste matrix. The standard quantifies the maximum spacing factor required to gain a moderate resistance to freezing and thawing as 0.008 in. (0.20 mm). The corresponding specific surface (alpha) is also limited to 1100 $in.^{-1}$ (45 mm^{-1}) for moderate freezing-and-thawing resistance.

Of the 13 Phase II and III materials, four exceeded the maximum spacing factor given in ASTM C 457 for moderate freezing-and-thawing resistance. These materials are P-3, P-AAFA, CAC-3, CAC-Latex, and PC Type III. All materials meet the specific surface value. In later sections, a comparison will be made from these relevant air content values and the specific materials' resistance to salt scaling and freezing-and-thawing damage.

9.4 Salt Scaling

Salt scaling is a mechanism in concrete that causes deterioration of the finished surface due to cyclical freezing and thawing. This is particularly relevant in the flatwork that is the focus of this project due to the importance of the finished surface. Salt scaling is exacerbated by potential deficiencies in the finished surface, loss of air at this location due to finishing, and inadequate curing leading to larger freezable water content and lower strength at the surface (Mindess, Young, & Darwin, 2003).

It is now commonly accepted that salt scaling is due to the glue-spall mechanism (Valenza II & Scherer, 2006). This mechanism includes the propagation of stress concentrations due to salt in water freezing on the concrete's surface. Scaling damage does not increase linearly with salt concentrations in the water; however, at a point of approximately 3 to 4% salt solution, the freezing point of the water drops and virtually never freezes.

9.4.1 Experimental Procedures

Salt scaling susceptibility was tested by closely following ASTM C 672. This test uses a visual rating scale to determine the damage due to salt scaling and is outlined as follows.

Specimens of dimensions 3.5 in. (89 mm) deep and 9 in. (229 mm) square were cast for each material according to the aforementioned standard. The samples were broom-finished, cured with wet burlap for 1 day, wet-cured for 14 days, and then stored at 73 °F (23 °C) and 50% relative humidity for 14 more days.

A "dam" was then created on each specimen to allow ponding of salt solution. Polyvinyl chloride (PVC) pipe with a 1 in. (25 mm) diameter was attached along the finished edges of specimens and attached and sealed using Liquid Nails construction adhesive. A typical specimen is shown in Figure 9.7:

Figure 9.7: Liquid Nails adhesive and typical specimen used in ASTM C 672 testing

After the dams were built, a 4% calcium chloride solution was ponded on the surface. The specimens were placed in a chamber that cycles between freezing at 0 °F (-17.78 °C) and typical lab temperatures of 73 °F (23 °C) every 16 hours.

The surface is photographed and visually rated after 5, 10, 15, 25, and 50 cycles and rated according to ASTM C 672 using the following scale (Figure 9.8):

Rating	Condition of Surface
0	no scaling
1	very slight scaling (3 mm [⅛ in.] depth, max, no coarse aggregate visible)
2	slight to moderate scaling
3	moderate scaling (some coarse aggregate visible)
4	moderate to severe scaling
5	severe scaling (coarse aggregate visible over entire surface)

Figure 9.8: Visual rating of salt scaling specimen surfaces according to ASTM C 672

It is important to note that visual ratings were performed by the same person whenever possible to eliminate potential discrepancies.

9.4.2 Results and Discussion

After two samples of each material were exposed to 50 cycles according to the procedures of ASTM C 672, the materials displayed various levels of salt scaling damage. Figures 9.9 through Figure 9.20 show each slab's surface after 50 cycles. In addition, the slabs at 0, 5, 10, 15, and 25 cycles are provided in Appendix F. It is important to note that P-1 degraded very early, so pictures are not always presented.

Figure 9.9: P-2 samples after 50 cycles according to ASTM C 672

Figure 9.10: P-3 samples after 50 cycles according to ASTM C 672

Figure 9.11: P-AAFA samples after 50 cycles according to ASTM C 672

Figure 9.12: CSA-2 samples after 50 cycles according to ASTM C 672

Figure 9.13: CAC-1 samples after 50 cycles according to ASTM C 672

Figure 9.14: CAC-Latex samples after 50 cycles according to ASTM C 672

Figure 9.15: PC Type III samples after 50 cycles according to ASTM C 672

Figure 9.16: CSA-3 samples after 50 cycles according to ASTM C 672

Figure 9.17: CAC-3 samples after 50 cycles according to ASTM C 672

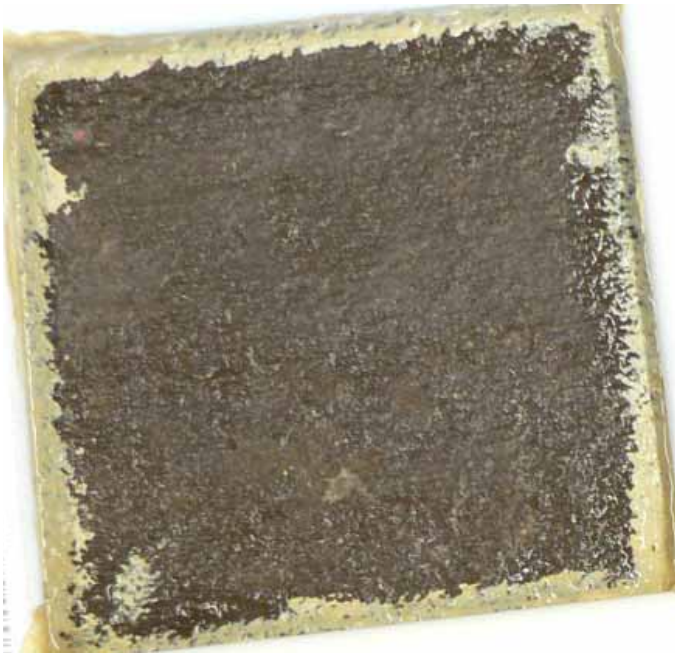

Figure 9.18: CAC-2 samples after 50 cycles according to ASTM C 672

Figure 9.19: CSA-1 samples after 25 cycles (50 unavailable) according to ASTM C 672

Figure 9.20: CSA-Latex samples after 25 cycles (50 unavailable) according to ASTM C 672

Based on these samples, each specimen from both Phase II and III was visually rated based on the criteria of ASTM C 672. The extent to which the sample met this criteria was carefully evaluated by a single member of the project team and the ratings assigned are presented in Table 9.3.

Table 9.3: Visual rating at 50 cycles in accordance with ASTM C 672

Material	ASTM C672 Visual Rating
P-1	5
P-2	0
P-3	3
P-AAFA	2
CSA-1	5
CSA-2	1
CSA-3	0
CSA-Latex	5
CAC-1	1
CAC-2	0
CAC-3	2
CAC-Latex	2
PC Type III	3

Although the standard does not present any failure criteria for the salt scaling visual rating, the materials P-1, CSA-5, and CSA-Latex were both rated 5 after 50 cycles. No air-entraining admixture was added to these mixtures as the manufacturers of these products claim that none is needed. Although no conclusions may be drawn from the severe rating received by P-1, the rating of CSA-1 and CSA-Latex implies that a calcium sulfoaluminate binder and the accompanying admixture offers little resistance to salt scaling, especially without additional air entrainment. Both materials binders comprise entirely of CSA.

The other materials were each rated 3 or better, indicating that, in general, they are at least fairly resistant to salt scaling. Among the most resistant include P-2, CSA-3, and CAC-2. Each alternative binder may be resistant to salt scaling if proportioned and used correctly.

9.5 Freeze-Thaw Testing

Freeze-thaw damage is a prime durability concern in flatwork and structural concrete exposed to freezing and thawing cycles. Through osmotic pressure, water in other locations attempts to dilute the highly charged ionic solution within the pores as water freezes; if fine pores are not finely spaced, the water will fail to reach its destination. This causes damage in transit due to high pressures as water travels through the concrete's matrix. In addition, water increases in volume by about 9% when it freezes, which may increase damage caused by osmotic pressure (Mindess, Young, & Darwin, 2003).

9.5.1 Experimental Procedure

To determine the resistance to this freeze-thaw damage, ASTM C 666 was followed. First, specimens of dimensions 4 in. x 3 in. x 16 in. (102 x 76 x 406 mm) were cast using the aforementioned air-entrained mix when applicable. These specimens were then wet-cured for 14 days, frozen to a temperature less than 4 °F (2 °C), and the initial resonant frequency is measured as shown in Figure 9.21.

Figure 9.21: Equipment for testing the fundamental transverse frequency of concrete samples according to ASTM C 666

Freeze-thaw testing proceeded by placing specimens in metal containers, surrounding them with water and subjecting the specimens to repeated freezing-and-thawing cycles. The fundamental frequency is measured during the thawing phase every 36 cycles. It is important to note that fundamental frequency was measured by the same technician as often as possible to eliminate user error and differences in judgment. In addition, each specimen is weighed during this period to further characterize damage done by repetitive freezing and thawing. After measurement, specimens are returned to random locations within the freezing-and-thawing chamber, as shown in Figure 9.22.

Figure 9.22: Specimens for ASTM C 666 in the freezing-and-thawing chamber

The individual cells are then filled with water, and freezing-and-thawing cycles continued. Each specimen was subjected to at least 300 freezing-and-thawing cycles or until the relative dynamic MOE reaches 60% of the original modulus. The relative dynamic MOE can be calculated for each specimen according to ASTM C 666 as shown in Equation 9.1:

$$P_c = (n_1^2/n^2) \times 100 \qquad (9.1)$$ *(ASTM C 666, 2008)*

where:

P_c = relative dynamic modulus of elasticity, after c cycles of freezing and thawing, percent,

n = fundamental transverse frequency at 0 cycles of freezing and thawing, and

n_1 = fundamental transverse frequency after c cycles of freezing and thawing.

When the test has ended due to the above criteria, the durability factor may be calculated to further characterize the material's resistance to freezing-and-thawing damage. This durability factor is given at the point of tests termination, and may be calculated according to ASTM C 666 as shown in Equation 9.2:

$$DF = PN/M \quad (9.2)$$ *(ASTM C 666, 2008)*

where:

DF = durability factor of the test specimen,

P = relative dynamic modulus of elasticity at N cycles, %,

N = number of cycles at which P reaches the specified minimum value for discontinuing the test or the specified number of cycles at which the exposure is to be terminated, whichever is less, and

M = specified number of cycles at which the exposure is to be terminated.

9.5.2 Results and Discussion

In general, calculating the durability factor and comparing it to time is a strong indicator of a material's resistance to freezing-and-thawing damage, at least in a manner relative to the other materials. The rate of degradation due to freezing-and-thawing damage and the resultant drop in this modulus is relatively slow in most materials. As shown in Figures 9.23 and 9.24, the majority of both Phase II and III materials held relatively high dynamic moduli through approximately 300 cycles.

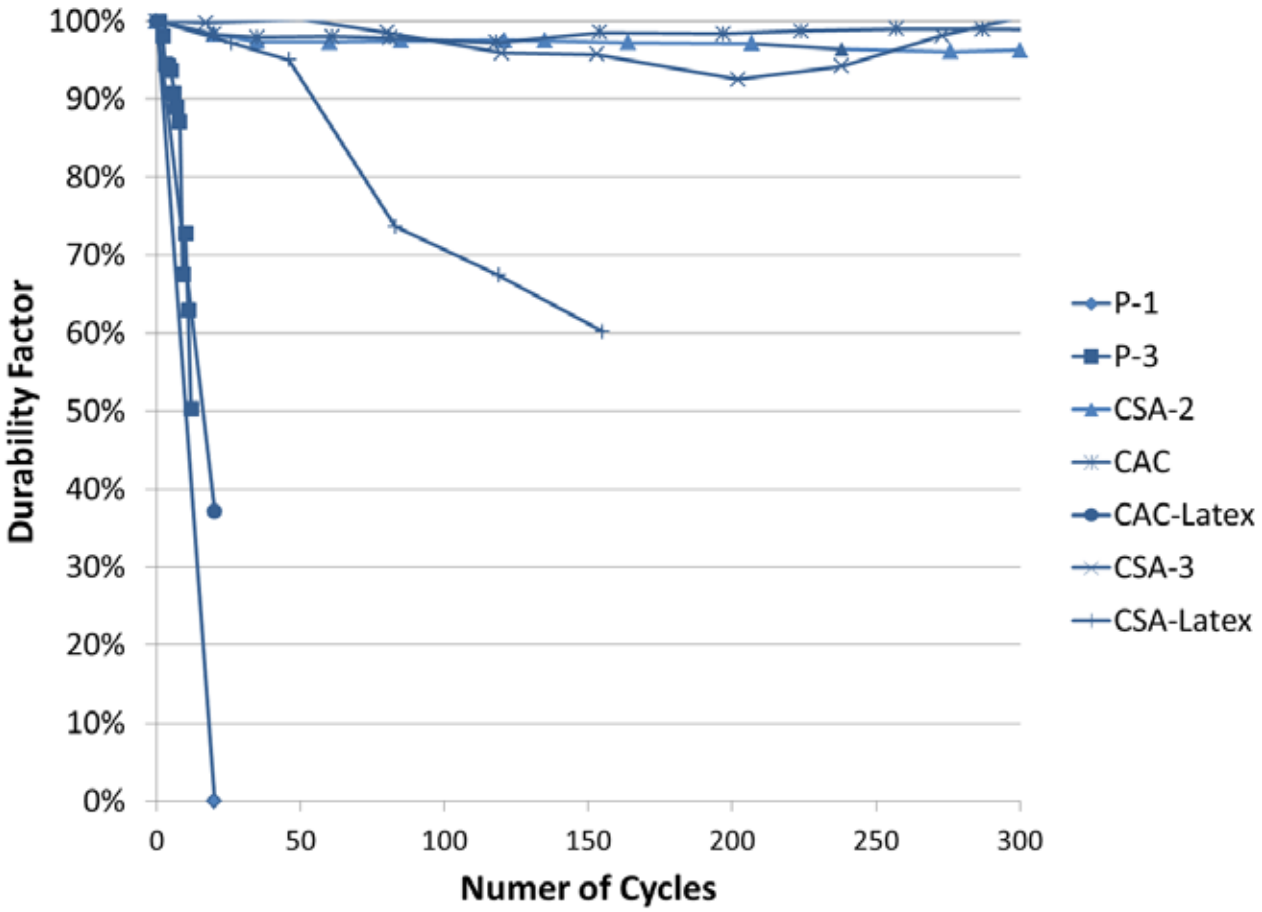

Figure 9.23: Relative dynamic MOE of Phase II materials

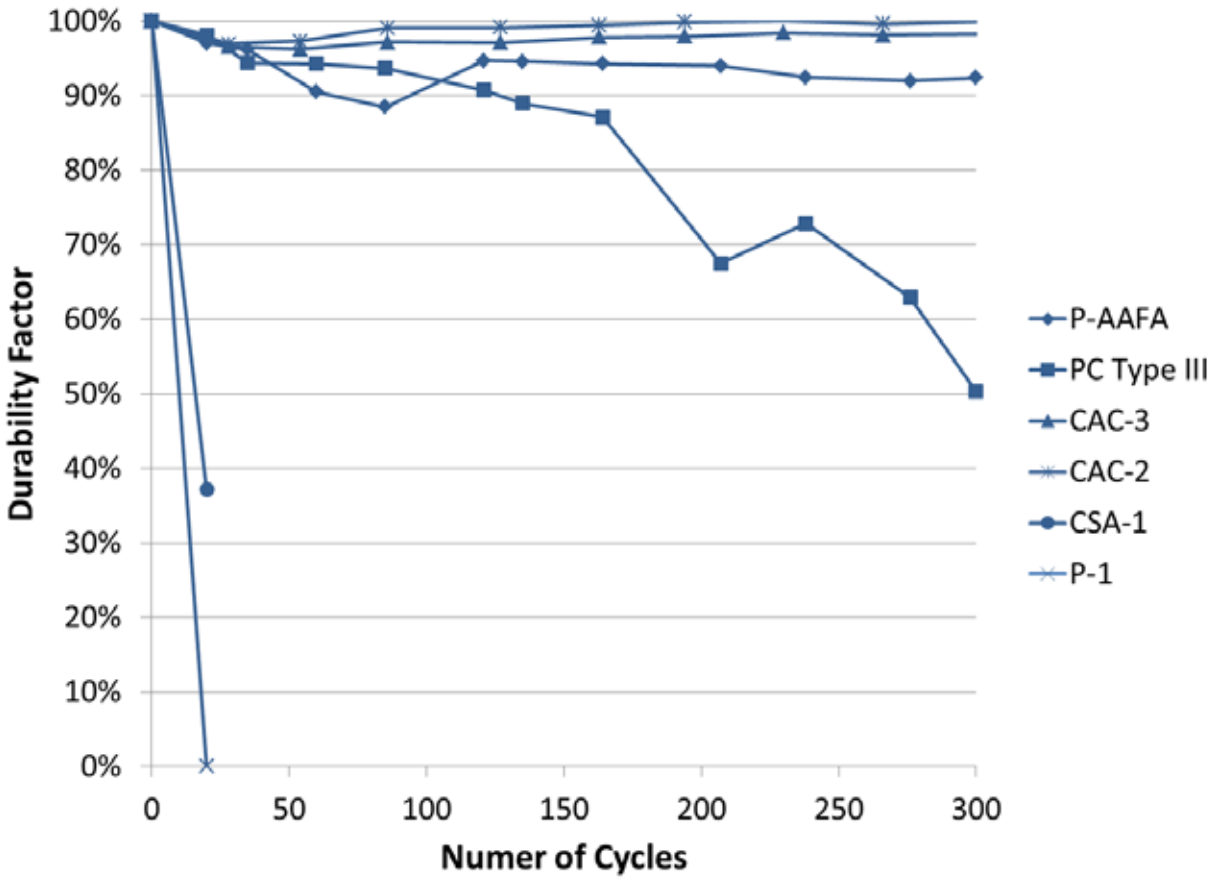

Figure 9.24: Relative dynamic MOE of Phase III materials

Only 4 of the total 13 materials displayed a drop in the relative dynamic MOE to below 60% before the 300-cycle limit. These materials included P-1, CSA-1, CSA-Latex, and PC Type III, covering all binder types relevant to this project besides CAC. The final durability factor and the materials final compliance with ASTM C 666 is shown in Table 9.4. Compliance was determined based on the number of cycles equaling or exceeding 300 (also shown) and a dynamic MOE.

Table 9.4: Relevant values and compliance with ASTM C 666 criteria

Material	Durability Factor	ASTM C666 Compliance	No. of Cycles	L > 0.008 inches (0.20 mm)?
P-1	0	Fail	20	No
P-2	92.5	Pass	300	No
P-3	93.25	Pass	300	Yes
P-AAFA	92.25	Pass	300	Yes
CSA-1	2.5	Fail	20	No
CSA-2	96	Pass	300	No
CSA-3	100.75	Pass	300	No
CSA-Latex	31	Fail	155	No
CAC-1	108	Pass	327	No
CAC-2	100.5	Pass	302	No
CAC-3	99	Pass	302	Yes
CAC-Latex	93.75	Pass	300	Yes
PC Type III	50.5	Fail	300	Yes

When performing a typical ASTM C 666, there seems to little correlation between the alternative concrete systems used and the spacing factor of 0.008 in. (0.20 mm) recommended by ASTM. Of the four materials with spacing factors over this value found by the hardened air void analysis, only one, PC Type III—the only full OPC materials of the group—failed to comply with ASTM C 666 and produced a high spacing factor. With the other materials, there was no correlation, possibly due to the individual differences between the materials relative to OPC concrete. It is possible that different binders have different critical spacing factors, owing to the differences in the materials and resultant microstructure. More work is needed to determine if this is in fact the case, but is an interesting finding that deserves further attention. These results suggest that performance testing using ASTM C 666 is likely a better evaluation method for assessing alternative binders, rather than applying the 0.008 in. (0.20 mm) spacing factor that is typically applied only to portland cement concrete mixtures.

The OPC, PC Type III, outperformed three other materials, but upon reaching the 300th freezing-and-thawing cycle, it was determined that it had dropped below the dynamic modulus limit of 60% between 276th and 300th cycle.

9.6 Summary and Conclusions

The summary of the air content and freeze-thaw performance of the materials is as follows:

- Although both fresh and hardened air content generally correspond, greater than 5% fresh air content does not necessarily correspond to an adequate spacing factor for moderate frost resistance, according to ASTM 1556.
- The ASTM C 672 salt scaling test yielded three materials with the worst visual rating of 5. Each of these materials was found to have an adequate spacing factor.

- ASTM C 672 and C 666 closely correspond. All materials with a visual rating of 5 also failed to comply with the freeze-thaw requirements. Only PC Type III failed the ASTM C 666 compliance with a visual rating of less than 5. It was rated 3.
- Materials P-3, P-AAFA, and CAC-3 maintained a good visual rating and ASTM C 666 compliance despite failing both the 5% fresh air limit and spacing factor requirements. This is likely due to the inclusion of fibers in P-AAFA. P-3 and CAC-3 may gain the resistance due to the combination of cements in the mix.
- Materials other than OPC concrete do not abide by typical rules of critical spacing factor, possibly due to difference in microstructure. Additional investigation will be required. Until this time, performance testing such as ASTM C 666 or ASTM C 672 should be used with materials containing alternative binders.

Chapter 10. Alkali-Silica Reaction

10.1 Introduction and Background

ASR occurs in portland cement concrete when silica within aggregates dissolves in the high-pH pore solution in concrete. The attack is triggered initially by hydroxyl ions in the pore solution and then by the alkalies in the pore solution, creating an expansive gel. This expansive alkali-silica gel in OPC concrete and other conventional concrete materials "may cause abnormal expansion and cracking of concrete in service" (Farzam et al., 2005). It requires water to proceed, and, thus, is only a concern in potentially moist environments. This cracking can lead to other durability problems such as corrosion of reinforcing steel. It allows for moisture and/or chlorides to penetrate into the concrete, potentially increasing the potential for freeze-thaw distress and/or corrosion of reinforcing steel. In addition, the cracking may lead to loss of strength in structural applications.

ASR is readily prevented by limiting the pH of the pore solution, controlling the alkali concentrations, controlling active silica within the aggregates, reducing the moisture that the concrete may be exposed to, and altering the gel to a unexpansive product (Mindess, Young, & Darwin, 2003). After ASR has been initiated in the field, it is very difficult to control. It is much easier to reduce the likelihood of ASR by selecting materials and mixture proportions using available prescriptive specifications or by using performance tests, with ASTM C 1293 (concrete prism test) being the most reliable test.

10.2 Materials and Mixture Proportions

To accelerate ASR for lab testing, the use of a reactive aggregate is needed. In addition, ASTM C 1293 provides for the evaluation of either the reactivity of either fine or coarse aggregates by using an aggregate known to be nonreactive. In this testing, a highly reactive fine aggregate was used in combination with a non-reactive coarse aggregate. The gradation of the coarse aggregate, a limestone, is provided in Table 10.1. The specific gravity of this limestone was 2.75 with an absorption capacity of 2.75%. The coarse aggregate was used in the as-received gradation.

Table 10.1: ASTM C 33 Gr. 57 limestone coarse aggregate sieve analysis

Sieve Size	Percent Passing
1.5 in. (38.1 mm)	100
1 in. (25.4 mm)	100
3/4 in. (19.05 mm)	85
1/2 in. (12.7 mm)	44
3/8 in. (9.53 mm)	19
No. 4	6
No. 8	2

In contrast, the fine aggregate is a siliceous sand from El Paso, Texas. The sand contains large amounts of quarts (64%), chert (17.1%), and feldspar (11.5%). In addition, the aggregate meets the gradation requirements of ASTM C33 for fine aggregate. It is important to note that mixing procedures did not allow aggregate modification in any of the "all-in-one" mixes, including P-1, P-2, P-3, and P-AAFA, as these mixtures already contain aggregates. Lastly, because the intention of this project was to evaluate specific rapid repair mixtures and most of these contained binders other than portland cement, NaOH was not added to the mixing water as is the case in ASTM C 1293, where the boosted alkalies are added to increase the alkali content to 1.25% Na_2O_e. Although the materials studied in this project do not necessarily meet the intended cement or aggregate composition used in ASTM C 1293, by combining selected binders with a highly reactive aggregate or by testing the as-received bag materials in ASTM C 1293 testing conditions (above water at 100 °F [38 °C]), one can still evaluate the relative susceptibility of these materials and mixtures to ASR.

10.3 Experimental Procedures

10.3.1 ASTM C 1293

Experimental procedures for quantifying alkali-silica reactivity in the rapid, cement-based repair materials studied in this project generally followed ASTM C 1293 characterized the expansion do to ASR due to the aggregate, alkaline pore solution, and ingress of moisture into the system. Although this expansion will likely greatly differ from field conditions, it allows for a general assessment of reactivity, especially when compared to other materials as was done in this project.

To perform these tests, four 3 x 3 x 11.25 in. (750 x 750 x 2850 mm) concrete prisms were cast in steel molds with steel gauge pins cast into each end. These prisms were then left to

cure in the temperature controlled mixing room and demolded at 24 hours. Next, each prism was stored in a typical 5-gallon bucket, as shown in Figure 10.1. Each bucket was lined with felt and 0.80 in. (20 mm) of water placed in the bottom to maintain a high relative humidity within the system.

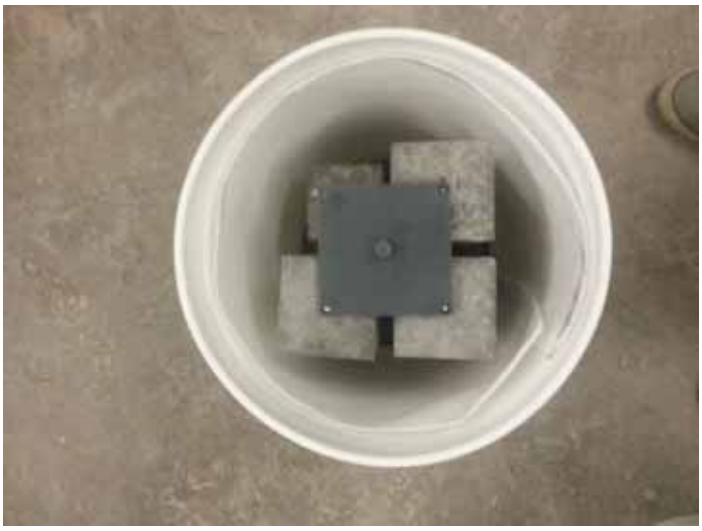

Figure 10.1: Container for moisture and orientation control of prisms for ASTM C 1293 testing

It is important to note that a high relative humidity was maintained without actively saturating the prisms. The prisms were placed on a plastic rack to raise them above the water level. The buckets were then sealed and stored in a 100 °F (38 °C) chamber, as shown in Figure 10.2, throughout the life of the test.

Figure 10.2: Temperature and humidity controlled room for ASTM C 1293 testing

This high temperature specified in ASTM C 1293 accelerates the test for experimental use. Each specimen was measured at 7 days from casting, but removed 24 hours before measuring to acclimate to a consistent "room temperature" of 73 °F (23 °C). Measurements were performed using a comparator, and each specimen was weighed for consistency.

After each measurement, the specimens were "flipped top to bottom" relative to their original position and returned to the five gallon buckets. The water level was then checked, and the bucket returned to the high temperature room.

ASTM C 1293 specifies for measurements to be taken at days 7, 28, and 56 and months 3, 6, 9, and 12. The aforementioned procedure was repeated for each measurement.

10.3.2 Pore Press

Because ASR is driven by aggregates being exposed to a high pH pore solution, characterizing pore solution composition at various points of maturity for the material may be important in alkali-silica reactivity. This characterization was especially desired for P-AAFA because an alkali activator is used in the cement, and it is of technical interest to quantify the effects of alkali activator addition on pore solution composition. To access the pore solution, the pore press, as shown in Figure 10.3, was used.

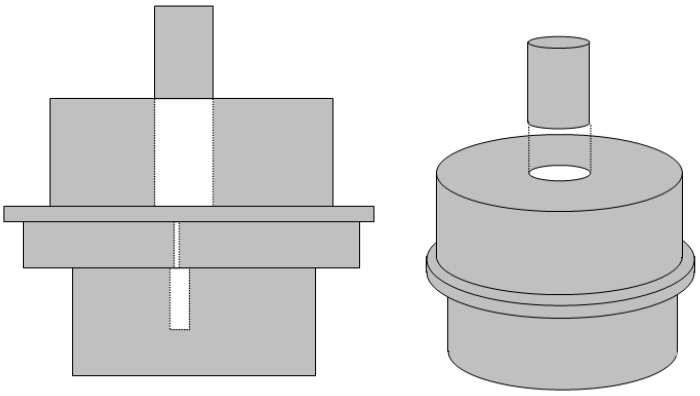

Figure 10.3: Schematic diagram of pore press used in extracting concrete pore solution

First, the concrete sample was crushed into pieces smaller than 0.375 in. (10 mm) in size. Approximately 250 grams of the crushed sample were used in the pore press and this value recorded.

Next, the equipment was set up. To do this, the base was set on the lower bearing block of the compression testing machine. The sample weight was recorded and then the container placed into the pore press base. Next, Part B of the base was set on the lower piece. The O-ring was then greased and seated properly. The area of Part B where the sample rests was lubricated with Teflon lubricant and the positioning ring was placed on Part B. The interior cavity of Part A was lubricated with Teflon lubricant. Finally, Part A was centered over and lowered onto Part B. Careful attention was paid to not move Part A after it was set in place so the O-ring was not disturbed.

Then, approximately one-third of the 250 grams of sample was poured into the cavity of Part A using a modified funnel and compacted using a small pestle. This process was repeated for two more lifts and leveled at approximately 0.5 in. (13 mm) from the cavity's top. A 0.1875 in. (4.8 mm) Teflon disc was placed on top of the sample.

Next, the surface of the piston was lubricated with the aforementioned lubricant and inserted into the cavity on top of the Teflon disc. The piston was checked to ensure it was perpendicular to the pore press setup. The protective disc was centered on top of the piston and stacked with bearing plates to allow the compression testing machine to make contact and continue through the entire stroke of the equipment.

To extract the pore solution, a load of approximately 5000 lbs (22 kN) was applied with a compression machine (shown in Figure 10.4) and then released. The piston was checked to guarantee it was turning freely. Next, a load of approximately 500,000 lbs (2,220 kN) was applied at a load rate of 30,000 to 40,000 lbs per minute (133 to 178 kN per minute). The maximum load was held for about 1 minute. The piston was then unloaded.

Figure 10.4: Forney FX700 compressive testing machine

The pore press was then dismantled and the sample removed. The concrete specimens were removed and examined, with their appearance similar to Figure 10.5.

Figure 10.5: P-AAFA samples after attempting pore solution extraction via pore press

10.4 Results and Discussion

In general, the material in this study performed well based on a single-year expansion limit of 0.04% cited in Appendix X1.2 of ASTM C 1293. The mixtures that exceeded this expansion limit at 1 year or less include P-AAFA, CAC-3, P-1, and CAC-Latex. The ASTM C 1293 results are shown in Figures 10.6 and 10.7. It is important to note that the pore press yielded no pore solution for material P-AAFA despite the relatively high load. The pore solution composition for this material is currently unknown and will not be speculated at this time.

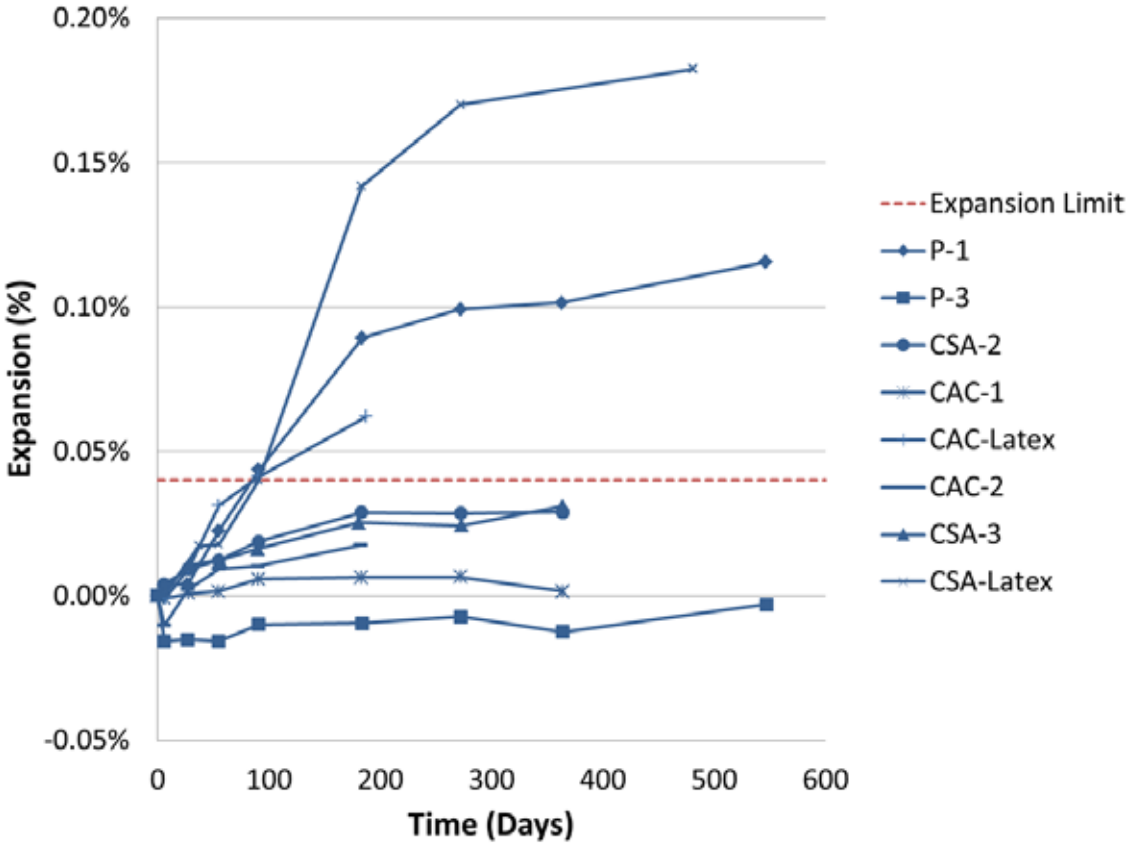

Figure 10.6: Expansion of Phase II materials via ASTM C 1293

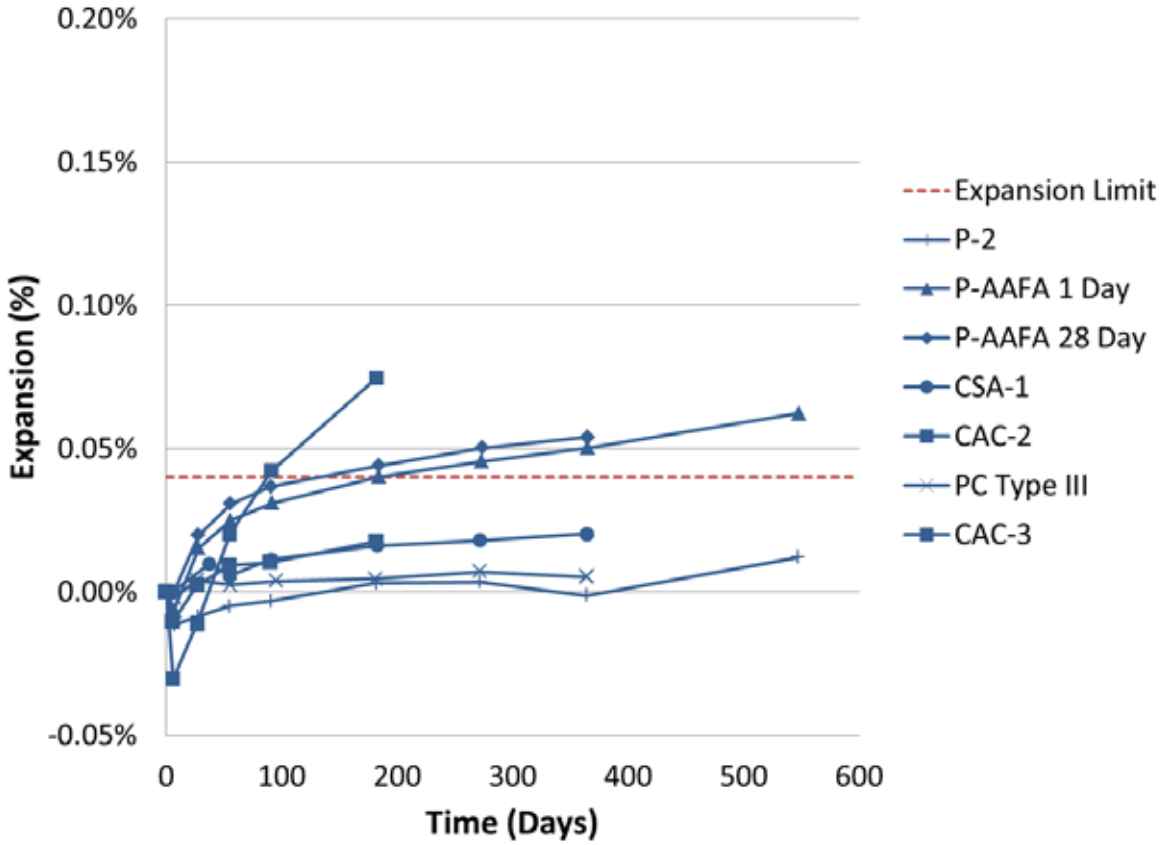

Figure 10.7: Expansion of Phase III materials via ASTM C 1293

Because ASR is created by a combination of siliceous aggregate and pore solution alkali content, it appears logical that all pre-packaged, all-in-one products other than P-2 succumbed to this reaction. For materials P-1, P-2, and P-AAFAA, it is likely that the pore solution is high in alkalinity and that the aggregate is reactive, or alternately, another reaction may have caused the expansion. Of these, it is known that P-AAFA has a highly alkaline pore solution due to its nature as a, alkali-activated fly ash product. The other pre-packaged materials all remained below the 0.04% expansion limit given in ASTM C 123, suggesting that either the aggregates were non-reactive or the pore solution pH was too low to dissolve the reactive aggregates. It is also possible that some binder systems lacked sufficient calcium to generate expansive ASR gel. More generally, the other materials (not all-in-one) performed well when tested for ASR. All materials outside of those mentioned were below the expansion limit.

10.5 Summary and Conclusions

The summary of the materials' ASR performance is as follows:

- Only four materials failed the ASTM C 1293 expansion limit of 0.04% at 2 years. One of these materials is P-AAFA, an alkali-activated fly ash material, which is expected to have a very highly alkaline pore solution.

- Styrene-butadiene latex increased the expansion of CAC (CAC-1 to CAC-Latex) and CSA (CSA-1 to CAC-Latex) significantly. More work is needed to understand the underlying mechanism for this behavior.
- Besides latex-modified materials and P-AAFA, the only materials to exceed the 0.04% expansion limit were P-1 and CAC-3. The content of the aggregate was not analyzed for material P-1.

Chapter 11. Sulfate Attack

11.1 Introduction and Background

One form of distress observed in concrete structures worldwide is external sulfate attack. The sulfates that cause this reaction are often present in soils and groundwater. External chemical sulfate attack leads to deleterious expansion in concrete due to the degradation of C_3A, then the formation of gypsum, and finally the formation of ettringite. In addition, transportation structures are susceptible due to the presence of sulfates in soils, water, and pollution (Mindess, Young, & Darwin, 2003).

In general, cements with lower C_3A content are more resistant to external chemical sulfate attack than are cements with higher C_3A contents. In addition, a less permeable microstructure and the consumption of $Ca(OH)_2$, both typically helped by SCMs, are also known to help prevent sulfate attack.

11.2 Materials and Mixture Proportions

Prisms for sulfate attack follow the typical mixing procedures and materials outlined in Zuniga (2013). ASTM C 1012 is the most commonly used sulfate attack test in the United States, but it relies on the testing of small mortar bars. Although ASTM C 1012 specifies suggested properties and proportions, this specification was modified to allow the use of concrete prisms of the typical material proportions developed in Phase I or provided by the material manufacturer. The modifications are as follows:

- ASTM C 1012 specifies an aggregate-to-cementitious-material ratio of 2.75 and a w/c of 0.485. For this project, both proportion requirements were ignored so typical rapid setting material proportions could be used. This also includes the use of 2-in. (50 mm) concrete prisms of 10-in. (250 mm) length instead of the typical 1-in. (50 mm) mortar bars.
- The test was also modified to use the same fine aggregate proposed in Zuniga (2013). This differs from the standard.

For each material, at least three 2-in. x 2-in. x 11.25-in. (500 x 500 x 2850 mm) prisms were cast to develop average properties of the specimens under sulfate attack.

11.3 Experimental Procedures

Experimental procedures for quantifying susceptibility to external chemical sulfate attack in concrete are provided in ASTM C 1012. Although the specification calls for curing of specimens until a compressive strength of 2850 psi (20 MPa), most specimens were instead cured for 1 day, 28 days, or both to compare the materials at similar ages. Each concrete prism was cast in steel molds with typical comparator pins at each end.

After the designated curing periods, each concrete prism was placed in sealed container filled with 5% sodium sulfate solution. At 1 day, the prisms are measured using a comparator as shown in Figure 11.1.

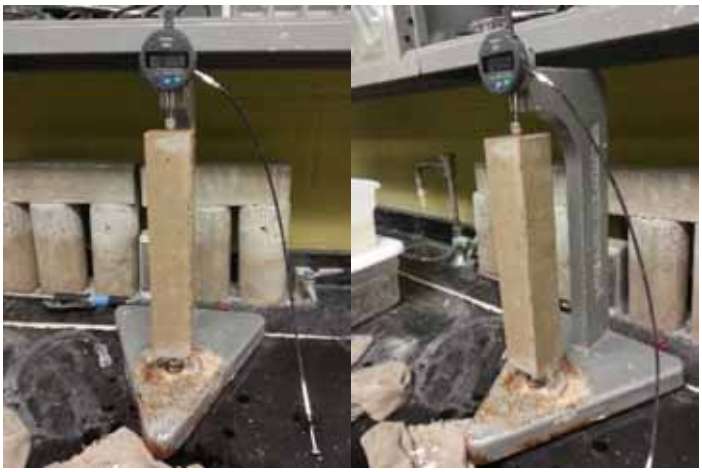

Figure 11.1: Comparator for measuring length change in concrete

The sulfate solution in the containers was replaced after each measurement. Subsequent measurements are taken at 2, 3, 4, 8, 13, and 15 weeks and after 4, 6, 9, 12, 15, and 18 months.

11.4 Results and Discussion

The expansion values for Phase II and III materials using both 1- and 28-day cures were recorded at the aforementioned times through 18 months. After this time period, the test was stopped. The results are shown in Figures 11.2 through 11.5. Please note that some Phase II and III materials have not yet reached 18 months under testing at the time of this report. The data will be recorded and reported at a later date.

Because there are no standard limits for the expansion of concrete exposed to external sulfates, an expansion of 0.04% is used herein as it represents the level of expansion that typically causes concrete to crack. This value is also consistent with concrete expansion limits used for ASR, both in ASTM C 1293 and for outdoor exposure blocks stored on the UT exposure site at the J.J. Pickle Research Campus.

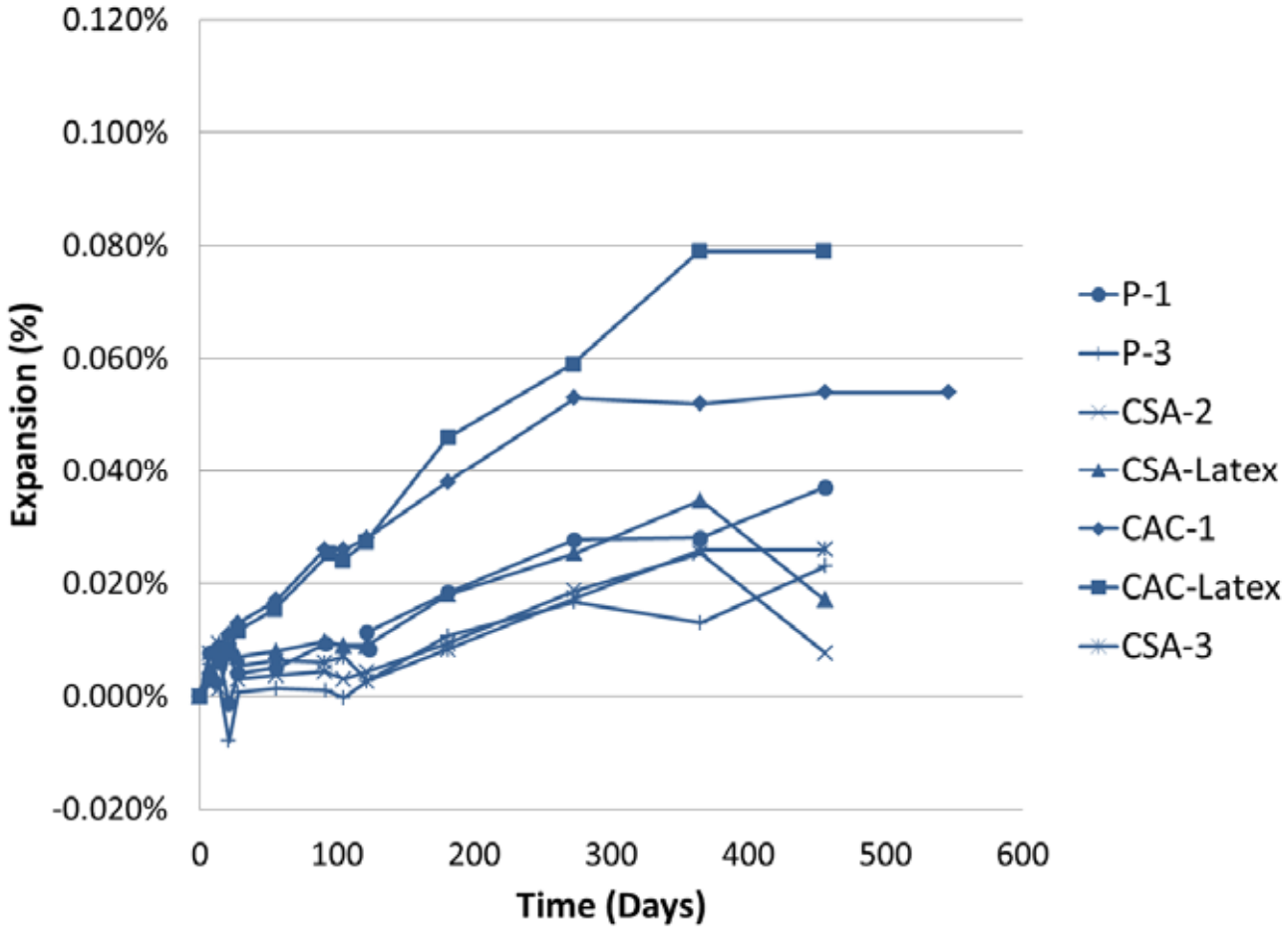

Figure 11.2: ASTM C 1012 expansion of Phase II materials after 1-day cure

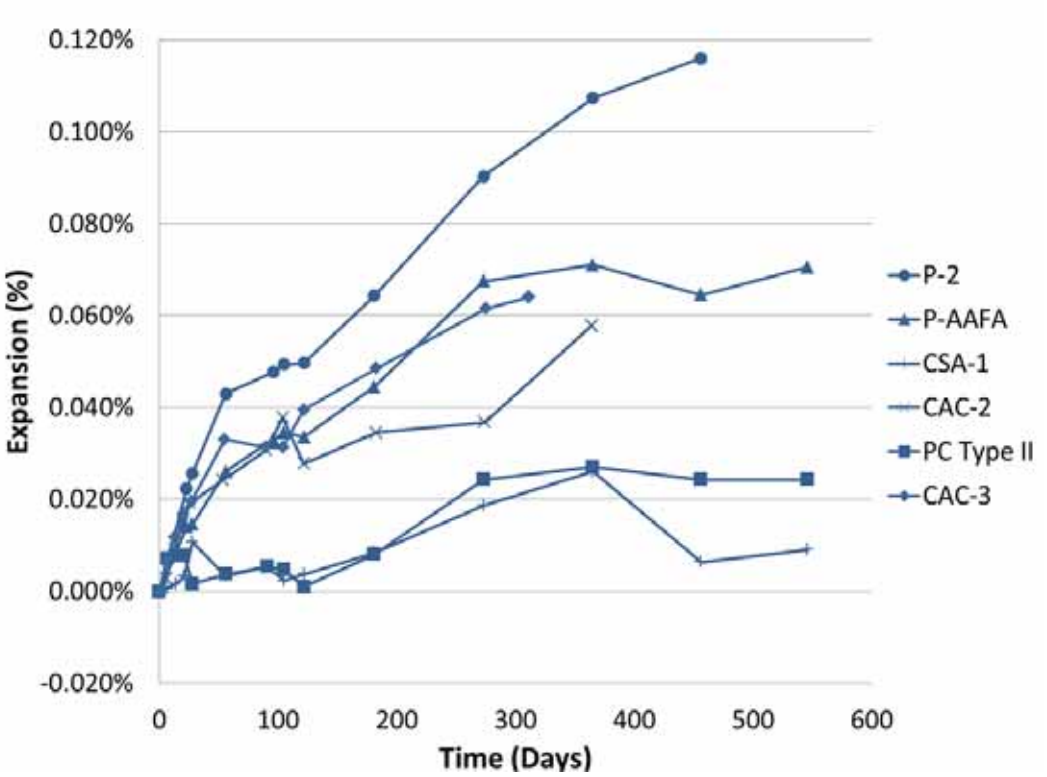

Figure 11.3: ASTM C 1012 expansion of Phase III Materials after 1-day cure

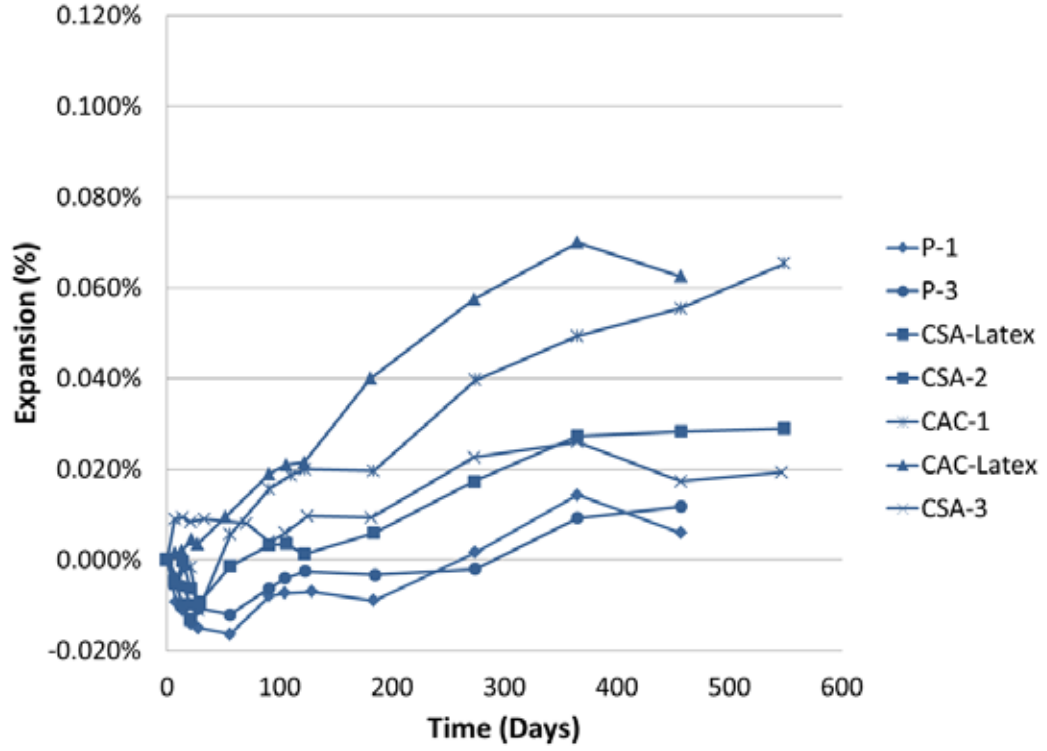

Figure 11.4: ASTM C 1012 expansion of Phase II Materials after 28-day cure

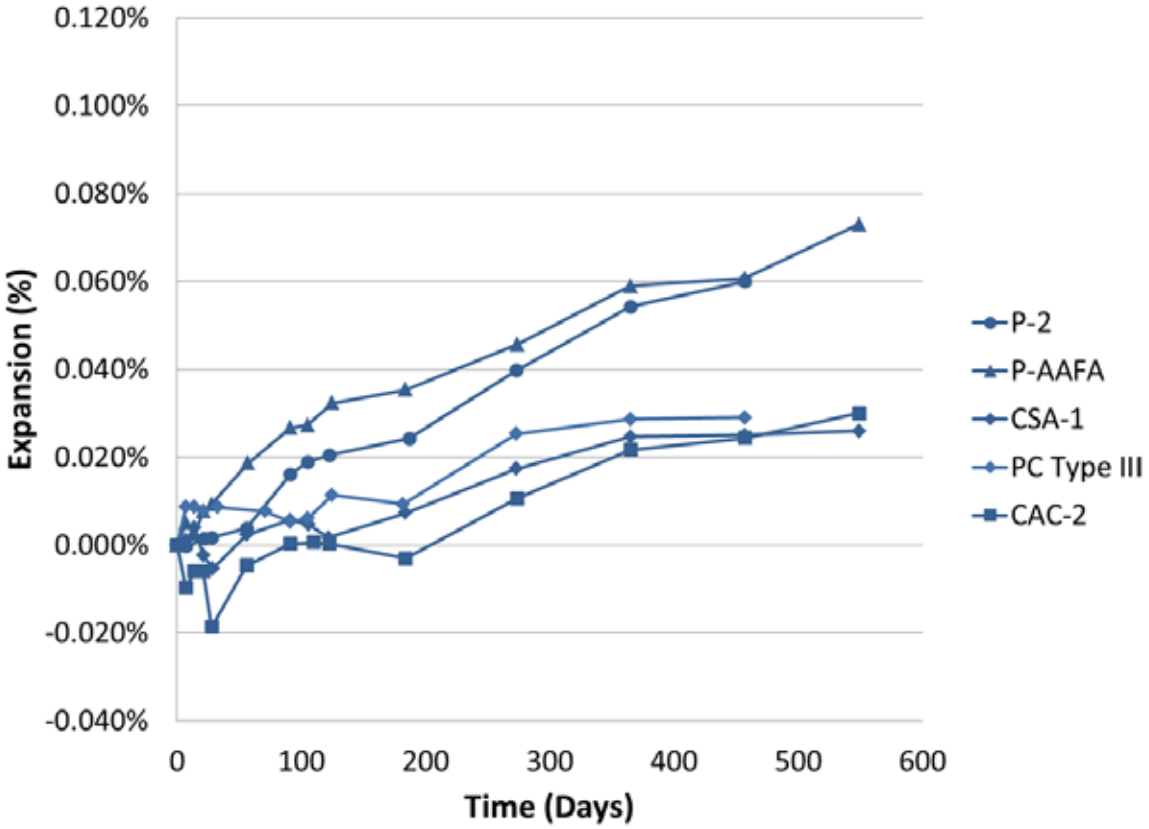

Figure 11.5: ASTM C 1012 expansion of Phase III Materials after 28-day cure

Materials P-2 and P-AAFA exhibited the most expansion with maximum values of 0.126% and .071% under 1-day curing conditions and 0.054% and 0.059% under 28-day curing conditions, respectively. Despite this, P-2 and P-AAFA expanded less than the limit of 0.4%.

Another unexpected outcome of the ASTM C 1012 testing performed for this project was the effect of the styrene-butadiene latex modifying of both CAC and CSA. The effect of sulfate attack on both specimens was more pronounced than when not modified by the latex. General knowledge of latex modifying anticipates a denser pore structure and higher resistance to sulfate attack when modified with styrene-butadiene latex (Shaker, El-Dieb, & Reda, 1997).

11.5 Summary and Conclusions

The summary of the materials' performance in a sulfate environment is as follows:

- In all materials, increasing curing time from 1 day to 28 days improved resistance to sulfate attack.
- The addition of styrene-butadiene latex (CAC-1 to CAC-Latex and CSA-1 to CSA-Latex) worsened the sulfate resistance in both instances.
- CAC was not resistant to sulfate attack in our tests. This is contrary to common knowledge of CAC.

- Nearly half of the materials (6 of 13) failed when only subjected to a single day of curing.

Chapter 12. Permeability and Corrosion

12.1 Introduction and Background

Transportation structures are particularly susceptible to corrosion due to deicing salts and other salt solutions. A truly durable structure would not allow the corrosive solutions to reach reinforcing steel and degrade the structural performance.

There are two primary sources of corrosion of reinforcing steel in concrete: chlorides and carbonation. In this project, chloride penetration was tested using three methods. First of all, the team used a simplified version of the ASTM C 1202 rapid chloride permeability test (RCPT), as created by Riding et al. (2008). The apparent chloride diffusivity of concrete was measured using ASTM C 1556, and the impact of chloride ingress into repaired, reinforced concrete beams was evaluated using a modified ASTM G 109. Carbonation was tracked over the course of 11 months as detailed in CEN/TS 12390-10:2007.

12.2 Materials and Mixture Proportions

In the simulated bridge deck for fatigue corrosion testing, the following materials and mixture proportions were used:

- **Fine aggregate**: River sand from the Colorado River in Austin, Texas. The aggregate has a fineness modulus of 2.71, with percent passing gradation as shown in Figure 12.1.
- **Coarse aggregate:** Grade 57 river gravel with an absorption capacity of 1.29% and a specific gravity of 2.60. This aggregate is further described in Table 12.1.
- **Volumetric mix design:** The mix design shown in Table 12.2 was used in Pesek (2011) with the cubic feet of each constituent expressed per cubic yard of concrete.
- The mixtures were deemed both small and workable enough to go without any admixtures when mixed with the aid of a vibrating table.

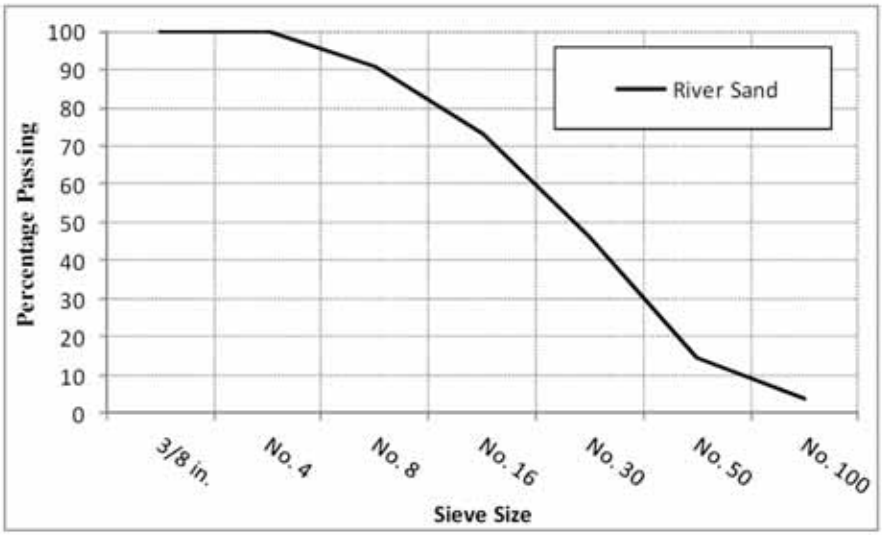

Figure 12.1: Gradation analysis of fine aggregate (Pesek, 2011)

Table 12.1: Gradation analysis of Gr. 57 river gravel for bridge deck mix

Sieve Size	Percent Passing
1.5 in (38.1 mm)	100
1 in (25.4 mm)	100
3/4 in (19.05 mm)	79
1/2 in (12.7 mm)	58
3/8 in (9.53 mm)	41
No. 4	7
No. 8	1

Table 12.2: Volumetric mixture design of bridge deck mix

Cement (ft^3/yd^3)	Water (ft^3/yd^3)	Paste Volume (ft^3/yd^3)	Coarse Aggregate (ft^3/yd^3)	Fine Aggregate (ft^3/yd^3)	Total Aggregate (ft^3/yd^3)
2.58	3.66	6.25	12.08	8.53	20.61

It is important to note that the upper portions of the simulated bridge deck sections contain concrete that was mixed with 0.5% calcium chloride per pound of cement to increase the rate of corrosion for testing. This procedure was suggested by Dr. Michael D. A. Thomas, P.Eng. of the University of New Brunswick. It will be further described in Section 12.5.1

12.3 Rapid Chloride Permeability Testing

The RCPT protocol was performed in accordance to the simplified concrete resistivity and RCPT method developed by Riding et al. (2008). This method greatly simplifies the typical RCPT, ASTM C 1202, by "avoid[ing] cutting samples, dessication, test duration, and sample heating" (Riding et al., 2008). It also produces better results when SCMs are used or when certain admixtures are present. Since the composition of some of the repair materials presented in this project are at least partially unknown, the rapid method was greatly preferred.

12.3.1 Experimental Procedures

To perform the aforementioned simplified test, two 4-in. x 8-in. (100 x 200 mm) cylinders were cast for each mixture according to the mixing guidelines. Each mixture was given typical proportions as outlined in Zuniga (2013). From each mixture, one sample was moist-cured for 28 days and the other moist-cured for 56 days.

After moist-curing, the specimen is covered with a 7.4 in. (188 mm) long acrylic sleeve instead of the sleeve specified in the original test. The specimen was then inserted between each half of the test cell and the two halves clamped onto the specimen with long bolts. A seal was created between the sleeve and the halves of the test cells.

Next, the cell at the top surface of the concrete cylinder specimen was filled with 3.0% NaCl solution. The other cell was then filled with 0.3 N NaOH solution. The cell at the top surface was connected to the negative terminal and the opposite side to the positive. After connection, the terminal was turned on and set to 60 volts. At this point, the initial current was read and recorded. After 5 minutes, according to Riding et al. (2008), the current was once again recorded and the test potentially stopped. The total charge passed through the sample, which is required by ASTM C 1202, was ignored.

12.3.2 Results and Discussion

In general, the mixtures tested in both Phases II and III performed well when subjected to the simplified RCPT. All but one (P-1) showed noticeable improvement when cured at approximately 56 days versus 28 days as curing is typically prescribed. The results are shown in Figures 12.2 and 12.3.

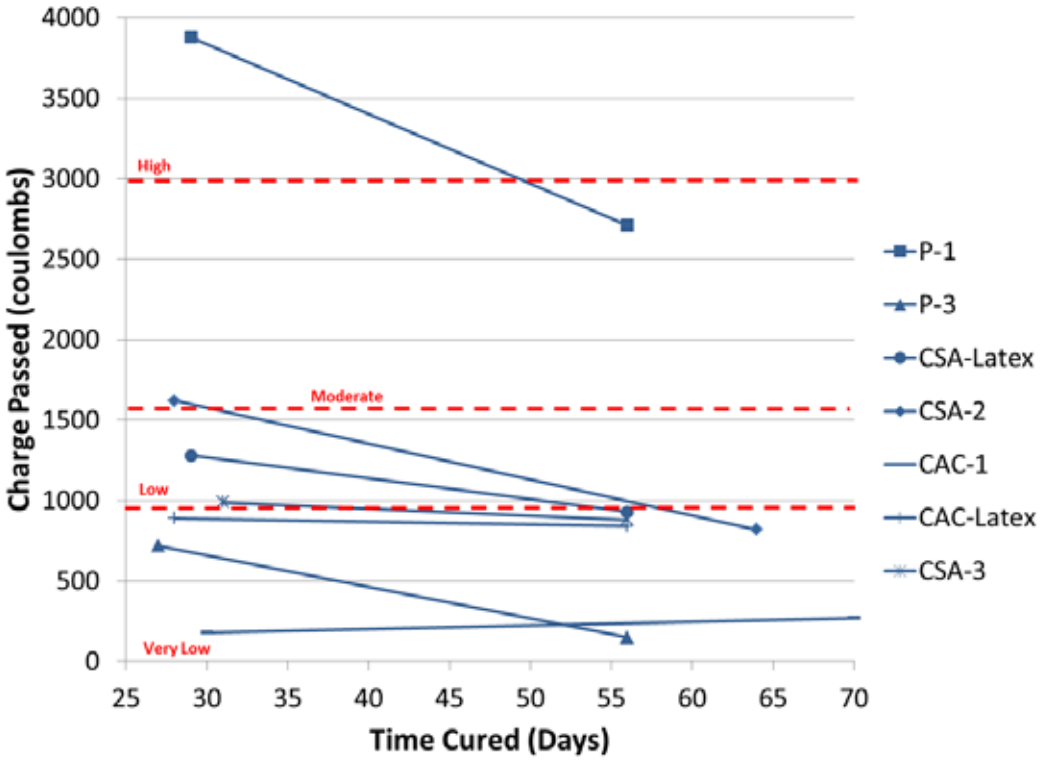

Figure 12.2: Results of simplified RCPT for Phase II materials

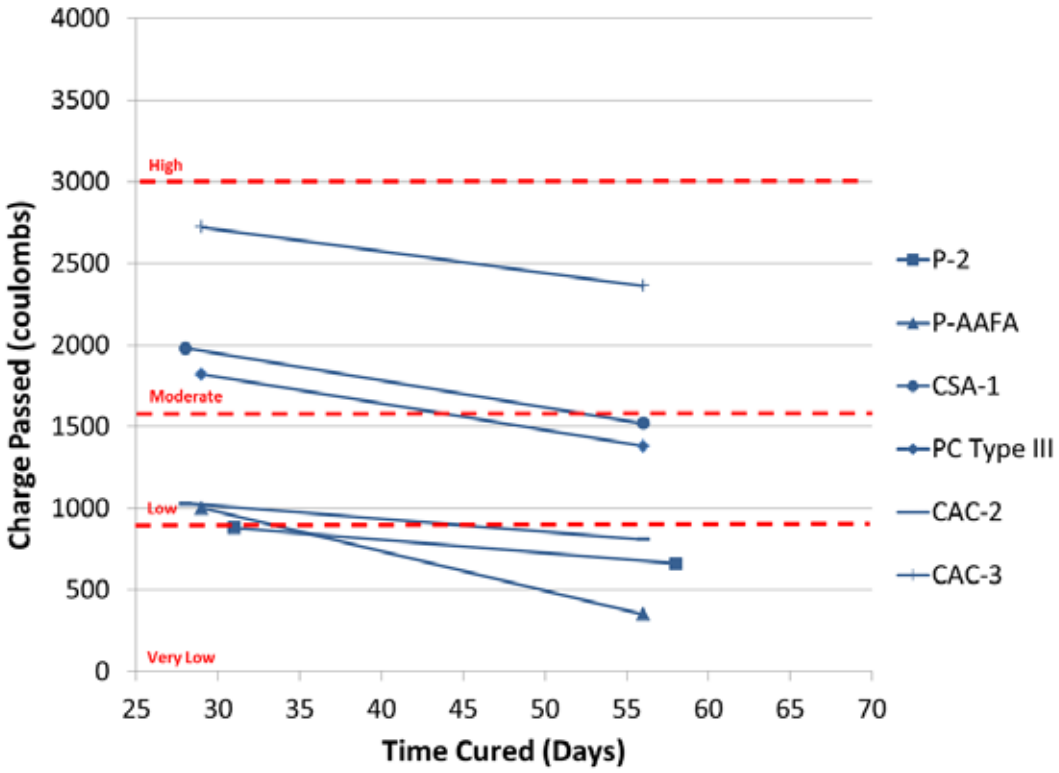

Figure 12.3: Results of simplified RCPT for Phase III materials

As shown in Figure 12.2, only P-1 could be classified as having high permeability according to the method. It should also be noted that if this material is cured for 58 days instead of 28 days, it is no longer above the 3000 coulomb limit for high permeability concrete.

Also, only three materials may be classified as having moderate permeability within the range of 1600 and 3000 coulombs. These materials are CSA-1 and PC Type III of Phase II and CSA-2 of Phase III, although each passes into the low permeability category of cured for 58 days.

Although curing for extended periods of time in a transportation-related situation that calls for rapid, cement-based repair materials is unlikely, this study highlights the benefit of curing time. In general, even minimal curing can have a marked effect on the ability of a material to resist intrusion by creating a more tortuous pore structure. Curing should be implemented whenever possible and for as long as possible.

12.4 Carbonation

Carbonation is the absorption of carbon dioxide gas into the concrete structure and the eventual conversion of calcium hydroxide and other hydration products to carbonates by atmospheric carbon dioxide. This conversion causes the concrete's pH to drop below the corrosion threshold of about 11.5. This drop in pH will initiate corrosion in the reinforcing steel if it reaches the appropriate depth, so the rate and penetration of carbonation is important to maintain the durability of concrete structures. Carbonation depths in well cured concrete with a low w/c seldom exceed 1 in. (25 mm) in depth, but it is important to test the alternative rapid-repair materials used in this project for differences (Mindess, Young, & Darwin, 2003).

12.4.1 Experimental Procedures

Carbonation was measured over a period of 11 months following procedures detailed in CEN/TS 12390-10:2007. Prisms of dimensions 4 in. x 4 in. x 16 in. (100 x 100 x 400 mm) were cast and placed outside. For each material to be studied, a single sample was placed both inside an enclosure and outside, as shown in Figure 12.4.

Figure 12.4: Test location of carbonation prisms

At intervals of 6 months and 11 months, carbonation depths were measured through the use of a Phenolphthalein pH indicator. The samples were broken perpendicular to the long faces and sprayed with indicator. Since carbonation lowers the pH of concrete to below 11.5, the indicator only "colors" the uncarbonated portions of concrete. This depth was then measured using a ruler as shown in Figure 12.5.

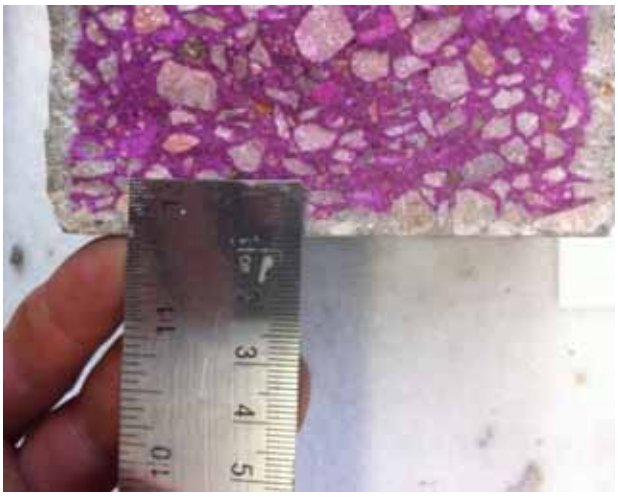

Figure 12.5: Action of Phenolphthalein pH indicator and measurement of carbonation depth

After the depths for each material are measured, pictures of each specimen are taken. Also, Sikagard 550W Elastocolor white base is applied onto the broken plane to prevent carbonation from reaching the ends of the specimen. The prisms are then placed outside in their previous location and facing the previous direction.

12.4.2 Results and Discussion

In general, every material performed worse than the Type III OPC. This result, as shown in Table 12.3, is likely due to the ill effects of most common SCMs on the ingress of carbonation. Figures 12.6 through 12.11 provide the carbonation on the various rapid repair materials.

Figure 12.6: P-AAFA sample displaying carbonation depth at 11 months using Phenolphthalein PH indicator

Figure 12.7: CSA-1 sample displaying carbonation depth at 11 months using Phenolphthalein PH indicator.

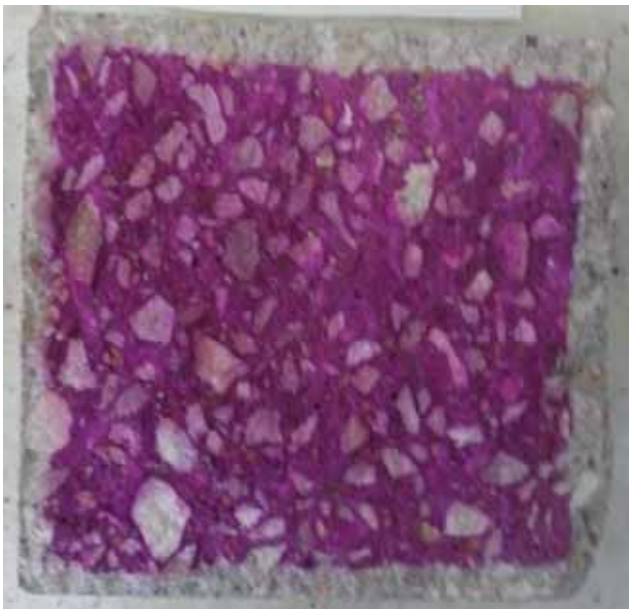

Figure 12.8: CAC-3 sample displaying carbonation depth at 11 months using Phenolphthalein PH indicator

Figure 12.9: P-2 sample displaying carbonation depth at 11 months using Phenolphthalein PH indicator

Figure 12.10: PC Type III sample displaying carbonation depth at 11 months using Phenolphthalein PH indicator

Figure 12.11: CAC-1 sample displaying carbonation depth at 11 months using Phenolphthalein PH indicator

Table 12.3: Carbonation depths for Phase III materials at 6 and 11 months

Material	6 Months		11 Months	
	Inside	Outside	Inside	Outside
P-2	0.15 in	0.05 in	0.11 in	0.04 in
	0.75 mm	1.2 mm	2.8 mm	0.98 mm
PC Type III	0.00 in	0.00 in	0.05 in	0.00 in
	0.02 mm	0.02 mm	1.28 mm	0.13 mm
CAC-3	0.02 in	0.01 in	0.25 in	0.13 in
	0.51 mm	0.30 mm	6.29 mm	3.30 mm
CAC-2	0.01 in	0.01 in	0.14 in	0.12 in
	0.24 mm	0.30 mm	3.48 mm	3.13 mm
P-AAFA	0.02 in	0.01 in	0.29 in	0.17 in
	0.56 mm	0.30 mm	7.28 mm	4.28 mm
CSA-1	0.03 in	0.01 in	0.34 in	0.14 in
	0.65 mm	0.30 mm	8.68 mm	3.48 mm

In addition, each specimen showed more carbonation when placed inside an enclosure. The standard supports this data by stating that the Stevenson screen allows the movement of atmospheric conditions yet prevents the exposure of specimens to precipitation and solar radiation (CEN, 2007).

As anticipated, all materials performed worse than PC Type III. Typically, secondary cementitious materials or other alternative binders create an environment more conducive to carbonation.

Of the Phase III materials, CSA-1 and P-AAFA allowed the most carbonation to take place, with a value greater than 0.25 in. (6.4 mm) when inside the carbonation enclosure. Although well below the minimum cover requirement of 0.75 in. (19 mm) called for in ACI 318, the carbonation depth may become more of an issue over the full life of a structure or roadway.

12.5 Chloride Diffusion

The ingress of chlorides into concrete and the rate at which this occurs can cause corrosion of the reinforcing steel when deicing salts or other chloride solutions are ponded on or applied to concrete.

It is important to understand the diffusion of chlorides into the concrete's matrix to allow for an indirect correlation to overall permeability and corrosion resistance of a concrete material.

12.5.1 Experimental Procedures

Following the procedure given in ASTM C 1556, the apparent chloride diffusion coefficient can be found. First, 4-in. (100 mm) x 8-in. (200 mm) cylinders of the Phase III materials were cast according to standard mixture proportions. The cylinders were cured for 28 days. After curing, the specimens were cut using a wet saw in accordance to ASTM C 1556 as shown in Figure 12.12 and frozen until further use.

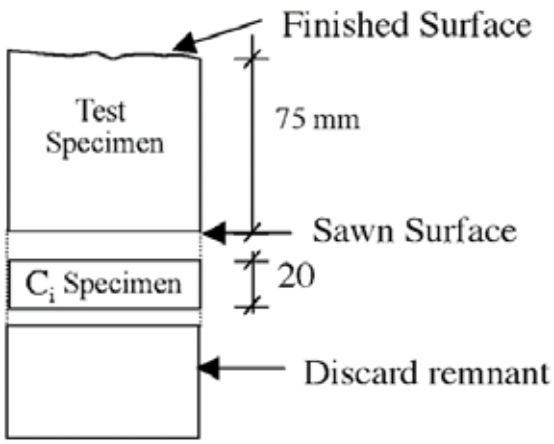

Figure 12.12: Preparation of test specimens for chloride diffusion test (ASTM 1556)

After all specimens were cast and cut, the test specimens were removed from the freezer and Sikadur Injection Gel was applied to all sides other than the finished surface. The specimens were left to cure at standard temperature and 50% relative humidity for 24 hours. When the epoxy set, each specimen was weighed and then submerged in a saturated calcium hydroxide water bath. After 24 hours, the surface was lightly dried and mass weighed. The specimen was then submerged again and reweighed at 24-hour intervals until the mass did not change by more than 0.1% over this time period.

After the mass remained stable, they were rinsed with water and submerged in an exposure liquid, "[a]n aqueous NaCl solution prepared with a concentration of 165 ± 1 g NaCl per L of solution" (ASTM C 1556, 2011a) for 35 days. After 35 days, the specimens were frozen until profile grinding began.

Profile grinding was performed at depths of 1 or 2 mm at a time. These depths, from the finished face, are listed as follows: 1 mm, 2 mm, 3 mm, 4 mm, 6 mm, 8 mm, 10 mm, and 12 mm. Each sample was ground at these depths despite differing w/c and pozzolan and slag contents. It was more relevant to the project that each material be compared in the same manner than follow the specification in this instance.

To perform profile grinding, each test specimen was clamped to a table and slowly and carefully ground using a profile grinder commonly used for this test. The concrete powder from each layer was carefully gathered in a plastic bag, labeled, and stored for later use. After each layer was collected, the C_i specimen was ground to develop a baseline sample to be tested.

Finally, the collected concrete powder was tested for chloride content. Each layer was analyzed using James Instruments, Inc., CL-2020 chlorimeter according to modified SHRP Product 2030: Standard Test Method for Chloride Content in Concrete (Islam, 2004). The following solutions were mixed according to this document to aid in the measurement of chloride ions in the powdered concrete:

- A digestion solution used for extracting chloride ions, made up of a ratio of 60 grams glacial acetic acid, 50 g isopropyl alcohol, and distilled water up to 1 liter.
- Calibration solutions with a wide range of chloride concentrations purchased from James Instruments.

- Stabilizing solution made up of “a dilute NaCl solution containing 3.75 ppm chloride” that “helps in controlling the temperature of the extraction solution” (Islam, 2004).

After calibration using the solutions and onscreen prompts, the chloride content was measured. Three grams of powder was mixed with the 20 mL digestion solution, the lid to the container was closed, and the container was shaken by hand for 30 seconds. After shaking, the solution was left to stand for 2.5 minutes and then 80 mL of stabilizing solution was added. Finally, the chloride content was measured with the CL-2020 as shown in Figure 12.13. The chloride content for each depth was recorded. This procedure was then repeated for every sample.

Figure 12.13: Measuring chloride content using James Instruments CL-2020 chlorimeter

12.5.2 Results and Discussion

Diffusion of chloride ions may cause corrosion of the reinforcing steel, so it is important to know both the innate chloride content of a particular concrete and the ability for ponded chlorides to penetrate. During the conducting of ASTM C 1556, the initial chloride content of each of the Phase III materials was calculated. These values are shown in Table 12.4 and Figure 12.14 provides the diffusion curves.

Table 12.4: Initial chloride content of each Phase III materials

Material	Initial Chloride Content
PC Type III	0.01150%
CAC-2	0.00605%
CAC-3	0.02800%
P-2	0.03735%
CSA-1	0.00810%
P-AAFA	0.00565%

As shown, PC Type III has an initial chloride content of 0.115%, more than three times that of the next highest, P-2. Also, as expected, this material allowed the penetration of a relatively large amount of chloride ions, at least within the first few millimeters. The PC Type III binder is made up of Type III portland cement and lacks alternative binders such as silica fume that could make a less permeable pore structure.

Generally speaking, CSA-1 allowed the most penetration of chloride solution during the ASTM C 1556 testing. In contrast, P-2, one of the premanufactured concrete all-in-one products, allowed the least penetration by chloride solution. This product likely performed well because of its optimized blend of cements, allowing for a more tortuous pore structure both due to the development of cementitious products and physical packing of the cement particles (Mindess, Young, & Darwin, 2003).

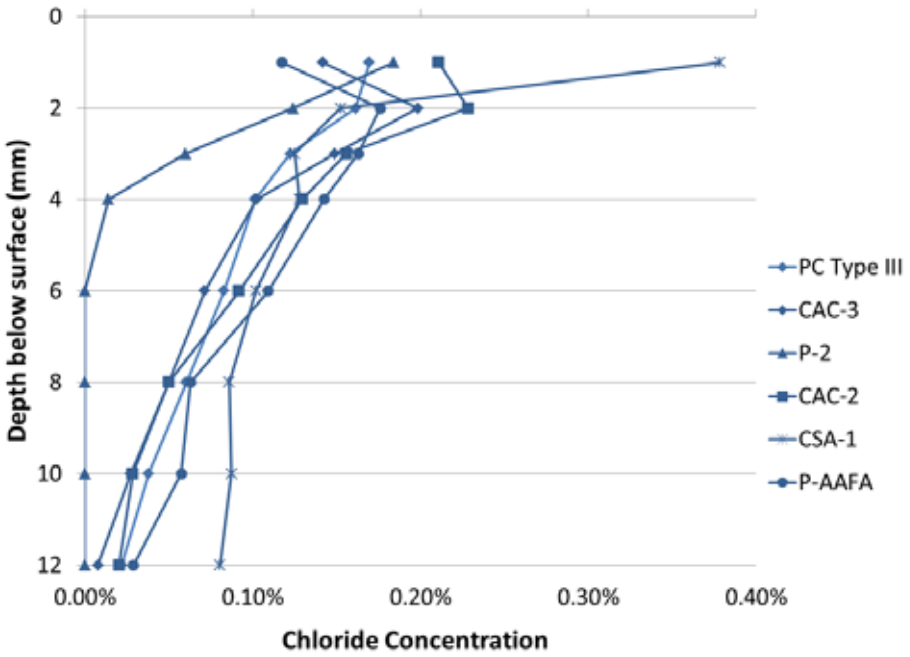

Figure 12.14: Diffusion of chloride ions into Phase III materials.

12.6 Combined Fatigue and Corrosion Testing

Pavements and transportation structures are subject to repetitive axel loading as vehicles pass. These loads only stress the structures to a fraction of their theoretical strength, and, because repetitive, may be considered fatigue loads.

When a damaged section is repaired and the aforementioned loads are repetitively applied, debonding of the repair is a concern. Bond strength in a more general sense is given in (Dornak, 2014). As requested by TxDOT, this project intended to develop a correlation between the fracturing of repair bonds under fatigue loading and the potential ingress of chlorides through this "gap" reaching the reinforcing steel and causing corrosion.

12.6.1 Experimental Procedures

At the request of TxDOT, a more thorough experiment representative of an actual in-place bridge deck pavement was designed. With assistance from Dr. Harovel Wheat of the Department of Mechanical Engineering at The University of Texas at Austin and Dr. Michael D. A. Thomas, P.Eng. of the University of New Brunswick, a highly modified version of ASTM G 109 was developed.

First, small "beams" were created with 6 in. x 6 in. x 21 in. (152 x 152 x 533 mm) dimensions and a nominal portion of 3 in. by 6 in. by 6 in. (76 x 76 x 262 mm) "removed" from the center. In these prisms, four no. 3 bars were cast with a cover of 0.75 in. (19 mm) at the top and bottom and 0.5 in. (13 mm) on each side. Typical dimensions of these beams are shown in Figure 12.15 with molds and reinforcing steel shown in Figure 12.16.

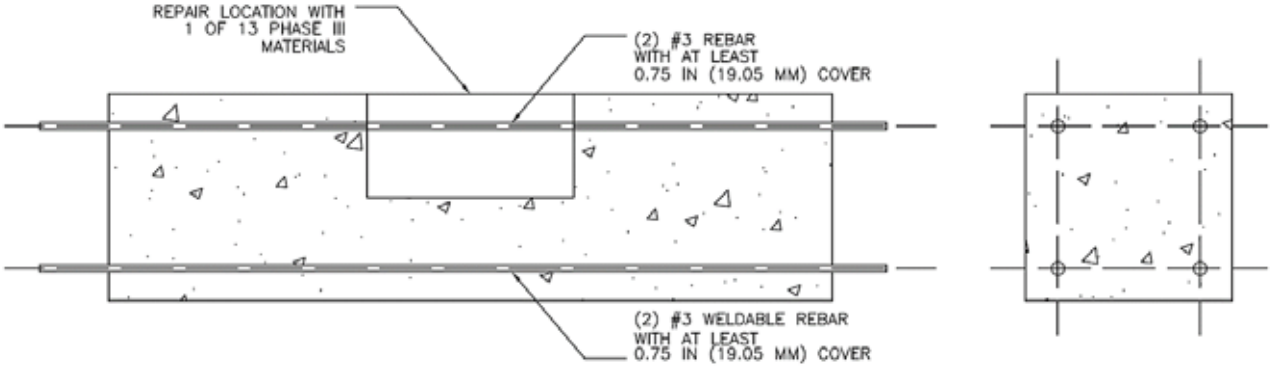

Figure 12.15: Design drawings of fatigue-corrosion beams

Figure 12.16: Molds for fatigue corrosion specimens displaying reinforcing steel and welded plates for development

It is important to note that each of two 7.5-in. x 6-in. x 3-in. (190 x 152 x 152 mm) portions of the top layer also contained 3% calcium chloride to help induce corrosion. The bottom layer was cast according to the mix procedure outlined by Zuniga (2013) and shown in Figure 12.17.

Figure 12.17: Casting the bottom layer of fatigue-corrosion beams

Then a foam insert was used as the second layer containing calcium chloride. Both layers were consolidated with a vibrating table to prevent honeycombing around the reinforcing steel. The top layer casting, reinforcing steel, and foam inserts are shown in Figure 12.18.

Figure 12.18: Casting top layer of fatigue-corrosion beams and displaying foam inserts for eventual repair material casting

The beams were then placed in a 100% humidity moist room to cure for 7 days. On the 7th day, the base was moved to a standard drying shrinkage room for 20 additional days. After 27 days from original casting, a repair of one of the final subset of six materials was cast in "removed" center portion. Once again, this portion was consolidated with a vibrating table to prevent honeycombing despite the rapid time of set. This repair was cured with wet burlap for a single day. An example of the final specimen is shown in Figure 12.19.

Figure 12.19: Example of final fatigue-corrosion beam and inset repair material

After 24 hours, the half-depth repaired specimens were placed in the MTS Systems fatigue loading machine. This machine allows repetitive application of low loads in a cyclic manner for fatigue testing. The specimens were simply supported as shown in Figure 12.20 and point-loaded at the center of the repair. Loads cycled between 2300 and 8000 force-pounds (10.2 to 35.6 kN) for 1 million cycles.

Figure 12.20: Loading fatigue-corrosion beams under repetitive loads using an MTS loading machine

At the conclusion of the cyclical fatigue loading, sample beams were removed from the loading apparatus and a rectangular plastic dam with base dimensions 6 in. (152 mm) by 12 in. (305 mm) was attached around the repair and surrounding concrete with Liquid Nails construction adhesive. Next, the specimen coated with Sikadur Injection Gel structural epoxy, excluding the dammed portion and bottom. The reinforcing steel penetrating from the ends of the specimen were also carefully avoided when applying the structural epoxy. The coat was allowed to cure for one week in standard temperatures.

After one week of curing, provisions for measuring both half-cell potential and macrocell corrosion were applied to the reinforcing steel at one end. Brass grounding claps with attached copper wire were mounted to each bar. In addition, a 100-ohm resistor was attached between the two lower bars and a single upper bar.

After one week in this configuration, 3% calcium chloride solution was ponded in the dam 1.5 in. (40 mm) above the concrete's surface. At this point, macrocell corrosion was measured in a manner similar to Maruya et al. (2007). The voltmeter was attached to a reference electrode with the ground and a single reinforcing bar with the other connection. Voltage readings were recorded for each bar by placing the reference electrode in the salt solution as shown in Figure 12.21. One week later, the calcium chloride solution was removed from the dam, and the cycle repeated.

Figure 12.21: Measuring macrocell voltage of reinforcing steel using voltmeter and reference electrode

12.6.2 Results and Discussion

To show corrosion has initiated, a "remarkable decrease" (Maruya et al., 2007) must be shown in the voltage measurements using the reference electrode and performing half cell potential. At approximately 14 weeks (98 days) from the initial ponding, this remarkable decrease in potential has not occurred in any of the six Phase III materials as shown in Figures 12.22 through 12.28. In each chart, solid lines represent the measurements for the top reinforicng bars and dashed lines represent bottom reinforcing bars. Circular markers are the fatigue-loaded specimens and triangular markers are unloaded.

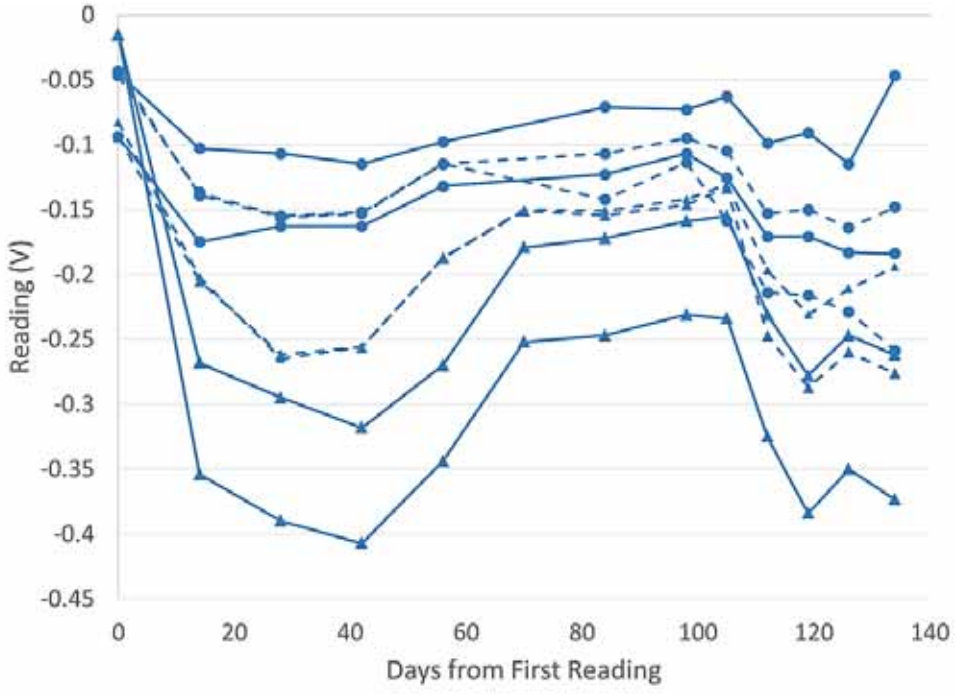

Figure 12.22: Macrocell potential measurement for PC Type III

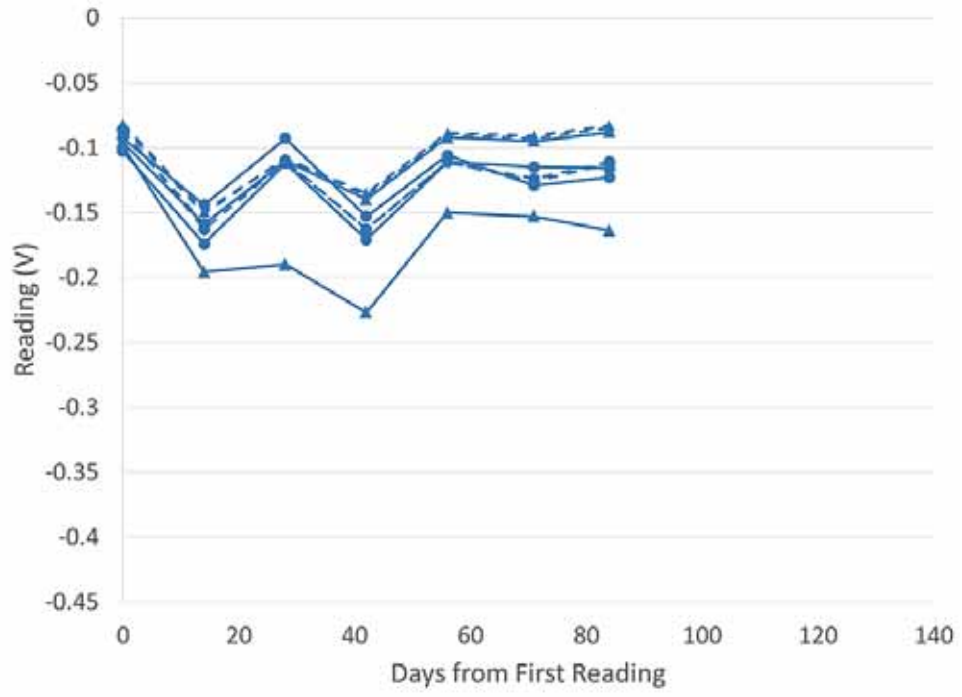

Figure 12.23: Macrocell potential measurement for CSA-1

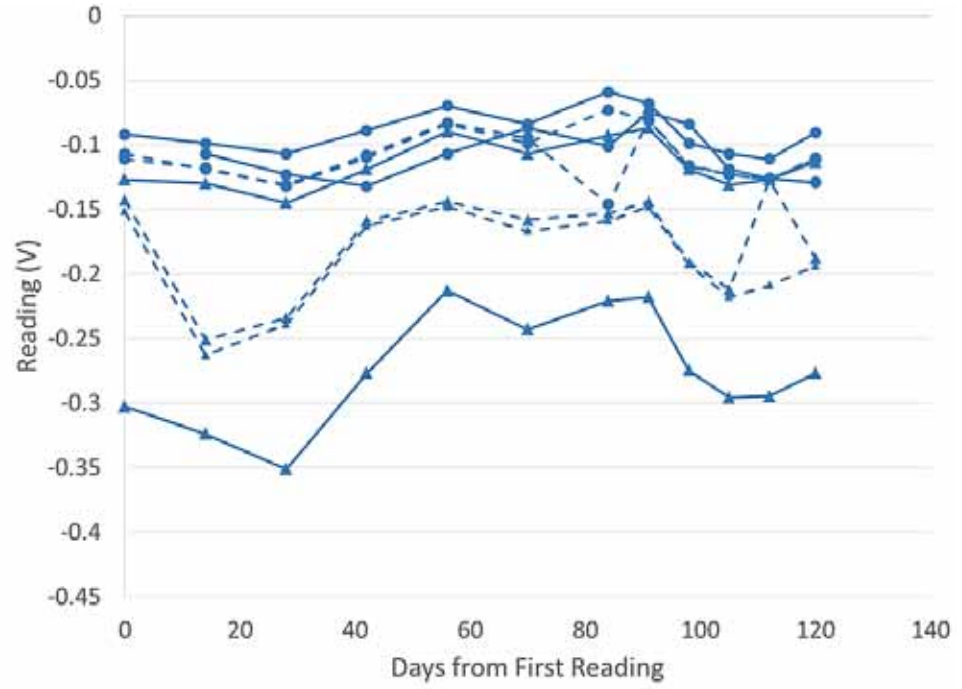

Figure 12.24: Macrocell potential measurement for CAC-2

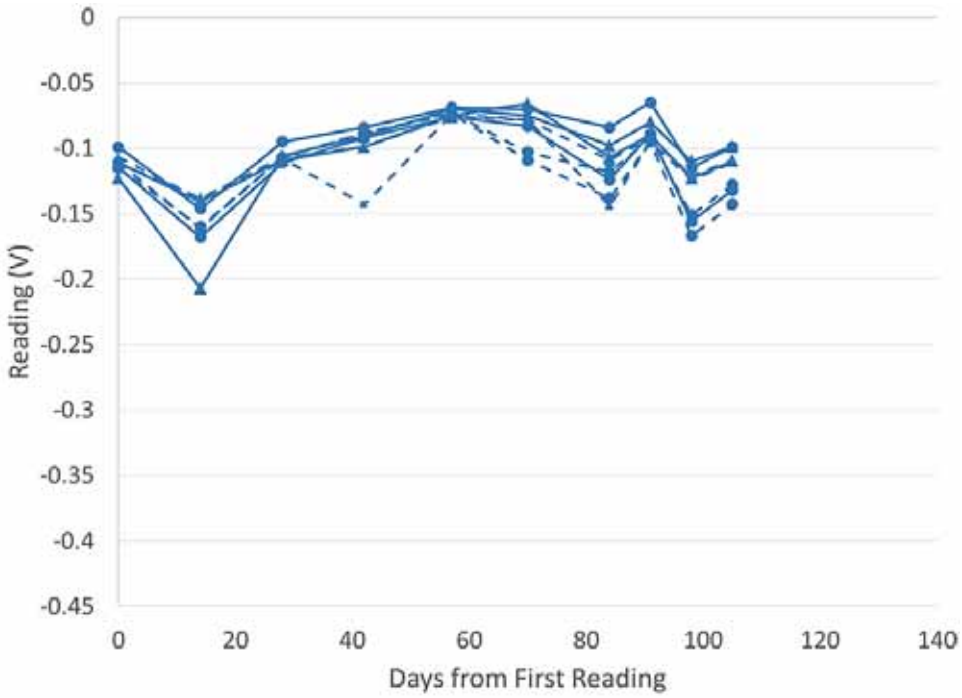

Figure 12.25: Macrocell potential measurement for CAC-3

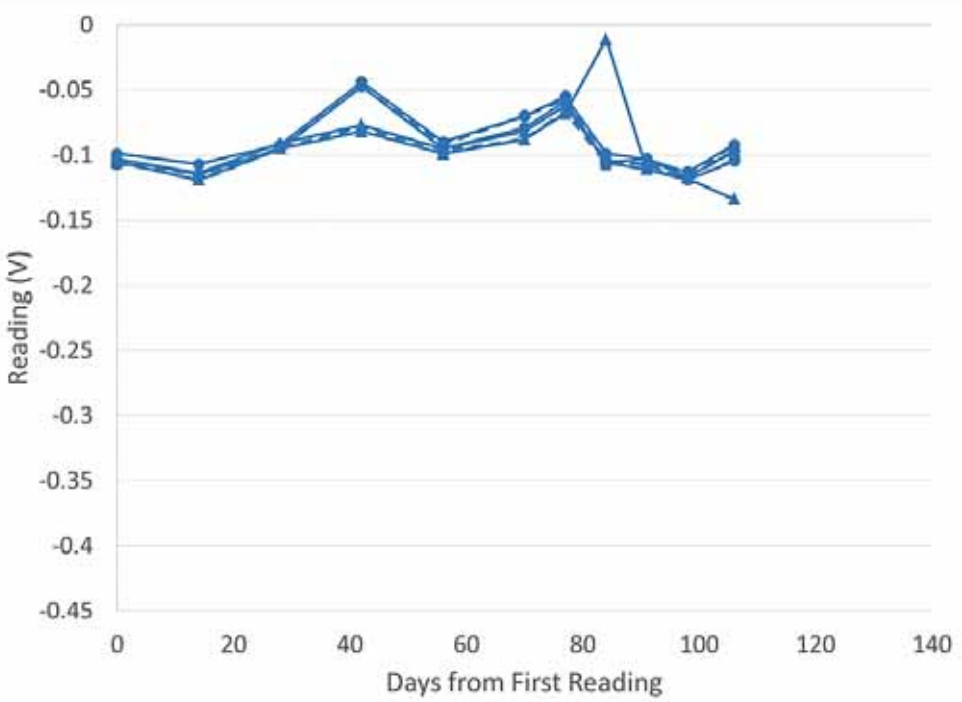

Figure 12.26: Macrocell potential measurement for P-2

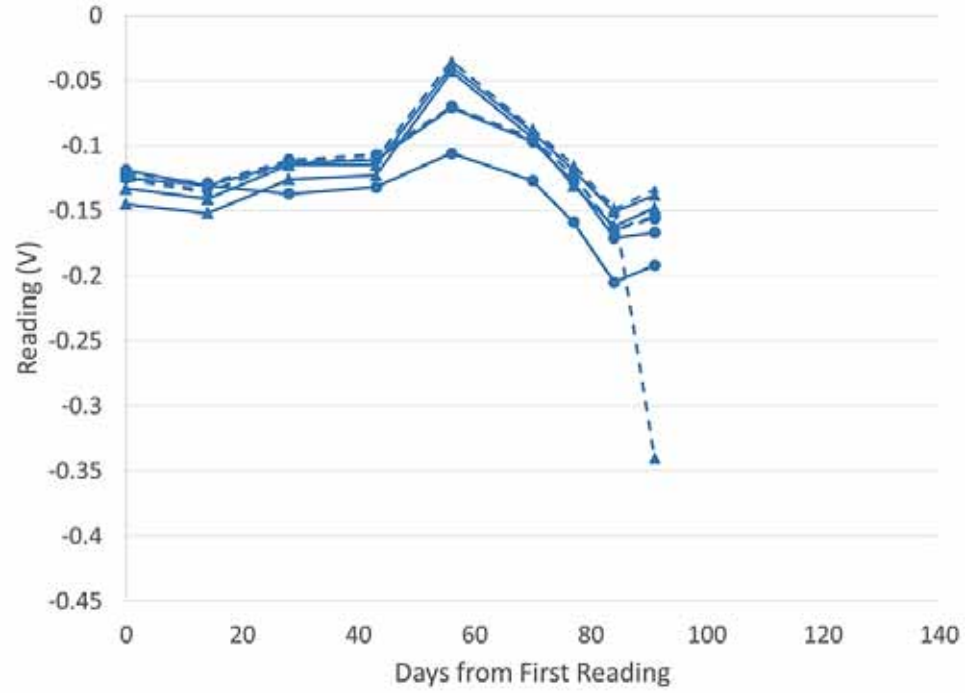

Figure 12.27: Macrocell potential measurement for P-AAFA

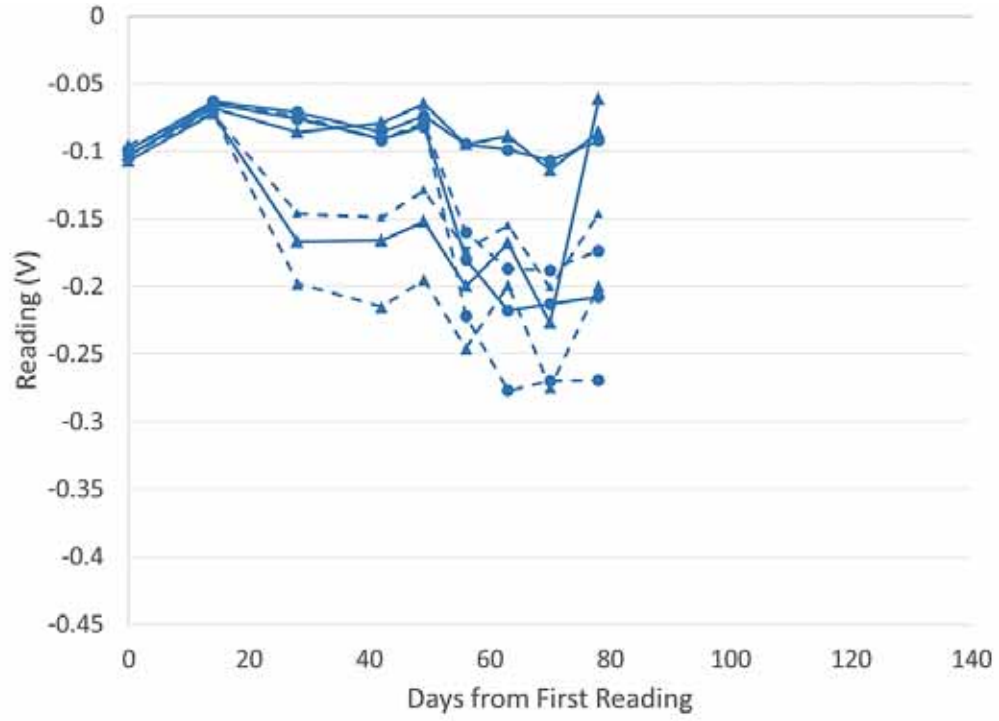

Figure 12.28: Macrocell potential measurement for control mix

For most materials, each reinforcing bar has performed similarly. It is to be expected that at corrosion initiation, likely occurring in the top bars, the voltage for those bars will drop

significantly from those shown in the aforementioned figures. With the chlorides mixed into the top layer of concrete and the frequent wetting-and-drying cycles (weekly), corrosion is expected to initiate sooner than similar studies. Despite this, there is little way to predict the onset of this corrosion, and it could still take significant time until it begins. These specimens will remain under testing well beyond the completion of this project.

12.7 Summary and Conclusions

The summary of the permeability and corrosion performance of the materials is as follows:

- All materials performed well according to the simplified RCPT when cured for 28 days. P-1 and CAC-3 displayed moderate permeability, with every other material displaying low permeability or better.
- The materials generally performed well according to the simplified RCPT when cured only for 1 day. Only P-1 displayed high permeability, with every other material displaying moderate or better permeability.
- In all instances, additional curing improved permeability according to the simplified RCPT.
- For all mixtures, carbonation depths increased between 6 and 11 months, with the exception of P-2. Although a slight reduction in carbonation was measured in this material, it can be assumed that discrepancies along the prism's length caused this difference. Carbonation cannot actually be reduced.
- In all instances, prisms within the Stevenson screen displayed increased carbonation depths when compared to those outside. Concrete not exposed to weather is expected to display increase carbonation depth.
- Carbonation at 11 months reaches depth that may cause concern if reinforcement cover in structural concrete is low.
- Simplified RCPT and chloride permeability due to the modified ASTM C 1556 generally correspond. The least permeable material according to the ponding test was P-2, which displayed very low permeability for both 1-day and 28-day curing conditions according to RCPT. CSA-1, the worst performing material according to the ponding test, was one of two materials displaying moderate permeability with a 1-day curing period.
- Although the time each fatigue and corrosion beam was tested varies, no material displayed corrosion during the test period. The test will be continued into the indefinite future.

Chapter 13. Conclusions

In summary, the following conclusions can be drawn from the research undertaken in this project.

- The selection of the repair materials should not be focused on the material with the strongest or highest values for the engineering properties. Instead, the focus should be on selecting a repair material with properties similar to those of the existing substrate. Selecting repair materials with this approach will increase the service life on any repair.
- The P-2 mixture satisfied the most criteria when considering all of the properties measured at standard temperatures.
- The CAC mixtures presented the best behavior during the temperature robustness study, highlighting its potential for use in cold weather repairs.
- Combining latex with either CSA or CAC had a significant impact on the engineering properties, reducing compressive strength, MOE, tensile strength (for CSA mixture only), and bond strength, and increasing the flexural strength. According to Bentivegna's field study, the latex-modified CAC overlays showed worse signs of deterioration when compared to plain CAC mixtures (2011).
- The CSA binder system had less drying shrinkage than did the CAC binder system at both 28 days and 64 weeks. Three of the four CAC mixtures exceeded the drying shrinkage limits specified by TxDOT.
- Mixtures containing fly ash contained more drying shrinkage than mixtures not containing fly ash.
- The CSA-1 mixture presented autogenous expansion and compressive stresses for both the FSF and RCF, confirming the shrinkage-compensating property for this binder.
- The CAC-2 mixture presented autogenous shrinkage and tensile stresses for both the FSF and RCF, which is behavior similar to that of a typical portland cement concrete with a low w/cm.
- The P-AAFA mixture has a rapid time to peak heat and generates about the same peak temperature when studied at 50 °F, 73 °F, and 100 °F (10 °C, 23 °C, and 38 °C).
- The CAC mixtures were the most variable as a whole, with the CAC-3 mixture having very slow heat generation, lower peak temperatures, and relatively no heat generation at 50 °F (10 °C) compared to the other three mixtures. Unlike the CAC-3 mixture, the remaining CAC mixtures had very rapid heat generation, the highest peak temperatures, the largest temperature gradient, and the best performance at 50 °F (10 °C) of any mixture.
- The CSA mixtures were retarded by the cooler temperatures at 50 °F (10 °C) but had one of the highest temperature gradients at 7.63 °F (4.24 °C) when cured at 73 °F (23 °C). For semi-adiabatic calorimetry, these mixtures yielded similar calorimetry data and temperature curves.

- The mixtures containing mostly portland cement, P-3 and PC Type III, had slower heat generation and lower peak temperature values than did the other rapid repair materials.
- All of the Phase III mixtures, excluding the PC Type III mixture, reached 3000 psi (20.7 MPa) at 3 hours after mixing for the simulated bridge deck repair.
- After the first 24 hours of the temperature gradient analysis, the heat evolution for each mixture had dissipated and the fluctuation in temperatures was due to the fluctuation in the ambient temperature.
- The CAC-3 mixture generated the highest heat and heat differential of all the Phase III mixtures. It also presented a quicker ettringite-induced peak, followed by a larger delayed peak approximately 8 hours later, which could be the portland cement hydrating.
- The P-AAFA mixture emitted as much heat as the ambient temperature 4 days after mixing, while the other mixtures experienced slightly elevated temperatures.
- All of the cracking in the repair sections occurred within the first 7 days after casting, except for the P-AAFA mixture.
- The CAC-2 mixture seemed to have excess water, which could have contributed to drying shrinkage or plastic cracking.
- The P-2 and CSA-3 mixtures performed the best at the Cotulla site; neither showed cracking or surface defections after 8 months of frequent and high axle loads.
- All three CSA mixtures have performed well, so far. The only issue is the transverse cracking with the CSA-2 mixture but this could suggest that it is not compatible with the existing pavement.

The durability of rapid repair materials is often overlooked when compared to their strength development. Despite this, a durable repair material will allow the repair to be replaced less often in transportation structures.

After extensive testing of the Phase II and III materials, their durability properties are tabulated in Table 13.1. This table should allow a general comparison of the materials and their overall resistance to freezing-and-thawing damage, ASR, sulfate attack, and corrosion.

Table 13.1: Durability comparison

Mix ID	Compliance or Relevant Value										
	>5% Fresh Air	Spacing Factor	ASTM C 672 Rating	ASTM C 666 Compliance	ASTM C 1012 Compliance		ASTM C 1293, <0.04% Exp.	RCPT Concrete Permeability		11 Month Carbonation Depth	Chloride Penetration (rank)
					1 Day	28 Day		1 Day	28 Day		
P-1		✓	5		✓	✓		High	Mod.	--	--
P-2*		✓	0	✓			✓	V. Low	V. Low	0.030 in (0.077 cm)	1
P-3			3	✓	✓	✓		V. Low	V. Low	--	--
P-AAFA*			2	✓				Low	V. Low	0.110 in (0.280 cm)	5
CSA-1*		✓	5		✓	✓	✓	Mod.	Low	1.370 in (3.475 cm)	6
CSA-Latex		✓	5		✓	✓	✓	Low	V. Low	--	--
CSA-2	✓	✓	1	✓	✓	✓	✓	Mod.	V. Low	--	--
CSA-3		✓	0	✓	✓	✓	✓	Low	V. Low	--	--
CAC-1	✓	✓	1	✓			✓	V. Low	V. Low	--	--
CAC-Latex	✓		2	✓				V. Low	V. Low	--	--
CAC-2*	✓	✓	0	✓		✓	✓	Low	V. Low	1.230 in (3.125 cm)	3
CAC-3*			2	✓		--		Mod.	Mod.	1.300 in (3.300 cm)	4
PC Type III*	✓		3		✓	✓	✓	Mod.	Low	0.050 in (0.125 cm)	2

Note: Phase III materials denoted with asterisk (*). Cells containing "--" indicate the mixture was not tested for that specific property.

In terms of the durability test program and the material's performances, the researcher team reached the following conclusions:

- Although not all materials met the required air content and spacing factors, the materials generally performed well according to ASTM C 672 and C 666. There is not always a correlation between a material's freeze-thaw performance and air content or makeup of that air.
- Several mixtures were not resistant to ASR or sulfate attack. It is important to note that CAC-1 and CSA-1 both exhibited some distress under each of these durability testing regimes.
- In general, styrene-butadiene latex creates a less permeable concrete matrix. Despite this, modified CAC and CSA worsen the effects of both ASR and sulfate attack.
- The materials are generally low in permeability according to ASTM C 1202.
- No conclusions could be drawn regarding the susceptibility of the materials to corrosion when placed as a repair and cyclically loaded. Corrosion was not initiated in any of the specimens.
- Carbonation depths are of a concern and are likely to cause corrosion if low reinforcement cover is specified.

References

AASHTO (2011). Standard Method of Test for Coefficient of Thermal Expansion of Hydraulic Cement Concrete AASHTO T 336-11, American Association of State Highway and Transportation Officials.

ACI Committee 318 (2011). Building Code Requirements for Structural Concrete. Farmington Hills, Mich.: American Concrete Institute.

ACI 548.4 (2011). *Specification for Latex-Modified Concrete Overlays.* The American Concrete Institute.

ASTM C 109 (2012). *Standard Test Method for Compressive Strength of Hydraulic Cement Mortars.* Conshohocken, PA: ASTM International.

ASTM C 1202 (2010). *Standard Test Method for Electrical Indication of Concrete's Ability to Resist Chlroride Ion Penetration.* Conshohocken, PA: ASTM International.

ASTM C1231 (2013). Standard Practice for Use of Unbonded Caps in Determination of Compressive Strength of Hardened Concrete Cylinders. Pennsylvania: American Society of Testing and Materials.

ASTM C 1293 (2008B). *Standard Test Method for Determination of Length Change of Concrete Due to Alkali-Silica Reaction.* Conshohocken, PA: ASTM International.

ASTM C138 (2013). Standard Test Method for Density, Yield, and Air Content of Concrete. Pennsylvania: American Society of Testing and Materials.

ASTM C143 (2012). Standard Test Method for Slump of Hydraulic-Cement Concrete. Pennsylvania: American Society of Testing and Materials.

ASTM C 150 (2012). *Standard Specification for Portland Cement.* West Conshohocken, PA: ASTM International.

ASTM C 1556 (2011a). *Standard Test Method for Determining the Apparent Chloride Diffusion Coefficient of Cementitious Mixtures by Bulk Diffusion.* Conshohocken, PA: ASTM International.

ASTM C157 (2008). Standard Test Method for Length Change of Hardened Hydraulic-Cement Mortar and Concrete. Pennsylvania: American Society of Testing and Materials.

ASTM C231 (2010). Standard Test Method for Air Content of Freshly Mixed Concrete by the Pressure Method. Pennsylvania: American Society of Testing and Materials.

ASTM C39 (2014). Standard Test Method for Compressive Strength of Cylindrical Concrete Specimens. Pennsylvania: American Society of Testing and Materials.

ASTM C403 (2008). Standard Test Method for Time of Setting of Concrete Mixtures by Penetration Resistance. Pennsylvania: American Society of Testing and Materials.

ASTM C 457 (2009). *Standard Test Method for Microscopical Determination of Parameters of the Air-Void System in Hardened Concrete.* Conshohocken, PA: ASTM International.

ASTM C469 (2010). Standard Test Method for Static Modulus of Elasticity and Poisson's Ratio of Concrete in Compression. Pennsylvania: American Society of Testing and Materials.

ASTM C496 (2011). Standard Test Method for Splitting Tensile Strength of Cylindrical Concrete Specimens. Pennsylvania: American Society of Testing and Materials.

ASTM C 618 (2011). *Standard Specification for Coal Fly Ash and Raw or Calcined Natural Pozzolan for Use in Concrete.* Conshohocken, PA: ASTM International.

ASTM C 666 (2008). *Standard Test Method for Resistance of Concrete to Rapid Freezing and Thawing.* Conshohocken,PA: ASTM International.

ASTM C 672 (2003). *Standard Test Method for Scaling Resistance of Concrete Surfaces Exposed to Deicing Chemicals.* Conshohoken, PA: ASTM International.

ASTM C78 (2010). Standard Test Method for Flexural Strength of Concrete (Using Simple Beam with Third-Point Loading). Pennsylvania: American Society of Testing and Materials.

ASTM C882 (2013). Standard Test Method for Bond Strength of Epoxy-Resin Systems Used With Concrete By Slant Shear. Pennsylvania: American Society of Testing and Materials.

Barborak, R. (2010). *Calcium Aluminate Cement Concrete (Class CAC Concrete) TxDOT Special Specification SS-4491 Tip Sheet.* Texas Department of Transporation.

BASF (2011). *Placement of Latex Modified Concrete.* BASF Corporation.

Bentivegna, A. (2012). *Multi-Scale Characterization, Implementation, and Monitoring of Calcium Aluminate Cement Based-Systems*. Austin: The University of Texas at Austin.

Campas, A., & Scrivener, K. (1998). Calcium Aluminate Cements. In A. Campas, & K. Scrivener, *Lea's Chemistry of Cement and Concrete* (pp. 709-771). Wobum: Butterworth-Heinemann.

Carmmond, N. (1990). Long-term performance of high alumina cement concrete in sulphase-bearing environments. In R. Mangabhai, *Calcium Aluminate Cements.* Cambridge: Great Britain at the University Press.

CEN. (2007). *UNI CEN/TS 12390-10:2008 Testing of Hardened Concrete - Part 10: Determination Of The Relative Carbonation Resistance Of Concrete.* CEN.

Chen, I. A. (2009). *Synthesis of Portland Cement and Calcium Sulfoaluminate-Belite Cement for Sustainable Development and Performance.* Austin: The University of Texas at Austin.

Day, R.L., & Haque, M. N. (1993). Correlation between Strength of Small and Standard Concrete Cylinders. ACI Materials Journal

Dow Chemical Company (1995). *Guidelines for: The Use of Dow Modifier A in Bridge Deck Overlayments.* Midland, MI: The DOW Chemical Company.

Dornak, M. L. (2014). *Engineering Properties, Early-age Volume Change, and Heat Generation of Rapid, Cement-based Repair Materials.*

Farzam, H., Bollin, G., Howe, R. H., Marin, J., Erlin, B. J., Isabelle, H. L., et al. (2005). *Cement and Concrete Terminology.* ACI Committee 116.

Fernandez-Jimenez, A. (2005). Composition and microstructure of alkali activated fly ash binder:Effect of the activator. *Cement and Concrete Research*, 1984-1992.

Garcia, A.M. (2014). Durability Testing of Rapid, Cement-based Repair Materials for Transportation Structures. Master's Thesis, University of Texas at Austin.

Ghafoori, N., & Tays, M. (2007). Abrasion Resistance of Early-Opening-to-traffic Portland Cement Concrete Pavements. *Journal of Materials in Civil Engineering*, 925-935.

Gosselin, C. (2009). *Microstructure Development of Calcium Aluminate Cement Based-Systems with and without Supplementary Cementitious Materials.* Lausanne, Switzerland: Ecole Polytechnique Federale De Lausanne.

Ideker, J. (2008). Early-age Behavior of Calcium Aluminate Cement Systems. PhD Thesis Austin, Texas: The University of Texas at Austin.

Islam, M. (2004). *SHRP Product 2030: Standard Test Method for Chloride Content in Concrete.* Washington, D.C.: Strategic Highway Research Program (SHRP).

Juenger, M. (2011). Advances in alternative cementitious binders. *Cement and Concrete Research*, 1232-1243.

Komljenovic, M. (2010). Mechanical and microstructural properties of alkali-activated fly ash geopolymers. *Journal of Hazardous Materials*, 35-42.

Kurtz, Balaguru, Consolazio, & Maher. (1997). *Fast Track Concrete For Construction Repair.* FHWA.

Ley, M. T. (2007). *The Effects of Fly Ash on the Ability to Entrain and Stabilize Air in Concrete. Dissertation: The University of Texas at Austin.* Austin, Texas. Liao, Y., & Wei, X. (2011). Early hydration of calcium sulfoaluminate cement through electrical resistivity measurement and microstructure investigations. *Construction and Building Materials*, 1572-1579.

Macadam, & Folwer. (1984). *Evaluation of Accelerated Concrete as a Rapid Setting Highway Repair Material.* FHWA.

Macias, A. (1996). Corrosion behaviour of steel in high alumina cement mortar cured at 5, 25, and 55°C: chemical and physical factors. *Journal of Materials Science*, 2279-2289.

Mamlouk, M.S. & Zaniewski, J.P. (2006). Materials for Civil and Construction Engineers. 2nd Ed. New Jersey: Pearson Prentice Hall, Inc.

Maruya, T., Takeda, H., Horiguchi, K., Koyama, S., & Hsu, K.-L. (2007). Half-Cell Potential as an Indicator of Chloride-Induced Rebar Corrosion Initiation in RC. *Journal of Advanced Concrete Technology, 5(3).*

Mindess, S., Young, J. F., & Darwin, D. (2003). *Concrete.* Upper Saddle River: Pearson Education, Inc.

Mehta, P.K. & Monteiro, J.M. (1993). Concrete: Structure, Properties, and Methods. 2nd Ed. New Jersey: Prentice Hall, Inc.

National Cooperative Highway Research Program. (2004). NCHRP Synthesis 333 Concrete Bridge Deck Performance. Transportation Research Board

Neville, A.M. Properties of Concrete. 3rd ed. London: Pitman Books Ltd, 1981.

PCA. (2010). Fly Ash, Slag, Silica Fume, and Natural Pozzolans. In P. C. Association, *PCA Manual* (pp. 57-72).

Pera, J., & Ambroise, J. (2004). New applications of calcium sulfoaluminate cement. *Cement and Concrete Research*, 671-676.

Pesek, P. W. (2011). *Temperature, Stress, and Strength Development of Early-Age Bridge.*

Pigeon, M., & Pleau, R. (1995). *Durability of Concrete in Cold Climates.* Taylor & Francis.

Poole, J. (2007). Modeling Temperature Sensitivity and Heat Evolution of Concrete. PhD Thesis, University of Texas at Austin.

Pradhan, B., & Bhattacharje, B. (2009). Half-Cell Potential as an Indicator of Chloride-Induced Rebar Corrosion Initiation in RC. *American Society of Civil Engineers*, 543-552.

Riding, K. (2007). Early age concrete thermal stress measurement and modeling. PhD Thesis, University of Texas at Austin, Civil Engineering.

Riding, K. A., Poole, J. L., Schindler, A. K., Juenger, M. C., & Folliard, K. J. (2008). Simplified Concrete Resistivity and Rapid Chloride Permeability Test Method. *ACI Materials Journal, 105(4)*, 390.

Shaker, F., El-Dieb, A., & Reda, M. (1997). Durability of Styrene-Butadiene Latex Modified Concrete. *Cement and Concrete Research 27(5)*, 711-720.

Scrivener, K. (2003). Calcium Aluminate Cement. In J. Newman, *Advanced Concrete Technology* (pp. 2/1-2/29). Oxford: Butterworth-Heinemann.

Shi, C., & Fernandez-Jimenez, A. (2011). New cements for the 21st century: The pursuit of an alternative to Portland cement. *Cement and Concrete Research*, 750-763.

Shi, C., & Roy, D. (2005). *Alkali-Activated Cements and Concretes.* Taylor and Francis (CRC Press).

TxDOT (2011). Departmental Material Specification: Concrete Repair Materials (DMS – 4655). Texas Department of Transportation.

Temple, M.A., Ballou, R.D., Fowler, D.W., and A.H. Meyer. (1984). *Implementation Manual for the Use of Rapid-Setting Concretes.* FHWA Research Report: FHWA/TX-85/37+311-7F.

Valenza II, J. J., & Scherer, G. W. (2006). Mechanisms of Salt Scaling. *Journal of th eAmerican Ceramic Society, 89(4)*, 1161-1179.

Whigham, J. (2005). Evaluation of Restraint Stresses and Cracking in Early-Age Concrete with the Rigid Cracking Frame. Master's Thesis, Auburn University.

Winnefeld, F. (2010). Hydration of calcium sulfoaluminate cements-Experimental findings and thermodynamic modelling. *Cement and Concrete Research*, 1239-1247.

Winnefeld, F., & Pelletier-Chaignat, L. (2011). Influence of the calcium sulphate source on the hydration mechanism of Portland cement-calcium sulphoaluminate clinker-calcium sulphate binders. *Cement & Concrete Composites*, 551-561.

Won, J.-P. (2011). Mix proportion of high-strength, roller-compacted, latex-modified rapid-set concrete for rapid road repair. *Construction and Building Materials*, 1796-1800.

Yang, Z., & Shi, X. (2009). Effect of styrene-butadiene rubber latex on the chloride permeability and microstructure of Portland cement mortar. *Construction and Building Materials*, 2283-2290.

Zuniga, J. R. (2013). *Development of Rapid, Cement-based Repair Materials for Transportation Structures.* University of Texas at Austin Thesis Report. Austin, Texas..